Domain-Specific Function and Subcellular Localization of Components of the COP1/SPA Complex in *Arabidopsis thaliana*

Inaugural-Dissertation

zur

Erlangung des Doktorgrades

der Mathematisch-Naturwissenschaftlichen Fakultät

der Universität zu Köln

vorgelegt von

Konstantin Kerner

aus

Speyer

Köln, 2020

Berichterstatter: Prof. Dr. Ute Höcker

                                     Prof. Dr. Martin Hülskamp

Prüfungsvorsitzender: Prof. Dr. Thomas Wiehe

Tag der mündlichen Prüfung: 24. November 2020

TABLE OF CONTENTS

LIST OF FIGURES

LIST OF TABLES

LIST OF ABBREVIATIONS

Abbreviations used in this study are listed below. Units from the International System of Units (SI units) are not listed.

35S	35S promoter of the cauliflower mosaic virus
Å	Ångström
AA	Alanin/Alanin
AD	activation domain
ANOVA	Analysis of Variance
APS	ammonium persulfate
At	*Arabidopsis thaliana*
B	blue light
BCA	bicinchoninic acid
BD	binding domain
bHLH	basic helix loop helix
bp	basepair/basepairs
BSA	bovine serum albumin
bZIP	basic leucin zipper
CC	coiled-coil
cDNA	complementary DNA
CDS	coding sequence
CFP	cyan fluorescent protein
CLS	cytosolic localization signal
Col-0	Columbia-0 (wild type)
C-terminal	carboxy-terminal
DAPI	4',6-diamidino-2-phenylindole

ddH$_2$O	double-distilled water
DMSO	dimethyl sulfoxide
DNA	desoxyribonucleic acid
DNase	desoxyribonuclease
dNTPs	desoxynucleoside triphosphate
DTT	1,4-dithiothreitol
E. coli	*Escherichia coli*
e.g.	exempla gratia (for example)
EDTA	ethylenediaminetetraacetic acid
et al.	et alii (and others)
FAD	flavin adenine dinucleotide
FMN	flavin mononucleotide
FR	far-red light
GFP	green-fluorescent protein
H	histidin
HA	human influenza hemagglutinin
HIR	high irradiance response
HRP	horseradish peroxidase
Hs	*Homo sapiens*
HSC70	heat shock cognate protein 70
i.e.	id est (that is
IgG	immunoglobulin G
Indel	insertion/deletion
kanR	resistance to kanamycin
kb	kilobase/kilobases

kDa	kilodalton
L	leucin
LB	Luria-Bertani
LFR	low fluence response
LOV	light oxygen voltage
LRE	light-responsive element
MeOH	methanol
MS	Murashige & Skoog
NB	nuclear body
Nedd8	neural-precursor-cell-expressed developmentally down-regulated 8
NLS	nuclear localization signal
N-terminal	amino-terminal
OD	optical density
P	p-value
PAGE	polyacrylamide gel electrophoresis
PCR	polymerase chain reaction
Pfr	far-red light-absorbing conformer of phytochromes
PHR	photolyase-homologous region
Pr	red light-absorbing conformer of phytochromes
PVDF	polyvinylidene difluoride
qRT-PCT	quantitative real-time polymerase chain reaction
R	red light
RING	really interesting new gene
RNA	ribonucleic acid
ROI	region of interest

RT	room temperature
Rub1	related to ubiquitin1
S	Svedberg
SDS	sodium dodecyl sulfate
SV40	simian vacuolating virus 40
Taq	*Thermus aquaticus*
TBS	Tris-buffered saline
T-DNA	transfer-DNA
TE	Tris/EDTA
TEMED	tetramethylethylendiamine
Trib1	Tribbles1
Tris	tris(hydroxymethyl)aminomethane
UV	ultraviolet light
UV-A	ultraviolet A
UV-B	ultraviolet B
v/v	volume per volume
VFLR	very low fluence response
VP	valine, proline
w/v	weight per volume
WD	aspartic acid, tryptophan
Wt	wild type
YEB	yeast extract broth
YFP	yellow fluorescent protein
YPD	yeast extract peptone dextrose

NOMENCLATURE

NOMENCLATURE OF ARABIDOPSIS GENES AND PROTEINS

COP1	Gene, locus, wild-type allele
cop1-4	Mutant allele
COP1	Protein
cop1-4	Mutant protein

EXCEPTION: NOMENCLATURE OF PHOTORECEPTORS

PHYA	Gene, locus, wild-type allele
phyA	Mutant allele
PHYA	Apoprotein (without chromophore)
phyA	Holoprotein (with chomophore)

ABSTRACT

Light affects almost all stages of plant development. To adequately adapt to changes in ambient light, plants have evolved a complex regulatory network to perceive and subsequently transmit light signals. One of the central regulators of light signaling in the model plant *Arabidopsis thaliana* is the COP1/SPA complex. This tetrameric complex is part of an E3 ubiquitin ligase complex which marks positive regulators of photomorphogenesis for degradation by polyubiquitination, thereby regulating important light-dependent processes like seedling de-etiolation, shade-avoidance responses, vegetative growth, and the induction of flowering. Both COP1 and SPA proteins contain C-terminal WD-repeats which are essential for interaction with many different players in the light-signaling cascade, and by extension for COP1/SPA function. The COP1/SPA complex has been studied extensively over the past two decades, but many aspects of COP1/SPA function are yet to be fully understood.

In the first part of this study, I analyzed both structural and functional differences between the COP1 and SPA1 C-terminal WD-repeat domains. First, by using structural X-ray data of the COP1 WD-domain, I generated a homology model of the SPA1 WD-repeat domain. I was able to identify several structural differences between both domains. First, sequence homology analysis showed that one residue that has previously been shown to be involved in the interaction of COP1 with a peptide of HY5 containing the VP binding motif is not conserved within SPA1. Second, two residues which are involved in the interaction with COP1 and a substrate of its homolog in humans, Trib1, are oriented differently in the substrate binding pocket of SPA1. Third, the homology model showed that two loops in the SPA1 WD-repeat domain are likely structurally different from COP1. Next, I generated chimeric hybrid proteins of COP1 and SPA1 that had their WD-repeat domains interchanged (CC1 and 11C). These proteins were proven to be functionally active in yeast two-hybrid and colocalization analysis. When expressed in plants, *CC1* was able to rescue the mutant phenotype of dark-grown *cop1* mutants. In contrast, *11C* was unable to rescue the mutant phenotype of dark-grown higher order *spa* mutants, indicating that the SPA1 WD-repeat domain is essential for COP1/SPA function, whereas the COP1 WD-repeat domain is not. *CC1* was able to partially rescue adult phenotypes of *cop1* mutants, but *11C* triggered a dominant negative phenotype in adult higher order *spa* mutants. Lastly, molecular analysis showed that endogenous COP1 accumulated in dark-grown seedlings expressing *11C*, indicating that 11C proteins may inactivate endogenous COP1. Taken together, these results indicate that the SPA1 WD-repeat domain is both structurally and functionally divergent from the homologous region of COP1.

In the second part of this study, I investigated the light-dependent subcellular localization of COP1 and SPA1 proteins. Nuclear exclusion of COP1 was dependent on SPA proteins in white light, but nuclear COP1 in *spaQn* mutants appeared to be inactive, demonstrating at least a dual role of SPA proteins in the regulation of COP1 activity. Analysis of COP1 localization in monochromatic light showed that nuclear exclusion of COP1 is likely regulated by a complex, non-additive interplay between phytochromes and cryptochromes. Finally, SPA1 also failed to localize into nuclear photobodies in white light, but whether this is due to nuclear exclusion of SPA1, SPA1 degradation or a combination of both remains unclear. In conclusion, these results show that SPA proteins are required both for the nuclear exclusion of COP1 and COP1 activity in general, whereas light-dependent nuclear localization of SPA1 remains to be investigated further.

ZUSAMMENFASSUNG

Licht beeinflusst so gut wie alle Phasen der Entwicklung von Pflanzen. Um angemessen auf Änderungen der umgebenden Lichtbedingungen reagieren zu können, hat sich in Pflanzen ein komplexes regulatorisches Netzwerk entwickelt, um Lichtsignale wahrnehmen und weiterleiten zu können. Einer der zentralen Regulatoren der Lichtsignaltransduktion ist der COP1/SPA Komplex. Dieser tetramerische Komplex ist Teil eines E3 Ubiquitinligasekomplexes, welcher positive Regulatoren der Photomorphogenese durch Polyubiquitinierung zur Degradation markiert und dadurch wichtige lichtabhängige Prozesse wie Deetiolierung von Keimlingen, Schattenvermeidungsantworten, vegetatives Wachstum und die Induktion der Blüte reguliert. Sowohl COP1 als auch SPA Proteine besitzen C-terminale WD-Wiederholungen, die essenziell für die Interaktion mit vielen verschiedenen Mitspielern in der Lichtsignalkaskade und damit für die Funktionalität von COP1/SPA, sind. Der COP1/SPA Komplex wurde in den letzten zwei Jahrzehnten umfangreich studiert, doch viele Aspekte der Funktion von COP1/SPA sind noch nicht voll und ganz verstanden.

In dem ersten Teil dieser Studie habe ich sowohl strukturelle als auch funktionelle Unterschiede zwischen der C-terminalen WD-Wiederholungsdomänen von COP1 und SPA1 analysiert. Durch die Nutzung von strukturellen Infrarotdaten der COP1 WD-Wiederholungsdomäne habe ich ein homologes Modell der SPA1 WD-Wiederholungsdomäne generiert. Ich konnte einige strukturelle Unterschiede zwischen beiden Domänen feststellen. Erstens hat die Analyse von Sequenzhomologie gezeigt, dass ein Aminosäurerest, von dem zuvor gezeigt worden war, dass er in die Interaktion zwischen COP1 und einem HY5 Peptid, welches das VP Bindemotif enthielt, nicht in SPA1 konserviert ist. Zweitens sind zwei Aminosäurereste, die in die Interaktion von COP1 und einem Substrat seines Homologs in Menschen, Trib1, involviert sind, in der Substratbindetasche von SPA1 anders orientiert. Drittens hat das Homologie Modell gezeigt, dass zwei Schleifen in der SPA1 WD-Wiederholungsdomäne sich wahrscheinlich von COP1 strukturell unterscheiden. Als nächstes habe ich chimärische Hybridproteine zwischen COP1 und SPA1, deren WD-Wiederholungsdomänen miteinander ausgetauscht wurden (CC1 und 11C), generiert. Diese Proteine waren funktionell aktiv in Hefe zwei-Hybrid- und Colokalisationsstudien. In Pflanzen exprimiert war *CC1* in der Lage, den Mutanten Phänotyp von in Dunkelheit angezogenen *cop1* Mutanten zu rekonstituieren. Dagegen war *11C* nicht in der Lage den Mutanten Phänotyp von höherrangigen, in Dunkelheit angezogenen *spa* Mutanten zu retten, was zeigt, dass die SPA1 WD-Wiederholungsdomäne essenziell für die Funktionalität von COP1/SPA ist, die COP1 WD-Wiederholungsdomäne hingegen nicht. *CC1* war in der Lage, adulte Phänotypen von *cop1* Mutanten partiell zu retten, wohingegen *11C* dominant negative Phänotypen in adulten höherrangigen *spa* Mutanten hervorgerufen hat. Zuletzt haben molekulare Analysen gezeigt, dass endogenes COP1 in im Dunkeln angezogenen Keimlingen, die *11C* exprimieren,

akkumuliert, was andeutet, dass 11C möglicherweise endogenes COP1 inaktiviert. Zusammengefasst zeigen diese Ergebnisse, dass die SPA1 WD-Wiederholungsdomäne sich sowohl strukturell als auch funktionell von ihrer homologen Region in COP1 unterscheidet.

Im zweiten Teil dieser Studie habe ich die lichtabhängige subzelluläre Lokalisation von COP1 und SPA1 Proteinen untersucht. Der Ausschluss von COP1 aus dem Nukleus ist abhängig von SPA Proteinen in weißem Licht, doch nuklear lokalisiertes COP1 scheint inaktiv in *spaQn* Mutanten zu sein, was zeigt, dass SPA Proteine mindestens eine zweiteilige Rolle in der Regulation der Aktivität von COP1 haben. Die Analyse der Lokalisation von COP1 in monochromatischem Licht hat gezeigt, dass der Export von COP1 aus dem Nukleus wahrscheinlich von einem komplexen, nichtadditiven Zusammenspiel von Phytochromen und Cryptochromen reguliert wird. SPA Proteine waren ebenfalls nicht in Lichtkörper im Nukleus lokalisiert, doch ob dies aufgrund des Exports von SPA1 aus dem Nukleus, der Degradation von SPA1 oder einer Kombination von beidem zu beobachten ist, ist noch unklar. Als Fazit zeigen diese Ergebnisse, dass SPA Proteine sowohl für den Ausschluss von COP1 aus dem Nukleus als auch für die Aktivität von COP1 im Allgemeinen notwendig sind, wohingegen der lichtabhängige Export von SPA1 aus dem Nukleus noch weiter untersucht werden muss.

1 INTRODUCTION

1.1 LIGHT PERCEPTION AND SIGNAL TRANSDUCTION

Plants are highly plastic organisms. As predominantly sessile life forms, they are forced to adapt to sometimes vastly diverse ranges of habitats to complete their life cycle. To this end, they have developed highly sensitive mechanisms to perceive key environmental cues such as light, temperature, moisture, and composition of nutrients in the soil. Once perceived, these signals are then integrated into a complex molecular regulatory network composed of receptors, transcription factors and other effectors to elicit responses to environmental changes. Because of this, plants are highly adaptable in terms of their life cycle, morphology, and growth phases. In addition to serving as an energy source for CO_2 fixation during photosynthesis, light is one of the most influential environmental signals for plants. Light affects all stages of a plant's life cycle. Plants can perceive light via an array of photoreceptors which enable them to sense light quality, direction, periodicity, and intensity. The underlying regulatory network orchestrates key aspects of plant development and morphology such as germination, seedling de-etiolation, phototropic growth, shade avoidance, vegetative growth and initiation of flowering (Neff et al., 2000) (Figure 1.1).

1.1.1 Plant photoreceptors perceive diverse aspects of light

Plants have developed a diverse set of photoreceptors to sense different wavelengths of the light spectrum. In the model plant *Arabidopsis thaliana* (Arabidopsis), five sets of photoreceptors have so far been described: (1) The red/far red light perceiving phytochromes (phyA-E); (2) cryptochromes (cry1 and cry2); (3) phototropins (phot1 and phot2); (4) F-box containing flavin binding proteins (FKF1/LKP2, ZEITLUPE), all of which perceive blue and/or UV-A light; and (5) the UV-B absorbing UV RESISTANCE LOCUS 8 (UVR8) (Paik and Huq, 2019)(Figure 1.1).

	seed germination	seedling de-etiolation	phototropism	shade avoidance	initiation of flowering
UVR8		+	+		+
cry1		+		+	
cry2		+		+	+
phot1/phot2			+		
ZTL					+
phyA	+	+		+	+
phyB-E	+	+		+	+
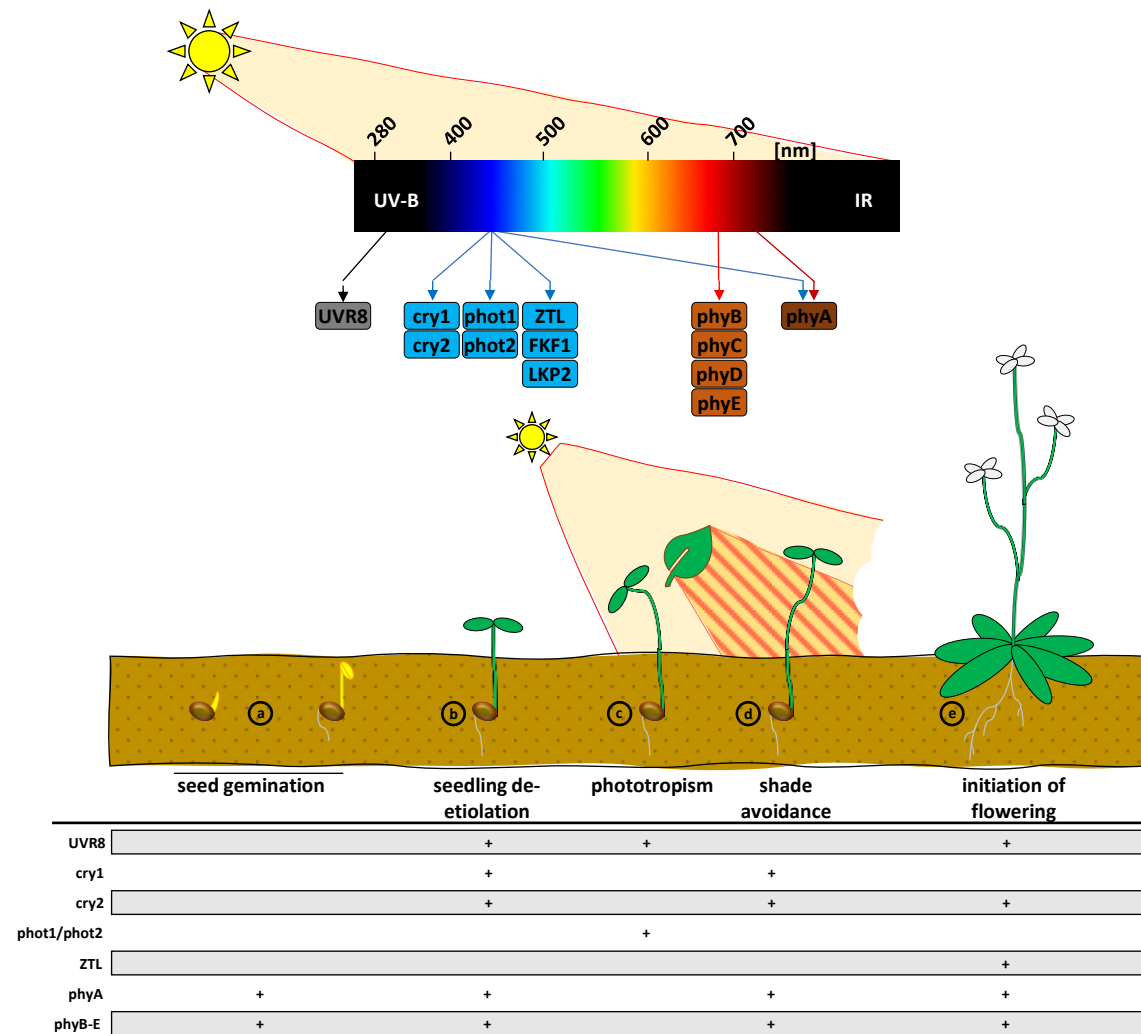
Figure 1.1: Light affects various stages of plant development.

Various types of photoreceptors perceive different wavelengths of light. Throughout plant development, different photoreceptors affect various aspects of light-regulated growth and development. The only known receptor capable of perceiving UV-B light is the UVR8 protein; UV-A and blue light is perceived by cryptochromes (cry1 and cry2), phototropins (phot1 and phot2), members of the Zeitlupe protein family and phyA; red light signals are regulated by the four existing type II phytochromes (phyB-E); and far-red light signals are regulated by the only type I phytochrome (phyA). Light, perceived by photoreceptors, affects – among others - **(a)** seed germination (regulated by phytochromes), **(b)** seedling de-etiolation upon emergence from the soil (regulated by UVR8, cryptochromes and phytochromes), **(c)** phototropism (regulated by UVR8 and phototropins), **(d)** the R/FR-dependent shade avoidance response (regulated by cryptochromes and phytochromes) and **(e)** the initiation of photoperiodic flowering (regulated by cry2, the Zeitlupe family, phytochromes and UVR8).

Phytochromes are among the most well characterized plant photoreceptors. They can be found almost universally in all land plants (Li et al., 2015a). Most commonly, they are dimeric receptors and each apoprotein covalently binds to a linear tetrapyrrole, phytochromobilin, as a chromophore (Franklin and Quail, 2010; Lagarias and Rapoport, 1980). Phytochromes are synthesized in darkness in their biologically inactive, red light (R) absorbing (Pr) conformation. Upon R-absorption, they convert

2

to the biologically active, far-red light (FR) absorbing (Pfr) conformation and translocate to the nucleus upon photoconversion (Sakamoto and Nagatani, 1996; Nagatani, 2004; Kircher et al., 1999). Pfr can subsequently be inactivated upon either absorption of FR or by thermal relaxation, the latter of which is a temperature-dependent process (Rockwell and Lagarias, 2006; Klose et al., 2020). Phytochromes can be categorized into two types: The light labile type I, and light stable type II phytochromes (Legris et al., 2019; Clough and Vierstra, 1997). In Arabidopsis, five phytochrome-encoding genes have been described, one of which (*PHYA*) encodes a type I phytochrome while the remaining four (*PHYB-E*) encode type II phytochromes (Sharrock and Quail, 1989; Clack et al., 1994). Light labile phyA is highly abundant in etiolated seedlings and regulates responses such as germination in low light conditions (Very Low Fluence Response, VLFR) or seedling de-etiolation in continuous high irradiance of FR (FRc High Irradiance Response, HIR), both of which are non-photoreversible processes (Li et al., 2011). Due to its rapid degradation upon light exposure, phyA can act as a highly sensitive initial light sensor upon soil emergence (Hennig et al., 2000; Franklin and Quail, 2010). In contrast, light stable type II phytochromes (phyB-E) are imported into the nucleus upon R exposure (Sakamoto and Nagatani, 1996; Kircher et al., 2002), where they are responsible for the mediation of both R/FR photoreversible low fluence responses (LFR) and R-dependent non-photoreversible HIRs (Casal et al., 1998). Whereas phyA is translocated into the nucleus upon interaction with FAR-RED ELONGATED HYPOCOTYL 1 (FHY1) and FHY1-LIKE (FHL) (Hiltbrunner et al., 2006; Genoud et al., 2008), the transport of light-activated type II phytochromes (phyB-E) is not fully understood (Klose et al., 2015). The remaining phytochromes, phyC-E, play comparatively smaller roles in phy-signaling and mostly seem to act redundantly with phyB (Hennig et al., 2002; Franklin et al., 2003b, 2003a). Finally, phyB, which is the most abundant phytochrome in light-grown seedlings (Sharrock and Clack, 2002), has more recently been identified as a thermosensor in ambient temperature conditions through its temperature dependent Pfr-Pr reversion rate (Legris et al., 2016; Jung et al., 2016; Klose et al., 2020).

Cryptochromes are blue light (B) and UV-A light perceiving flavoproteins that mediate a plethora of B-induced responses, such as seedling de-etiolation or photoperiodic flowering (Wang et al., 2014; Ahmad and Cashmore, 1993; El-Din El-Assal et al., 2001; Mao et al., 2005; Guo et al., 1998). Blue light is perceived via a non-covalently bound flavin adenine dinucleotide (FAD) chromophore which binds to the N-terminal Photolyase Homologous Region (PHR) domain (Lin et al., 1995; Banerjee et al., 2007). The Arabidopsis genome contains three cryptochrome-encoding genes (*CRY1*, *CRY2* and *CRY3*); out of these, only cry1 and cry2 have been shown to function as B-perceiving photoreceptors, while *CRY3* encodes a CRY-DASH type protein which is involved in UV-induced damage repair of single-stranded DNA (Kleine et al., 2003; Pokorny et al., 2008; Ahmad and Cashmore, 1993). Similar to phytochromes, both cry1 and cry2 function as homodimers (Sang et al., 2005; Yu et al., 2007); whereas cry1 localizes both in the nucleus and cytoplasm, cry2 exclusively localizes to the nucleus (Guo et al.,

1999; Kleiner et al., 1999; Wu and Spalding, 2007). Signal transduction of B-activated cry1 and cry2 dimers occurs primarily in the nucleus, with the possible exception of B-dependent cotyledon expansion and root elongation mediated by cry1 (Wu and Spalding, 2007).

Phytochromes and cryptochromes cooperatively regulate various parts of plant development. For example, R, FR and B-mediated repression of seedling etiolation is regulated by phyB, phyA and cryptochromes, respectively (Nagatani et al., 1991, 1993; Dehesh et al., 1993; Parks and Quail, 1993; Reed et al., 1994; Ahmad and Cashmore, 1993). Shade avoidance syndrome (SAS), which is mainly regulated via R/FR ratios perceived by phyB, is also controlled by B-dependent signaling via cry1 (Franklin and Quail, 2010; Keller et al., 2011). Aside from these types of autonomous actions, synergistic co-action of phytochromes and cryptochromes has also been recognized (Sellaro et al., 2009; Su et al., 2017). Various phytochromes and cryptochromes can also physically interact, such as light activated phyA and cry1, phyB and cry2 or phyB and cry1 (Ahmad et al., 1998b; Devlin and Kay, 2000; Mas et al., 2000; Hughes et al., 2012). More recently, a negative feedback loop involving negative regulators of cryptochrome signaling BLUE-LIGHT INHIBITOR OF CRYPTOCHROMES 1 (BIC1) and BIC2, has also been shown to be partly influenced by phytochrome signaling (Wang et al., 2016, 2017). Phytochrome-cryptochrome coactions, and the various aspects of B, R and FR signaling crosstalk are highly complex and not yet fully understood (Wang et al., 2018a).

Apart from cryptochromes and phyA, B and UV-A light is perceived by two other families of photoreceptors in Arabidopsis: Firstly, phototropins are flavoproteins containing a C-terminal serine/threonine kinase domain and two Light, Oxygen or Voltage sensing (LOV1 and LOV2) domains, which non-covalently bind oxidized FMN as a chromophore (Fankhauser and Christie, 2015; Christie et al., 1999). The Arabidopsis genome contains two loci encoding phototropin genes, *PHOT1* and *PHOT2*. They are involved in a variety of light-regulated processes, such as chloroplast movement, stomatal opening, leaf flattening and phototropic growth (Christie et al., 1998; Kagawa et al., 2001; Jarillo et al., 2001; Kinoshita et al., 2001; de Carbonnel et al., 2010; Okajima, 2016). Secondly, several members of the ZEITLUPE (ZTL) family, such as ZTL, FLAVIN-BINDING KELCH REPEAT F-BOX 1 (FKF1) and LOV KELCH PROTEIN 2 (LKP2) are LOV-domain containing, B and UV-A light-perceiving photoreceptors that mainly involved in circadian clock function and circadian regulation of flowering time (Somers et al., 2000; Imaizumi et al., 2003; Baudry et al., 2010; Christie et al., 2015). Besides their amino-terminal LOV domain, they contain an F-box and six kelch-repeats in their carboxy-terminal region (Ito et al., 2012), and transmit signals via protein degradation as part of Skp Cullin F-box (SCF)-type E3 ubiquitin ligases (Ito et al., 2012; Christie et al., 2015).

Lastly, UV-B light (280-315 nm) is perceived by the atypical photoreceptor UVR8 (Rizzini et al., 2011). In contrast to all other known photoreceptors in Arabidopsis, UVR8 does not bind a

chromophore. Instead, UV-B photons are perceived by specific tryptophans within the UVR8 peptide sequence (Rizzini et al., 2011; Christie et al., 2012; Di Wu et al., 2012; Zeng et al., 2015). UVR8 consists of two subdomains: a seven-bladed β-propeller domain, formed by RCC1-repeats, and an unstructured C-terminal domain comprised of 27 amino acids, therefore named the C27 domain (Cloix et al., 2012; Rizzini et al., 2011; Di Wu et al., 2012). UV-B-activated UVR8 dissociates from its inactive homodimeric conformation into active monomers (Liu et al., 2014; Voityuk et al., 2014; Wu et al., 2014; Mathes et al., 2015; Heilmann et al., 2016, 2015) which subsequently translocate from the cytosol into the nucleus and interact with downstream effectors to transmit UV-B signals (Kaiserli and Jenkins, 2007; Yin et al., 2016; Qian et al., 2016). UVR8-mediated responses include hypocotyl growth inhibition, regulation of photoperiodic flowering and UV-B stress attenuation responses such as accumulation of flavonols and anthocyanins, DNA repair and protection against oxidative stress (Li et al., 2015b; Davey et al., 2012; Stracke et al., 2010; Morales et al., 2013; Favory et al., 2009; Brown et al., 2005; Kliebenstein et al., 2002; Arongaus et al., 2018).

1.1.2   Attenuation of photoreceptor signals by negative feedback loops

Some photoreceptors regulate their own activity via negative feedback mechanisms. In the recent decade, various types of such negative feedback loops have been elucidated. As such, expression of the afore-mentioned *BIC1* and *BIC2* genes is indirectly regulated by cry1 and cry2. BICs subsequently interact with CRYs to prevent the formation of active cry oligomers (Wang et al., 2016, 2017). Consistently, *bic1 bic2* double mutants are hypersensitive to B, while transgenic BIC overexpressing plants are hyposensitive to B (Wang et al., 2016). More recently, the structure of BIC2-CRY2 crystals has been determined, revealing that BIC is composed of four α-helices and a loop, which form a wide surface area for contact with the N-terminal region of CRY2 (Ma et al., 2020).

Similar to cryptochromes, the UV-B receptor UVR8 regulates its own activity by indirectly inducing the expression of two genes encoding WD-repeat proteins called *REPRESSOR OF UV-B PHOTOMORPHOGENESIS 1 (RUP1)* and *RUP2*. Expression of *RUP1* and *RUP2* is induced by UV-B light in a UVR8-dependent manner (Gruber et al., 2010). RUPs interact with the C27 domain of UVR8 to promote reversion of UVR8 to its inactive dimeric ground state, thereby attenuating UV-B signals (Gruber et al., 2010; Heijde and Ulm, 2013). Consistent with this mechanism, *rup1 rup2* double mutants are hypersensitive to UV-B light (Gruber et al., 2010; Yin and Ulm, 2017).

1.1.3   Photoreceptors transmit light signals via direct control of transcription factors

Light signals perceived by photoreceptors are transmitted via multiple pathways; one such pathway is facilitated via the direct interaction of photoreceptors with transcription factors. The most well studied transcription factors of this kind are a family of basic Helix-Loop-Helix (bHLH) transcription factors named PHYTOCHROME INTERACTING FACTORS (PIFs). The Arabidopsis genome contains eight genes encoding *PIF*s, namely *PIF1*, *PIF3-8* and *PHYTOCHROME-INTERACTING FACTOR-LIKE 1* (*PIL1*) (Lee and Choi, 2017). PIFs act as repressors of light responses in the dark, regulating various aspects of skotomorphogenic growth such as hypocotyl elongation or suppression of chlorophyll biosynthesis (Oh et al., 2004; Kim et al., 2003; Koini et al., 2009; Huq and Quail, 2002; Fujimori et al., 2004; Leivar et al., 2008; Shin et al., 2009; Stephenson et al., 2009). Besides skotomorphogenic growth, PIFs have also been shown to play a pivotal role in shade-induced growth responses mediated by phyB signaling (Lorrain et al., 2008). These responses are facilitated by PIF binding to specific motifs in the Arabidopsis genome, named G- or E-boxes (CACGTG or CANNTG, respectively) (Huq and Quail, 2002; Leivar et al., 2008; Shin et al., 2007; Leivar and Quail, 2011; Zhang et al., 2013). Upon light-activation, phytochromes in their active Pfr form translocate to the nucleus, where they physically interact with the N-terminal Active Phytochrome B-binding (APB) or APA motifs of PIFs (Ni et al., 2014). Phy-PIF interaction leads to phosphorylation and subsequent degradation of PIFs, however the mechanism behind PIF phosphorylation is not fully understood (Shin et al., 2016; Ni et al., 2013; Al-Sady et al., 2006). Degradation of PIFs subsequently promotes photomorphogenic growth.

Similarly, cry signal transduction partly occurs through another set of bHLH transcription factors named CRYPTOCHROME-INTERACTING BASIC-HELIX-LOOP-HELIX (CIB). Light-activated cry2 interacts with the N-terminal region of CIB1 via its PHR domain (Liu et al., 2008a). CIB1 forms heterodimers with CIB2, CIB4 and CIB5 and binds to E-box (CANNTG) elements in the Arabidopsis genome in a CRY2-dependent manner (Liu et al., 2008a, 2013). Intriguingly, more recent studies have revealed that cryptochromes also interact with PIFs, specifically PIF4 and PIF5 via their PHR domains to inhibit PIF activity in B (Pedmale et al., 2016; Ma et al., 2016), suggesting that cryptochromes might be involved in shade avoidance responses via the regulation of PIFs (Fraser et al., 2016).

1.1.4   The COP1/SPA complex is a central repressor of photomorphogenesis in darkness

Besides direct regulation of transcription factors such as PIFs and CIBs, photoreceptors also regulate gene expression via indirect mechanisms. One of the most well studied mechanisms is control of the activity of E3-ubiquitin ligase-subunit complex named COP1/SPA (Hoecker, 2017). *COP1* is a member of a group of genes named the *CONSTITUTIVE PHOTOMORPHOGENIC/DE-ETIOLATED/FUSCA* (*COP/DET/FUS*) genes (Schwechheimer and Deng, 2000; Serino and Deng, 2003). Many members of

this group were identified almost thirty years ago in several genetic screens for mutant seedlings that display a photomorphogenic phenotype in darkness (Deng et al., 1992; Pepper et al., 1994; Chory et al., 1989; Wei Ning et al., 1994; Serino and Deng, 2003). Several of these *COP/DET/FUS* loci – all of which are highly conserved in the entire eukaryotic lineage including humans - were found to encode proteins which are key regulators of the ubiquitin-proteasome system, and are associated with three distinct protein complexes: The COP1-SUPPRESSOR OF PHYA-105 (SPA) complex, the COP9 signalosome (CSN) and the COP10-DET1-DDB1 (CDD) complex (Yi and Deng, 2005; Lau and Deng, 2012). The CDD complex forms a complex with DNA DAMAGE-BINDING PROTEIN 1 (DDB1), which is itself an important linker protein for CULLIN 4 (CUL)-based E3-ubiquitin ligases, thus linking the CDD complex to CUL-based ubiquitination processes, however ubiquitin ligase activity has not been proven yet (Yanagawa et al., 2004; Schroeder et al., 2002; Jackson and Xiong, 2009; Wertz et al., 2004); the CSN, which contains six of the COP/DET/FUS proteins, is a multimeric protease complex that regulates the activity of CULLIN-RING E3 ligases (CRLs) (Wei et al., 2008); and lastly, COP1 is a REALLY INTERESTING NEW GENE (RING)-based E3 ubiquitin ligase which has been established as one of the central repressors of photomorphogenesis in darkness (Lau and Deng, 2012). Even though COP1 was initially identified in a genetic screen for seedlings with photomorphogenic growth in darkness, later studies revealed that COP1 regulates almost all other light-controlled processes in Arabidopsis besides seedling photomorphogenesis, such as flowering, circadian rhythm, stomatal development, shade avoidance responses, plant defense, crosstalk between light and hormone signaling and cold acclimation (Liu et al., 2008b; Jang et al., 2008; Yu et al., 2008; Mao et al., 2005; Kang et al., 2009; Crocco et al., 2010; Jeong et al., 2010; Catalá et al., 2011; Lau and Deng, 2012). As an E3 ubiquitin ligase, COP1 forms a likely tetrameric complex with SPA proteins and mediates the final step of the poly-ubiquitination of a variety of photomorphogenesis-inducing transcription factors, thereby marking them for degradation via the 26S proteasome (Huang et al., 2014; Hoecker, 2017) (Figure 1.2). Generally speaking, the process of poly-ubiquitination can be subdivided into three distinct steps which are mediated by different enzymes: ubiquitin activation (E1), ubiquitin conjugation (E2) and ubiquitin ligation (E3), whereas the E3 ubiquitin ligase unit also mediates substrate specificity (Hoecker, 2005). As a RING-type E3-ubiquitin ligase, COP1 is one of more than 1300 E3 ligases in Arabidopsis (Smalle and Vierstra, 2004) and mediates the poly-ubiquitination of transcription factors such as regulators of seedling de-etiolation such as LONG HYPOCOTYL 5 (HY5), HY5 HOMOLOG (HYH) or LONG AFTER FAR-RED LIGHT 1 (LAF1); the regulator of shade avoidance responses LONG HYPOCOTYL IN FAR-RED (HFR1); CONSTANS (CO), which is a key activator of photoperiodic flowering; and the activators of anthocyanin biosynthesis PRODUCTION OF ANTHOCYANIN PIGMENT 1 (PAP1) and PAP2 (Osterlund et al., 2000; Holm et al., 2002; Seo et al., 2003b; Maier et al., 2013; Liu et al., 2008b; Jang et al., 2008; Rolauffs et al., 2012; Jang et al., 2005; Yang et al., 2005b) (Figure 1.2).

Additionally, several members of the B-box (BBX) family of transcription factors have also been found to be targets of COP1 (Vaishak et al., 2019). Through the degradation of these activators of light responses, COP1 activity has been linked with more than 68% of light-regulated genes in transcriptomic analysis of Arabidopsis seedlings (Paik et al., 2019). Interestingly, a non-canonical role of COP1 has been uncovered in the UV-B mediated regulation of photomorphogenic growth; whereas COP1 usually acts as a suppressor of photomorphogenesis, it promotes photomorphogenesis in UV-B light by stabilizing the transcription factor HY5 (Favory et al., 2009; Huang et al., 2013) (Figure 1.3).
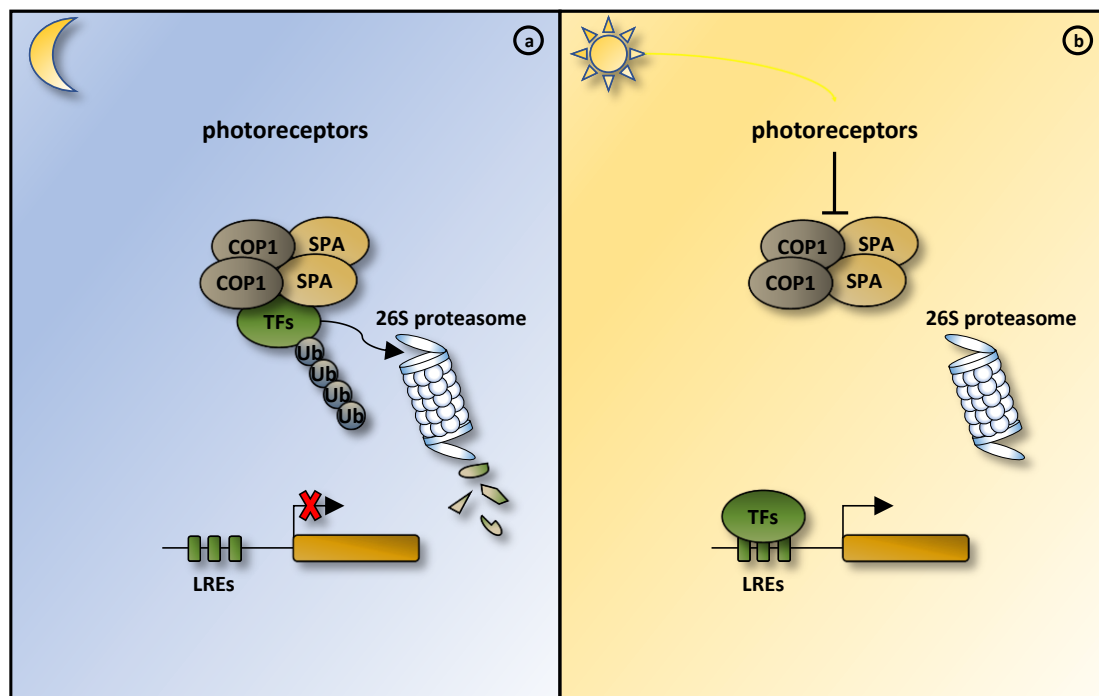
Figure 1.2: The COP1/SPA complex is a central repressor of photomorphogenesis in darkness.

The COP1/SPA complex, likely a tetrameric complex consisting of two COP1 proteins and two SPA proteins of any combination, acts as an E3 ubiquitin ligase to suppress light signals. **(a)** In the dark, the COP1/SPA complex is active and physically interacts with photomorphogenesis-promoting transcription factors. This interaction catalyzes the polyubiquitination of these transcription factors, which targets them for degradation via the 26S proteasome, thus suppressing photomorphogenesis. **(b)** Upon light-activation, photoreceptors suppress the activity of the COP1/SPA complex, preventing it from targeting photomorphogenesis-promoting transcription factors for degradation. Transcription factors accumulate and bind to Light-responsive Elements (LREs) in the genome to promote the expression of light-induced genes, thereby promoting photomorphogenic growth.

In Arabidopsis, COP1 interacts with SPA proteins (SPA1-4) to suppress photomorphogenesis in darkness. The *SPA1* locus was originally identified in a genetic screen for suppressors of the weak *phyA* mutation *phyA-105* (Hoecker et al., 1998). Later, *SPA1* was found to be part of a small gene family consisting of three additional *SPA*-like genes, *SPA1-related 2* (*SPA2*), *SPA1-related 3* (*SPA3*) and *SPA1-related 4* (*SPA4*) (Laubinger and Hoecker, 2003). Higher order *spa* mutants show various degrees of

photomorphogenic growth in darkness, but in contrast to *cop1* null mutants which arrest growth at the seedling stage, *spa* quadruple null mutants are viable plants that can complete their life cycle (Laubinger et al., 2004; McNellis et al., 1994a; Ordoñez-Herrera et al., 2015). The four *SPA* genes appear to have partially redundant, but also distinct functions, as evidenced by the fact that *spa* single mutants do not show any signs of de-etiolated growth in the dark (Menon et al., 2016; Laubinger et al., 2004; Hoecker et al., 1998). In the light, only the *spa2* mutant shows a normal response to light signals, while the *spa1*, *spa3* and *spa4* mutants exhibit exaggerated photomorphogenic growth (Hoecker et al., 1998; Laubinger and Hoecker, 2003; Laubinger et al., 2004; Fittinghoff et al., 2006). Phenotypic and molecular analysis of higher order *spa* mutants such as the *spa1 spa2* and *spa3 spa4* double mutants, as well as various *spa* triple mutants revealed that *SPA*-dependent suppression of photomorphogenesis in darkness is mediated redundantly by *SPA1* and *SPA2*, whereas *SPA3* and *SPA4* mainly regulate light-dependent vegetative growth in the adult stage (Laubinger and Hoecker, 2003; Laubinger et al., 2004). Furthermore, *SPA1* and *SPA4* were shown to be sufficient to promote shade-induced hypocotyl elongation in response to low R/FR, while *SPAs* were not required for the acceleration of flowering time in low R/FR (Rolauffs et al., 2012). Further functional divergence was found between *SPA1* and *SPA2*; while *SPA1* is involved in light-dependent processes like leaf expansion or photoperiodic flowering, *SPA2* seems to have no effect on light-dependent processes, which can be largely attributed to the fact that SPA2 proteins are being rapidly degraded upon light exposure (Fittinghoff et al., 2006; Laubinger et al., 2006; Balcerowicz et al., 2011; Chen et al., 2016).
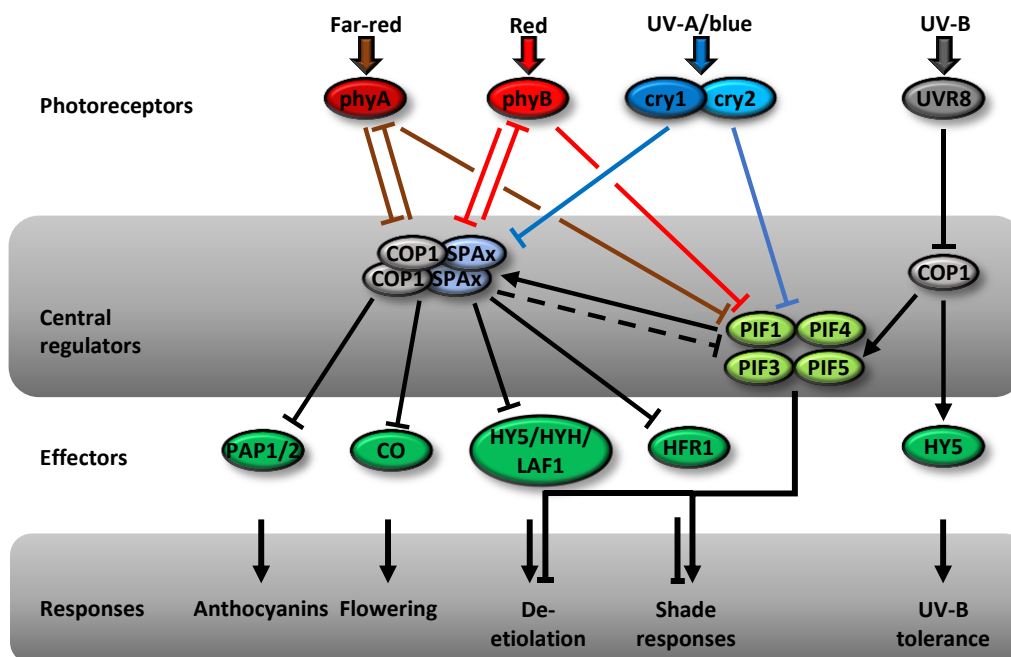
Figure 1.3: Light responses are controlled by a complex regulatory network.

A regulatory network, consisting of receptors, central regulators, and effectors, enables precise control of light-responses in Arabidopsis. First, light activates photoreceptors, which can detect light either via chromophores or via internal peptide structures. Different photoreceptors are activated by different wavelengths of light; phyA and phyB are mainly activated by FR and R, respectively, whereas cryptochromes are activated by B. UVR8 is the only known photoreceptor so far that is activated by UV-B light. Upon activation, photoreceptors suppress the activity of central regulators, mainly the COP1/SPA complex. Photoreceptors also suppress the activity of PIF transcription factors, which serve a dual function as central regulators and effectors. Effectors controlled by the COP1/SPA complex regulate a variety of responses to light signals, such as anthocyanin biosynthesis (mainly regulated by PAP1 and PAP2), photoperiodic flowering (mainly regulated by CO), seedling de-etiolation (mainly regulated by HY5, HYH, LAF1 and PIFs) and shade-avoidance responses (mainly regulated by HFR1 and PIFs). In UV-B light, COP1 has a unique function as a stabilizing factor of HY5 to promote UV-B tolerance responses. The COP1/SPA complex also affects PIFs and vice-versa, e.g. the SPA1-dependent phosphorylation of PIF1 or the COP1-dependent stabilization of PIF5 in UV-B light (REFs).

All four Arabidopsis SPA proteins physically interact with COP1 both *in vitro* and *in vivo*, where they likely form a tetrameric protein complex consisting of two COP1 and two SPA proteins (Hoecker and Quail, 2001; Zhu et al., 2008) (Figure 1.2). Interaction of COP1 and SPA1 is essential for light-dependent processes such as the regulation of HY5 activity (Saijo et al., 2003). Knock-out of all four *SPA* genes or mutations in *COP1* result in a constitutively photomorphogenic phenotype, further demonstrating that both *COP1* and *SPAs* are indispensable for the suppression of photomorphogenesis in darkness. In conclusion, the COP1/SPA complex is a central repressor of photomorphogenesis in darkness.

1.1.5 Crosstalk between COP1/SPA and PIF-dependent pathways

Both PIFs and the COP1/SPA complex are direct and indirect negative regulators of photomorphogenesis, respectively (Leivar and Quail, 2011; Hoecker, 2017). Initially, these pathways were believed to act in parallel to affect light-dependent processes. However, more recent studies have shown that the COP1/SPA complex and PIF proteins also work in synergy via multiple mechanisms (Martínez et al., 2018) (Figure 1.3). A report in 2014 demonstrated that HY5, itself a target of COP1/SPA, is stable in dark grown *cop1*, *spa* and *pif* mutant seedlings (Xu et al., 2014). The same report also demonstrated that the N-terminal domain of PIF1 physically interacts with both COP1 and SPA1 via their C-terminal domains *in vitro*, and that this interaction enhances ubiquitination activity of COP1 (Xu et al., 2014, 2015). Gene expression analysis also revealed that shade induced the convergence of the *cop1* and *pif1pif3pif4pif5* (*pifq*) transcriptome, and another report demonstrated that COP1/SPA indirectly promotes PIF3 stability by repressing the activity of a kinase of PIF3, BRASSINOSTEROID-INSENSITIVE 2 (BIN2), in the dark. Phosphorylation of PIF3 promotes its degradation via the 26S proteasome. COP1/SPA therefore promotes PIF3 activity by repressing PIF3 phosphorylation (Ling et al., 2017; Pacín et al., 2016). Lastly, COP1 has been shown to mediate the UV-B-induced repression of shade-avoidance responses; in the light, COP1 interacts with and stabilizes the positive regulator of shade-induced growth, PIF5; UV-B-activated UVR8 disrupts the COP1-dependent stabilization of PIF5, thereby repressing PIF5 activity in UV-B light in a COP1-dependent manner (Sharma et al., 2019). These results demonstrate that both central repressors of light signals, COP1/SPA and PIFs, act together in a synergistic fashion; it remains to be seen whether more mechanisms of COP1/SPA-PIF crosstalk can be elucidated.

1.1.6 Structural domains of COP1 and SPA proteins

Structural analysis of COP1 and SPA proteins reveals striking similarities between them; Arabidopsis COP1 is comprised of an N-terminal REALLY INTERESTING NEW GENE (RING)-finger domain followed by a Coiled-Coil (CC) domain and a C-terminal WD40-repeat domain (Yi and Deng, 2005). SPA proteins are structurally similar to COP1, especially towards the C-terminal end where all four SPA proteins show the highest level of conservation to COP1; accordingly, all four SPA proteins are also comprised of a C-terminal WD40-repeat domain and a central CC domain (Menon et al., 2016). However, SPA proteins do not contain RING motifs; instead, the large N-terminal extensions harbor vaguely conserved kinase-like domains that are similar to Serine/Threonine (Ser/Thr) kinases (Hoecker, 2017) (Figure 1.4).
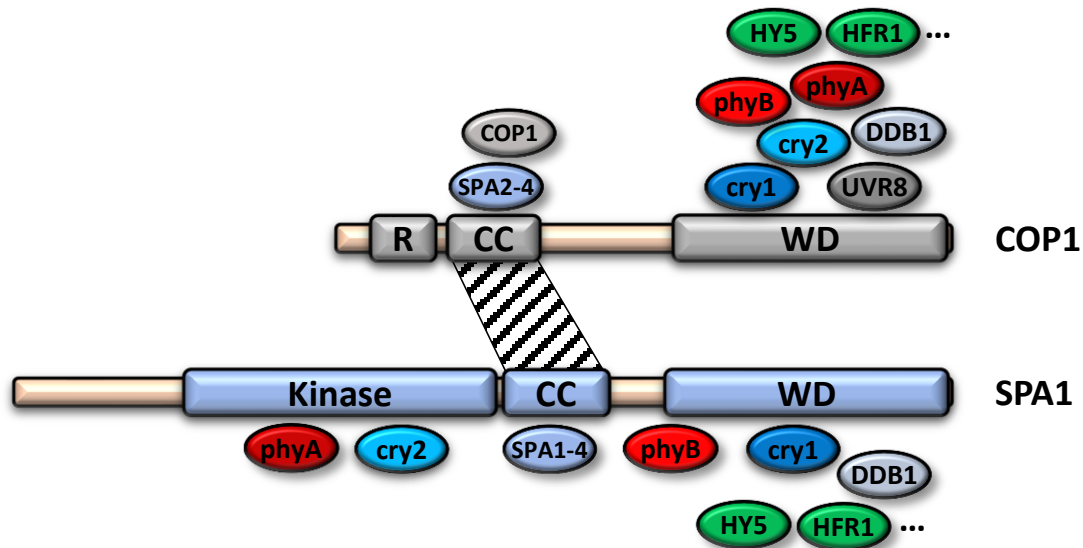
Figure 1.4: Arrangement of structural domains of Arabidopsis COP1 and SPA1.

COP1 possesses an N-terminal RING-finger domain (R) which confers E3 ubiquitin ligase activity. The N-terminal region of SPA1 contains a kinase domain which interacts with phyA, cry2 and PIF1. Both COP1 and SPA1 contain a central CC domain, which is required for assembly of the tetrameric COP1/SPA complex, as it is required for homo- and heterodimerization of COP1 and SPA proteins. The SPA1 CC domain is also required for phyB interaction (REF). The C-termini of both proteins contain a WD-repeat domain, which are required for the interactions of COP1 with downstream targets, the adapter protein DDB1 and the photoreceptors cry1 and phyB. The COP1 WD-repeat domain additionally interacts with phyA, cry2 and UVR8.

E3 ubiquitin ligase activity is conferred by the N-terminal RING-finger domain of COP1, which is a zinc binding domain that is characteristic for many E3 ubiquitin ligases (Deng et al., 1992; Yi and Deng, 2005; Deshaies and Joazeiro, 2009). Transgenic lines expressing COP1 proteins lacking a RING-finger domain display a seedling phenotype that is similar to transgenic plants expressing full-length COP1, which might indicate that the COP1 RING-finger domain is not necessary for COP1 functions in the light (Torii et al., 1998). In contrast, functionality of the large N-terminal extensions of SPA proteins is still not fully understood. Only a part of the N-terminal kinase-like domain is conserved among the four SPAs as well as among SPAs from early land plants such as *Physcomitrium patens* (Physcomitrium), while the remainder of the N-terminal region does not show high degrees of sequence conservation (Ranjan et al., 2014; Laubinger et al., 2004). Interestingly, the SPA1 N-terminus does not seem to be required for SPA1 function in seedlings, since transgenic seedlings expressing SPA1 lacking the N-terminal domain were able to complement a *spa* mutant phenotype in the light, but expression of a SPA1-CT509 construct lacking the kinase-like domain did not complement the early flowering phenotype of *spa* mutants in short day conditions (Fittinghoff et al., 2006; Yang and Wang, 2006; Zuo et al., 2011; Ponnu, 2020). B-activated cry2, but not cry1, physically interacts with the N-terminal domain of SPA1 both *in vitro* and *in vivo* (Lian et al., 2011; Liu et al., 2011; Holtkotte et al., 2016).

Similarly, phyA also physically interacts with the kinase-like domain of SPA1 in a light-dependent manner (Sheerin et al., 2015). The phyB-SPA1 interaction is mediated by both the SPA1 CC and WD-repeat domain, and was originally reported to be light-independent, but later studies showed that this interaction is light-dependent as well (Zheng et al., 2013; Sheerin et al., 2015). The SPA1 N-terminus also affects SPA1 stability and contributes to COP1/SPA complex formation, as SPA1 proteins lacking the N-terminal region are more stable when expressed in Arabidopsis seedlings and show reduced affinity to COP1 both *in vitro* and *in vivo* (Fittinghoff et al., 2006; Yang and Wang, 2006; Holtkotte et al., 2016). Lastly, while the kinase-like domains of SPA proteins have long been believed to not confer any kinase activity, a recent report has found that SPA1 acts as a Ser/Thr kinase to phosphorylate PIF1 both *in vitro* and *in vivo* (Paik et al., 2019). This provides a first piece of evidence for COP1-independent function of SPAs, as well as a novel mechanism of SPA1 signaling conferred by its N-terminal kinase-like domain.

The CC domains of both COP1 and SPAs mediate formation of the COP1/SPA complex. Biochemical analysis has demonstrated that the CC domains of COP1 and SPA proteins are essential for both homo- and heterodimerization (Torii et al., 1998; Yang and Wang, 2006; Hoecker and Quail, 2001; Laubinger and Hoecker, 2003; Saijo et al., 2003; Zhu et al., 2008). Consistent with this, COP1 and SPA proteins likely form a tetrameric complex consisting of two COP1 and two SPA proteins of any possible SPA combination according to gel filtration studies (Zhu et al., 2008). Formation of the tetrameric COP1/SPA complex via its CC domains is essential for COP1/SPA function, as evidenced by the fact that transgenic plants which overexpressed COP1 lacking its CC domain retained a hypocotyl length which was similar to the wild type, while plants overexpressing full length COP1 showed significantly longer hypocotyls, and plants overexpressing SPA1 lacking its CC domain did not rescue the *spa1* mutant phenotype in seedlings (Torii et al., 1998; Fittinghoff et al., 2006; Yang and Wang, 2006). Even though the tetrameric structure of the COP1/SPA complex has been known for more than a decade, the question of why this structure is essential for COP1/SPA function still remains to be answered.

Several *cop1* mutants expressing truncated COP1 proteins that lack the WD40-repeat domain display strongly de-etiolated seedling phenotypes and severe dwarfism, suggesting that the WD40-repeat domain is essential for COP1 function (McNellis et al., 1994a; Stacey et al., 2000). COP1 binding to its substrates such as HY5, HYH, PAP1, PAP2, members of the BBX family and others, is mediated by the COP1 WD-repeat domain (Holm et al., 2001, 2002; Jang et al., 2005; Maier et al., 2013). The binding motif of COP1 substrates was first identified in biochemical studies involving HY5 as well as the regulators of salt stress responses SALT TOLERANCE (STO) and SALT TOLERANCE HOMOLOG (STH); it is comprised of a canonical Valin-Proline (VP) core sequence, followed by one of the two negatively charged amino acids, aspartic acid or glutamic acid (E/D), a hydrophobic residue and a glycine (G)

residue (V-P-E/D-ɸ-G; ɸ = hydrophobic residue), in conjunction with an upstream stretch of 4-5 negatively charged amino acids (Holm et al., 2001). Many other COP1 substrates have later been shown to interact with COP1 via a VP motif as well (Jang et al., 2005; Datta et al., 2008; Maier et al., 2013). Interaction of substrates with the COP1 WD40-repeat domain enables substrate polyubiquitination and subsequent degradation via the 26S proteasome. Besides substrate recognition, the COP1 WD-repeat domain also binds DDB1 which acts as a linker protein for the COP1/SPA complex and the CUL4 complex (Chen et al., 2010). Many CUL4-based E3 ubiquitin ligases bind WD-domain-containing proteins, which function as substrate recognition modules for the E3 ligase complex, also known as DDB1-CUL4-associated factors (DCAFs) (Jackson and Xiong, 2009; Fonseca and Rubio, 2019; Tevatia and Oyler, 2018). The COP1 WD-repeat domain contains a conserved WDxR motif which is essential for DDB1 binding (Chen et al., 2010). More recently, however, the X-ray structure of both human and Arabidopsis COP1 WD repeat domains has been solved and demonstrated that the WDxR motif is buried in the WD-repeat structures of COP1, suggesting that the WDxR motif might be required for the general structural integrity of the WD-repeat domain, rather than for DDB1 binding (Uljon et al., 2016; Lau et al., 2019). Both human and Arabidopsis COP1 form structurally similar seven-bladed β-propellers with an unstructured loop at the bottom face of the propeller. Interestingly, both WD-repeat domains interact with TRIBBLES 1 (TRIB1), a substrate of human COP1, via the TRIB1 VP-motif, providing evidence that the mode of COP1 interaction with its substrates is highly conserved throughout eucaryotes. Additionally, TRIB1-binding residues in the Arabidopsis COP1 WD-repeat domain contain COP1W467, which has been previously reported as essential for HY5 binding (Holm et al., 2001). Finally, the COP1 WD-repeat domain also interacts with several light-activated photoreceptors such as cry1, cry2, phytochromes and UVR8 (Seo et al., 2004; Wang et al., 2001; Yang et al., 2001; Holtkotte et al., 2017; Lau et al., 2019; Ponnu et al., 2019). Structural and biochemical studies revealed that both cryptochromes and UVR8 interact with the COP1 WD-repeat domain via their VP motifs as well, providing a mechanism for competitive binding between photoreceptors and substrates to the COP1 VP-binding pocket at the top face of the WD-repeat donut structure (Ponnu et al., 2019; Lau et al., 2019). Taken together, the COP1 WD-repeat domain is an integral domain for COP1 function which provides a surface for a plethora of COP1 binding partners like photoreceptors, DDB1 and COP1 substrates.

The WD-repeat domains of all four SPA proteins share high sequence similarity to COP1-WD (Hoecker et al., 1999; Laubinger and Hoecker, 2003). In contrast to COP1, the X-ray structure of the SPA1 WD-repeat domain has not been solved yet, but it is assumed to form a seven-bladed β-propeller as well, estimated by sequence identity (Hoecker, 2017). The SPA1 WD-repeat domain is indispensable for SPA1 function, as transgenic *spa1* mutant seedlings expressing SPA1 proteins which lack the WD-repeat domain do not rescue the *spa1* mutant phenotype (Yang and Wang, 2006). Many proteins that

interact with the COP1 WD-repeat domain also interact with the SPA1 WD-repeat domain, likely in a similar fashion. The SPA1 WD-repeat domain has been demonstrated to be essential for interaction with HY5, HFR1, cry1, phyB and DDB1, the latter of which mediates the association of COP1/SPA with the CUL4-based E3 ligase complex (Saijo et al., 2003; Yang et al., 2005a; Lian et al., 2011; Lee et al., 2008; Zhang et al., 2008; Chen et al., 2010). Although both the COP1 and SPA1 WD-repeat domain are able to physically interact with DDB1, it is conceivable that both are required for CUL4-DDB1$^{COP1/SPA}$ complex formation. Notably, SPA proteins are necessary for the B-dependent interaction of COP1 and CRY1 *in vivo*, indicating that SPA proteins might act as adapter proteins to mediate interactions between COP1 and photoreceptors (Holtkotte et al., 2017). phyA- and phyB-SPA interactions also disturb the COP1-SPA interaction in a light-dependent manner, suggesting a mechanism of light-dependent disruption of the COP1/SPA complex by phytochromes (Sheerin et al., 2015). Taken together, even though the COP1 and SPA WD-repeat domains are structurally similar, several notable differences in their functions have been observed.

1.1.7 COP1 and SPA suppress photomorphogenesis as part of a CUL4-based E3 ubiquitin ligase

Intriguingly, all nine *COP/DET/FUS* genes that were cloned initially, namely *COP1*, *DET1*, *COP10* and the *CSN* subunits *1*, *2*, *3*, *4*, *7* and *8*, are either directly or indirectly involved in the activity of CULLIN-RING E3 ligases (CRL4s). The CSN is a protease consisting of eight subunits (CSN1-8) and is highly conserved among eukaryotes (Wei et al., 2008). Mechanistically, CSN mediates the removal of Nedd8/Rub1 modifications (deneddylation) from cullins within CRL ligase complexes (Cope et al., 2002; Lyapina et al., 2001; Schwechheimer et al., 2001; Wei et al., 2008). Recent studies also suggest that CSN regulates DNA methylation processes in Arabidopsis (Fonseca and Rubio, 2019; Tuller et al., 2019). The CDD complex, consisting of the two members of the COP/DET/FUS family COP10 and DET1 as well as DDB1, associates with CUL4 and RBX1 to form an E3 ligase in which COP10 acts as a small ubiquitin variant protein to enhance the activity of the E2 subunit (Schroeder et al., 2002; Yanagawa et al., 2004; Biedermann and Hellmann, 2011; Chen et al., 2006; Nixdorf and Hoecker, 2010). The 16 kDa protein DET1-, DDB1-ASSOCIATED (DDA1) also interacts with members of the CDD complex to form a heterotetrameric complex (CDDD) that associates with CUL4 *in vivo* (Pick et al., 2007; Fonseca and Rubio, 2019; Irigoyen et al., 2014). DDA1 acts as a substrate recognition module to interact with Abscisic Acid (ABA) receptors PYRABACTIN RESISTANCE-LIKE 4 (PYL4), PYL5 and PYL8 to mediate ubiquitination and subsequent degradation of PYLs (Lim et al., 2013; Irigoyen et al., 2014).

Arabidopsis COP1/SPA associates with DDB1 as part of a CRL4 complex (Fonseca and Rubio, 2019). Arabidopsis CUL4 is a member of the cullin family (Sarikas et al., 2011). It acts as a scaffolding protein for CRL4 complexes and is essential for a variety of developmental processes, evidenced by the

fact that *cul4* null mutations lead to embryo lethality. The CRL4 complex is formed by interaction of the CUL4 N-terminus with DDB1 and the C-terminus with the E2 subunit RBX1 (Bernhardt et al., 2006; Biedermann and Hellmann, 2011). The interaction of CRL4s with WD40-repeat containing proteins is conserved throughout eucaryotes (Angers et al., 2006; He et al., 2006). Interestingly, as is the case for COP1/SPA, the majority of these DDB1-CUL4-Associated Factors (DCAFs) contain WD motifs and mainly act as substrate recognition modules for CRL4 (van Nocker and Ludwig, 2003; Higa and Zhang, 2007; Zimmerman et al., 2010; Migliori et al., 2012; Fonseca and Rubio, 2019). COP1/SPA complexes associate with CUL4-DDB1 both *in vitro* and *in vivo* and synergistically repress photomorphogenesis in darkness (Lee et al., 2008; Chen et al., 2010) (Figure 1.5). In summary, the COP1/SPA complex acts as a substrate recognition module for the CRL4, forming a higher order CUL-DDB1$^{COP1/SPA}$ complex to regulate photomorphogenic growth (Chen et al., 2006, 2010; Fonseca and Rubio, 2019).

1.1.8 Activity of the COP1/SPA complex is suppressed by four distinct mechanisms

To accurately perceive and transduce light signals downstream of photoreceptors, tight regulation of the COP1/SPA complex is required. In Arabidopsis, this has led to the emergence of four distinct mechanisms of inactivation of the COP1/SPA complex that have been uncovered so far (Figure 1.5).
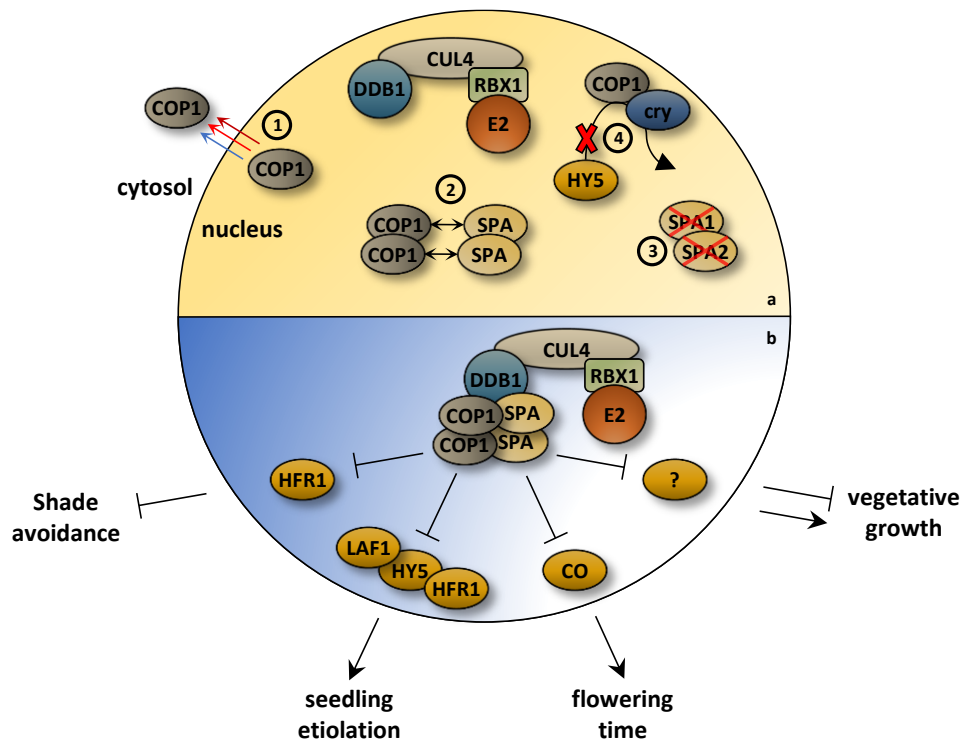
Figure 1.5: Mechanisms of inactivation of the CUL4-DDB1$^{COP1/SPA}$ complex.

(a) In the light, photoreceptor action inactivates the COP1/SPA complex via four distinct mechanisms: (1) Light causes translocation of COP1 from the nucleus to the cytosol, thereby physically separating it from its targets; (2) interaction of photoreceptors with COP1 disrupts COP1/SPA interaction, which is required for COP1 activity; (3) SPA proteins, especially SPA2 and to a lesser extend SPA1, are degraded in a light-dependent manner; (4) some light-activated photoreceptors (cry2, UVR8) compete for COP1 binding with COP1 substrates to the binding pocket, preventing physical interaction and subsequent polyubiquitination of substrates. **(b)** In darkness, the COP1/SPA complex acts as a substrate recognition unit for Cullin4-Related Ligases (CRLs) to catalyze the polyubiquitination of photomorphogenesis-promoting transcription factors like HFR1, LAF1, HY5 and CO. COP1 and SPA proteins bind to the protein DDB1, which acts as a bridging protein between COP1/SPA and CUL4. Physical interaction of the COP1/SPA complex catalyzes the transfer of ubiquitin from the ubiquitin conjugating E2 subunit, which also binds to CUL4 via the bridging protein RBX1. Mutations in the *COP1* or *SPA* genes affect many light-regulated phenotypes such as shade avoidance, seedling etiolation, photoperiodic flowering, and vegetative growth.

First, light causes the exclusion of COP1 protein from the nucleus, thereby prohibiting interaction with its nuclear localized substrates (Von Arnim and Deng, 1994; Subramanian et al., 2004). This process of nucleocytoplasmic partitioning is reversible, as nuclear abundance of COP1 increases in plants that have been exposed to shade when compared to non-shaded plants (Pacín et al., 2013). Initially, nuclear exclusion of COP1 upon light exposure was believed to be a slow process of 12-14 hours based on studies involving β-Glucoronidase (GUS)-COP1 fusion proteins (Von Arnim and Deng, 1994). But later studies revealed that COP1 fused to Yellow Fluorescent Proteins (YFP) relocated to the cytosol within 2-3 hours, suggesting that nuclear exclusion contributes to the quick stabilization of

COP1/SPA targets upon light exposure (Pacín et al., 2014; Moriconi et al., 2018). Nucleocytoplasmic partitioning of COP1 is dependent on two key motifs in the COP1 peptide sequence: first, a bipartite Nuclear Localization Signal (NLS) which is situated in the region between the CC and the WD-repeat domain, and second a Cytosolic Localization Signal (CLS) in the CC domain of COP1 (Stacey et al., 1999; Subramanian et al., 2004). Phytochromes and cryptochromes have both been shown to facilitate nuclear exclusion of COP1, albeit by mechanisms that are so far not fully understood (Gu et al., 2012; Osterlund and Deng, 1998). Both UV-B light and increased ambient temperature attenuate and counteract COP1 nuclear exclusion, but interestingly, the responses are very different; while temperature-dependent nuclear COP1 retention leads to increased COP1/SPA activity and amplified elongation growth, UV-B dependent nuclear retention of COP1 leads to the stabilization of HY5 and repression of elongation growth in response to UV-B (Oravecz et al., 2006; Park et al., 2017). It is unclear whether UV-B affects nucleocytoplasmic partitioning of COP1 directly. (Oravecz et al., 2006).

Second, SPA proteins, which are essential for COP1 activity in Arabidopsis, are degraded in the light. Rapid light-induced destabilization of SPA2, and to a lesser extend SPA1, via the 26S proteasome decreases COP1/SPA activity in the light and stabilizes transcription factors such as HY5 (Balcerowicz et al., 2011; Chen et al., 2015). SPA2 degradation is phyA-dependent and conferred by the SPA2 kinase-like domain (Chen et al., 2016). Intriguingly, SPA2 degradation is COP1 dependent, which raised the hypothesis that COP1 regulates its own activity by targeting subunits of the COP1/SPA complex for degradation, but so far, no evidence of direct SPA2 polyubiquitination by COP1 has been found (Zhu et al., 2008).

Third, The COP1-SPA interaction is disrupted in the light. In B, the cry1 C-terminal (CCT) domain interacts with the SPA1 WD-repeat domain (Wang et al., 2014; Liu et al., 2011; Lian et al., 2011; Fankhauser and Ulm, 2011). This interaction reduces SPA1 binding affinity to COP1 which reduces COP1/SPA activity and effectively stabilizes HY5 (Liu et al., 2011; Lian et al., 2011). In contrast, the N-terminal PHR domain of B-activated cry2 has been shown to interact with the SPA1 N-terminus, but this seems to strengthen the COP1-SPA interaction rather than causing COP1-SPA dissociation (Zuo et al., 2011; Holtkotte et al., 2017). In a similar fashion to cry1, light-activated phyA and phyB also interact with SPA proteins which disrupts COP1-SPA interaction and causes reorganization of the COP1/SPA complex and negatively affects its activity (Lu et al., 2015; Sheerin et al., 2015; Seo et al., 2004; Viczián et al., 2012).

Lastly, two recent major reports have demonstrated that light dependent inactivation of COP1/SPA is also facilitated by VP-mediated competition of COP1 binding between photoreceptors and COP1 targets (Lau et al., 2019; Ponnu et al., 2019; Ponnu, 2020). Competition between cryptochromes and HY5 for interaction with the COP1 VP-binding pocket has previously been

hypothesized (Müller and Bouly, 2015). The importance of cry VP motifs in the cry-COP1 interaction was then shown via several methods including co-crystallization of the COP1 WD-repeat domain with peptides containing cry VP motifs (Lau et al., 2019; Ponnu et al., 2019). *cry1 cry2* double mutants expressing cry2 with a mutated VP motif (VP to AA) are unable to complement *cry* mutant phenotypes, further solidifying the importance of the cry2 VP motif (Ponnu et al., 2019). B-activated CRY2 was then shown to significantly reduce the interaction of COP1 and PAP2 both in yeast-2-hybrid assays and in Foerster Resonance Energy Transfer-Fluorescence Lifetime Imaging (FRET-FLIM) experiments, while cry2 harboring VP to AA mutations failed to reduce COP1-PAP2 interaction, indicating that B-activated CRY2 displaces PAP2 from COP1 by competitive binding for the COP1 VP-binding pocket (Ponnu et al., 2019). A similar mechanism was reported in the same year for UVR8; which was shown to reduce the interaction of COP1 with HY5 in a VP-dependent manner, indicating that competitive binding of UVR8 promotes HY5 stability by preventing interaction of COP1 with its substrate (Lau et al., 2019). This novel mechanism raises intriguing questions regarding the co-evolution of binding motifs in COP1/SPA substrates and photoreceptors; however, the exact mechanistic process of this mode of COP1/SPA inactivation has yet to be deciphered.

1.1.9 Activity of light-regulated transcription factors causes vast genetic reprogramming of the Arabidopsis transcriptome

The tight regulation of various transcription factors by light leads to large-scale differential expression of genes between light-grown, and dark-grown Arabidopsis seedlings. Early microarray studies have shown that more than 20% of Arabidopsis genes are differentially expressed between light- and dark-grown seedlings (Ma et al., 2001; Tepperman et al., 2001; Jiao et al., 2005). Transcriptomic analysis on *pif* mutants, for example, has shown that the majority (80%) of genes which are differentially expressed in *pif1 pif3 pif4 pif5* (*pifq*) mutants grown in darkness overlaps with differentially expressed genes in light-grown seedlings (Shin et al., 2009; Lorrain et al., 2009; Leivar et al., 2009). Chromatin Immunoprecipitation (ChIP)-sequencing experiments combined with RNA-sequencing studies of dark- and light grown *pif* single and triple mutant as well as the *pifq* mutant revealed that 2,025 genes are regulated by the PIF quartet and described a complex interplay of differential contributions of individual PIFs to the PIF-regulated transcriptome (Zhang et al., 2013). Similarly, COP1 indirectly controls the expression of numerous light-regulated genes via the targeted destabilization of transcription factors. Early transcriptomic analysis of *cop1* mutants using microarrays showed that a large proportion of light controlled genes (up to 1321 out of 6126; 21%) is differentially expressed between dark-grown wild type and *cop1* mutant seedlings (Ma et al., 2002). Similarly, RNA-sequencing analysis of *spa* quadruple mutants showed that 7261 genes were differentially regulated

by the four SPAs, however the contribution of individual SPAs similar to PIFs has not been investigated yet (Pham et al., 2020). Intriguingly, the COP1- and SPA1-4-differentially regulated transcriptome in dark-grown seedlings strongly overlaps (Pham et al., 2020). Taken together, light regulates the expression of a large number of genes either directly or indirectly via the control of transcription factors by photoreceptors and a set of CUL4-based E3 ligases.

1.2 PHOTOBODY FORMATION

Upon light activation, many photoreceptors such as phytochromes, cryptochromes and UVR8 are rapidly localized to subnuclear foci, also called nuclear bodies (NBs) (Van Buskirk et al., 2012). NBs are distinct subnuclear domains that are hypothesized to provide microenvironments for molecular processes such as gene expression, DNA replication or protein dynamics (Shaw and Brown, 2004; Spector, 2006). Photoreceptor containing NBs, or photobodies, are a distinct type of NBs whose formation, function and size are regulated by light (Chen and Chory, 2011).

Photobody formation is best characterized in phytochrome signaling (Van Buskirk et al., 2012). Localization of light-activated phytochromes into subnuclear photobodies was first reported for phyB-GFP fusion proteins, but was described for all remaining phytochromes, including phyA, shortly after (Yamaguchi et al., 1999; Kircher et al., 1999, 2002; Kim et al., 2000). Steady-state dynamics of R-induced phyB photobody formation is dependent on the Pr/Pfr ratio of phyB (Chen et al., 2003). Differential dynamics of photobody formation of various phytochromes was reported in transgenic plants expressing GFP-fusion constructs of phyA-E (Kircher et al., 2002); formation of phyA-containing photobodies occurs rapidly and can be observed within 2-3 minutes after light exposure, reaching its maximum after 10 minutes followed by a rapid decline; formation of phyB-E-containing photobodies is considerably slower and reaches its maximum after 6-8 hours (Kircher et al., 2002). B-activated cry2 also translocates into nuclear and cytosolic photobodies, and cry1 has been observed in COP1 and SPA containing nuclear bodies, suggesting that cry1 could likely localize to phy-containing photobodies as well (Yu et al., 2009; Zuo et al., 2012; Wang et al., 2001; Gu et al., 2012; Lian et al., 2011; Liu et al., 2011; Zuo et al., 2011).

COP1 speckle formation is also well characterized. COP1 colocalizes into nuclear speckles with various photoreceptors as well as COP1 targets like HY5, HYH, LAF1 and HFR1 (Ang et al., 1998; Holm et al., 2002; Seo et al., 2003b, 2004; Duek and Fankhauser, 2003; Duek et al., 2004; Jang et al., 2005; Ponnu et al., 2019). Consistent with previously described mechanisms of nucleocytoplasmic partitioning, YFP-COP1 speckles are not observed in light-grown seedlings, and the COP1 CC domain is required for COP1 localization into speckles (Oravecz et al., 2006; Stacey and Von Arnim, 1999). SPA1

also colocalizes into nuclear speckles with COP1 and the requirement of the COP1 CC domain for COP1 speckle formation suggests that SPA proteins might be required for COP1 to localize into speckles (Van Buskirk et al., 2012; Stacey et al., 1999; Menon et al., 2016).

Although the exact function of photobodies has not been fully understood, several hypotheses have been proposed: First, photobodies might act as storage depots for photoreceptors to regulate the amount of active phytochrome in the nucleoplasm (Matsushita et al., 2003; Palágyi et al., 2010). Second, photobodies might be required for key steps of the regulation of light-regulated genes by transcription factors (Van Buskirk et al., 2012). And third, since the COP1/SPA complex acts as an E3 ubiquitin ligase, it is possible that photobodies are the sites of light-dependent protein degradation (Al-Sady et al., 2006; Van Buskirk et al., 2012).

2 AIMS OF THIS THESIS

The COP1/SPA complex is a central suppressor of photomorphogenesis in darkness. For the past two decades, components of the COP1/SPA complex have been extensively studied, but the detailed mechanisms of especially SPA proteins have not been fully understood. Genetic and biochemical analysis shows that SPA proteins enhance COP1 activity, but the mechanistic basis is still largely unclear. Hence, this thesis aimed to study the mechanisms of the regulation of COP1 activity by SPA proteins by aiming to investigate the following aspects of COP1/SPA function:

(1) **Structural and functional divergence of the COP1 and SPA1 WD-repeat domain.** The COP1 C-terminal region harbors a WD-repeat domain which forms a seven-bladed b-propeller structure. Based on sequence homology studies, the C-terminal end of SPA1 likely forms a similar structure. Since both COP1 and proteins are required for the suppression of photomorphogenesis in darkness, it is possible that the COP1 and SPA1 WD-repeat domains exert different functions *in planta*. To this end, the WD-repeat domains of both COP1 and SPA1 were investigated for structural and functional differences.

(2) **SPA-dependent nuclear exclusion of COP1.** COP1 activity is suppressed in the light via several mechanisms. Among others, COP1 is exported from the nucleus upon light exposure, thereby physically separating it from its nuclear localized substrates. However, the role of SPA proteins in the light-induced nucleocytoplasmic partitioning of COP1 is currently unknown. To this end, a *35S::YFP-COP1* transgene was crossed into the *spa1 spa2 spa3 spa4* quadruple mutant background (crosses performed by Dr. Martin Balcerowicz in previous studies) to investigate the role of SPA proteins in the nuclear exclusion of YFP-COP1.

3 RESULTS

3.1 STRUCTURAL AND FUNCTIONAL DIFFERENCES BETWEEN THE COP1 AND SPA1 WD-REPEAT DOMAINS

3.1.1 A homology model of the SPA1 WD40-repeat domain suggests structural variations to COP1

Multiple sequence alignment of the COP1 and SPA1-SPA4 amino acid sequences reveals high sequence identity among these proteins in the C-terminal region, with SPA1 having the highest similarity to COP1 in that region among all four SPA proteins (45% sequence identity, Supplemental Figure S 1). The COP1 C-terminal region contains seven WD40 repeats and has been shown to form a seven-bladed β-propeller structure(Uljon et al., 2016; Lau et al., 2019). Due to its high sequence similarity, the SPA1 C-terminal region may form a very similar structure.

By aligning the amino acid sequence of the Arabidopsis COP1 WD40 domain to the corresponding region in Arabidopsis SPA1, two major differences were identified: one insertion/deletion of 8 amino acids starting at position 926 of SPA1, and one insertion/deletion of 3 amino acids starting at position 988 of SPA1, henceforth called indel1 and indel2, respectively (Figure 3.1a). Based on sequence homology to COP1, the two indels are not positioned within the highly conserved β-sheets that form the propeller structure, but rather in the interconnecting loops in-between the conserved sheets. Specifically, indel1 is situated in the predicted loop connecting β-sheets 5C and 5D, while indel2 is in the predicted loop connecting 6D to 7A according to the naming scheme by Uljon et al., 2016. Interestingly, the region identified as indel2 has previously been described as an enriched sequence of acidic amino acids, and the equivalent region in human COP1 on the top face of the propeller is partially disordered (Uljon et al., 2016). The corresponding region (indel2) of SPA1 is more similar to *Homo sapiens* COP1 than Arabidopsis COP1. Thus, this region may also form a more disordered structure in SPA1 like human COP1 (Figure 3.1a).
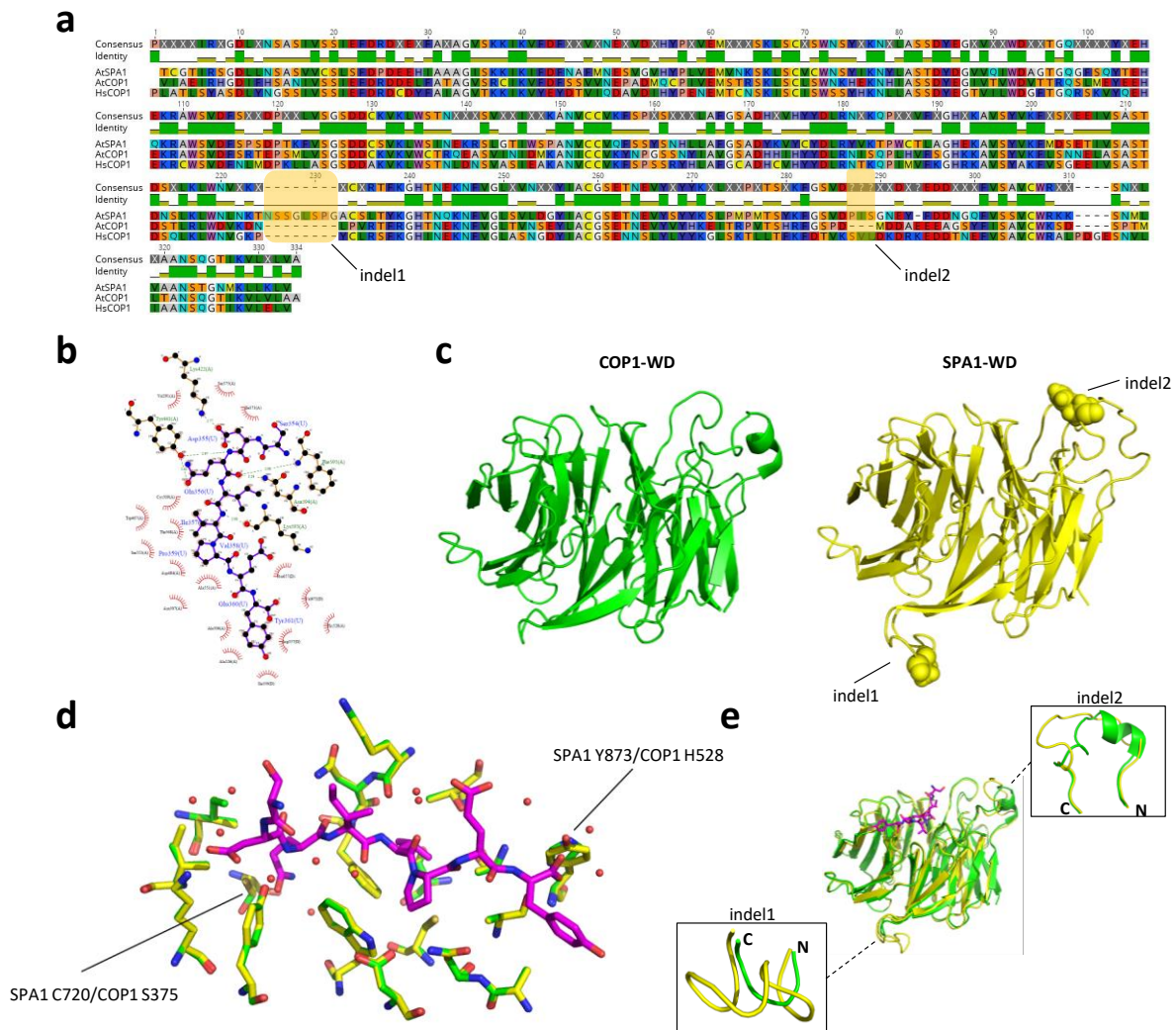
Figure 3.1: Theoretical homology model of the SPA WD-repeat domain.

(a) Amino acid sequence alignment of WD40-repeat domains of Arabidopsis COP1, Arabidopsis SPA1 and *Homo sapiens* COP1. Ranges of AtSPA1 (703-1029), AtCOP1 (358-675), and HsCOP1 (407-731) were aligned with ClustalW using standard settings. Two major polymorphisms were identified in the SPA1 sequence (indel1 and indel2, respectively), which are highlighted in the alignment. **(b)** Residues predicted to be involved in binding to Trib1 peptide. Ligplot (https://www.ebi.ac.uk/thornton-srv/software/LIGPLOT/) was utilized to predict residues beyond the ones previously identified. Blue stick model represents Trib1 peptide, orange stick molecules represent COP1 residues that form salt bridges with Trib1 peptide, and red „radial" molecules represent COP1 residues that make hydrophobic interactions with Trib1 peptide. **(c)** Table listing COP1 residues that contribute to the interaction with Trib1 peptide, with the equivalent residues in the SPA1 WD40-repeat domain sequence. Non-conserved residues are marked in grey. **(d)** Stick model representation of Trib1 peptide (magenta) interaction with both COP1 (green) and SPA1 (yellow) WD40-repeat domains (superimposed). Two mismatching residues (SPA1 Y873/COP1 H528 and SPA1 720/COP1 S375) are marked with arrows. **(e)** Structural model of PDB accession 5IGO, chain A (green), and homology model of SPA1 WD40 repeats (yellow). Two major polymorphisms identified in the SPA1 sequence are highlighted as spheres. Homology model was generated with I-Tasser (https://zhanglab.ccmb.med.umich.edu/I-TASSER/) based on 5IGO, chain A. (f) Superposition of PDB accession 5IGO, chain A (green) and homology model of SPA1 WD repeats (yellow). Polymorphisms in the SPA1 amino acid sequence result in structural differences in the homology model (highlighted in

boxes). Trib1 peptide (PDB accession 5IGO, chain U) binding site is located in close proximity to indel2. Data for **b-e** was generated in collaboration with Dr. Soshichiro Nagano, University of Giessen.

Several proteins that bind COP1 contain a characteristic valine-proline motif, often preceded by multiple negatively charged amino acids, which has been shown to be indispensable for binding to the COP1 WD40 domain (Holm et al., 2001; Uljon et al., 2016; Lau et al., 2019). Conversely, a binding pocket for the consensus VP motif has been described previously (Figure 3.1b; Uljon *et al.*, 2016). In the structure of Arabidopsis COP1 (5IGO), the residues which interact with the Trib1 peptides were identified by using the software LigPlot+ (2.1) (data generated in collaboration with Dr. Soshichiro Nagano, University of Giessen). The default parameters were used; the maximum distances for hydrogen-acceptor and donor-acceptor pairs were 2.70 Å and 3.35 Å, respectively, whereas the maximum and the minimum distances for the detection of hydrophobic contacts were 3.90 Å and 2.09 Å, respectively (Table 3.1, Figure 3.1d) (data generated in collaboration with Dr. Soshichiro Nagano, University of Giessen). Out of these, four amino acids were non-conserved in the SPA1 sequence, with SPA1 V718, C720, I736 and Y873 replacing COP1 I373, S375, V391 and H528, respectively. Notably, COP1 H528 has previously been described to form a salt bridge to HY5-E45 in co-crystals (Lau et al., 2019). It is possible that this salt bridge cannot be formed with the non-basic tyrosine contained in SPA1. These substitutions could result in differential binding properties between the COP1 and SPA1 WD-repeat domains.

Table 3.1: Amino acids which likely contribute to COP1-target binding.

Structural data from a COP1-Trib1 co-crystal was utilized to determine additional residues of the COP1 WD-repeat domain which likely contribute to COP1-Trib1 binding using the software LigPlot (https://www.ebi.ac.uk/thornton-srv/software/LIGPLOT/). Table shows a comprehensive list of all identified residues, the type of bond, the publication in which the residue was identified previously (if applicable) and the equivalent residue in SPA1. Non-conserved residues are marked in grey (data generated in collaboration with Dr. Soshichiro Nagano, University of Giessen).

COP1 residue	type of bond	previously described	equivalent SPA1 residue
I373	hydrophobic		V718
S375	hydrophobic	Uljon et al., 2016	C720
V391	hydrophobic		I736
K422	ionic	Lau et al., 2019,	K767
Y441	ionic	Lau et al., 2019	Y786
W467	hydrophobic	Uljon et al., 2016, Lau et al., 2019	W812
D484	hydrophobic		D892
A506	hydrophobic		A851
N507	hydrophobic		N582
C509	hydrophobic	Uljon et al., 2016	C854
A526	hydrophobic		A871
H528	hydrophobic	Lau et al., 2019	Y873
A551	hydrophobic		A896
S553	hydrophobic		S898
T568	hydrophobic	Uljon et al., 2016	T913
K593	ionic		K946
N594	ionic		N947
F595	ionic	Uljon et al., 2016, Lau et al., 2019	F948

To further analyze structural differences between the COP1 and SPA1 WD-repeat domains, a theoretical model of the SPA1 WD-repeat domain based on the available COP1 structure was generated using the software ITasser (Figure 3.1c, data generated in collaboration with Dr. Soshichiro Nagano, University of Giessen). As expected, the SPA1 WD-repeat sequence forms a donut-shaped seven-bladed propeller similar to COP1 in this homology model. As in COP1, the N-terminal β-strand of SPA1 is the last sheet of the seventh blade (7D), while the C-terminal strand is the second to last sheet of the seventh blade (7C). However, the above described larger insertions/deletions also result in structural differences between COP1 and SPA1 in this model: Indel1 is positioned at the bottom face of the donut and forms a slightly different, similarly disordered loop between sheets 5C and 5D. Indel2, however, is positioned at the top face of the propeller and is slightly more extensive than the homologous COP1 sequence (Figure 3.1e, data generated in collaboration with Dr. Soshichiro Nagano, University of Giessen). Interestingly, this loop in the SPA1 model is more similar to the human COP1

structure. Additionally, superposition of the COP1 and SPA1 VP-binding pockets revealed that two amino acids (COP1 S375/SPA1 C720 and COP1 H528/SPA1 Y873) were positioned slightly different and might thus influence binding affinities to VP motifs (Figure 3.1d). Taken together, due to several non-conserved residues in the VP-binding pocket and two structural differences, biochemical properties of the SPA1 WD-repeat domain might be slightly different from those of COP1.

3.1.2   Chimeric COP1/SPA1 proteins display similar molecular properties to full-length COP1 and SPA1

Given that the homology model of the SPA1 WD-repeat domain predicted a similar, but also partly distinct structure compared to COP1, it is possible that the COP1 and SPA1 WD-repeat domains might have slightly different functions and are thus not interchangeable. To test this hypothesis, chimeric COP1/SPA1 hybrid proteins were generated in which the respective WD-repeat domains were interchanged (Figure 3.2a). To determine a suitable swap site, sequence identity and conservation between the COP1 and SPA1 protein sequences were analyzed. A sequence of relatively high conservation located between the coiled-coil domain and WD-repeat domain of both proteins was identified. Additionally, this site had been used in similar previous studies in which chimeric hybrid proteins of SPA1 and SPA2 had been generated (Chen et al., 2016). Using this position (357 amino acids of COP1 and 702 amino acids of SPA1) as a swap site, two chimeric hybrids were generated: one with the N-terminal domains of COP1 fused to the SPA1 WD-repeat domain (hence called CC1) and another one with the N-terminal domains of SPA1 fused with the COP1 WD-repeat domain (hence called 11C) (Figure 3.2a).
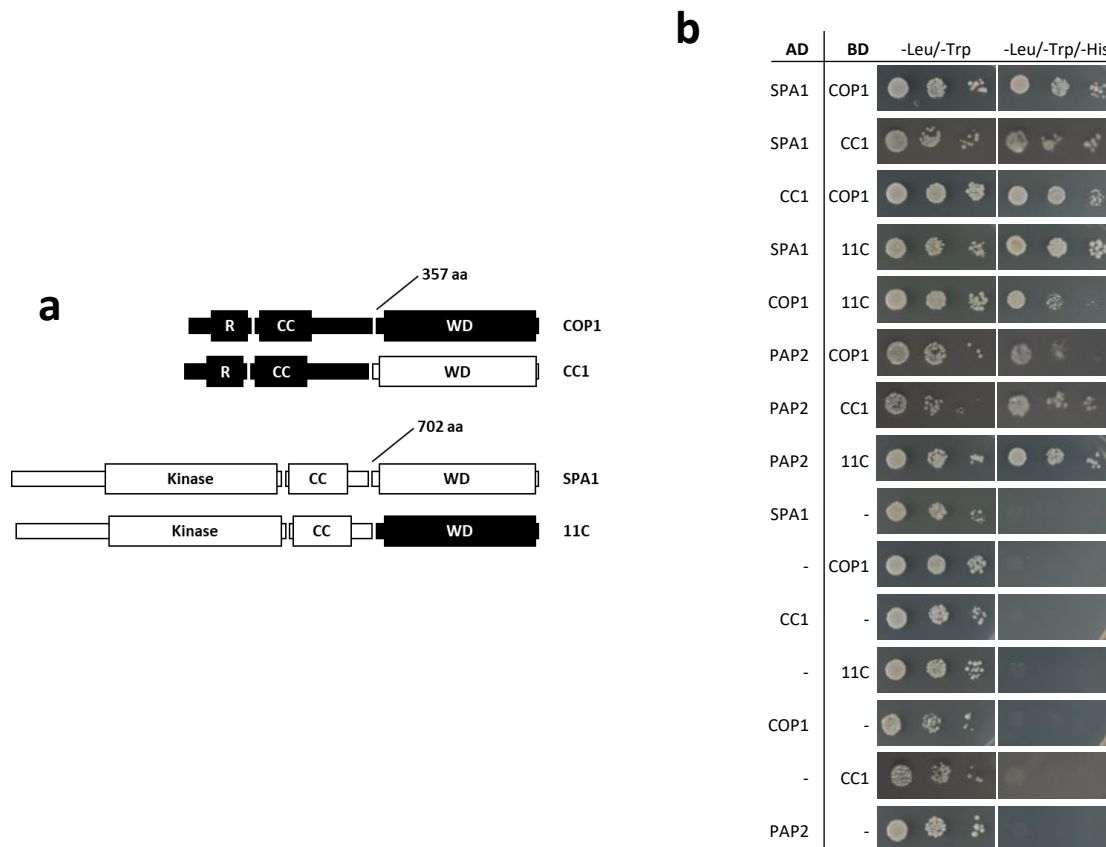
Figure 3.2: Chimeric COP1/SPA1 proteins interact with full-length COP1 and SPA1, as well as PAP2 in yeast.

(a) Schematic of chimeric COP1/SPA1 domain-swapped proteins; R: RING-Finger domain; CC: Coiled-coil domain; WD: WD40-repeat domain; KLD: Kinase-Like Domain. Black boxes represent COP1 protein domains, white boxes represent SPA1 protein domains. **(b)** Yeast-two-hybrid assays of chimeric COP1/SPA1 proteins and full-length COP1, SPA1 and PAP2. Proteins fused either to the GAL4 DNA binding domain (BD) or to the GAL4 activating domain (AD) were co-expressed in the yeast strain AH109 and plated on synthetic dropout (SD) medium lacking either leucin and tryptophane (-Leu/-Trp) or leucin, tryptophane and histidine (-Leu/-Trp/-His). Yeast cells were plated in droplets from cell suspensions of optical densities at 600 nm (OD600) of 1, 0.1 or 0.01 (left to right). Interactions of SPA1-CC1, PAP2-COP1 and PAP2-CC1 published in BS.c thesis of Annika Luebbe (Luebbe, 2016).

To exclude the possibility that the fusion caused major disfunction of the chimeric proteins such as misfolding of the individual domains, the question of whether known protein-protein interactions of COP1 and SPA1 were retained was investigated. Both COP1 and SPA1 have previously been reported to interact with each other in the yeast two-hybrid system via their coiled-coil domains (Yi and Deng, 2005; Hoecker and Quail, 2001). Additionally, protein-protein interactions with several downstream targets of the CUL4-DDB1$^{COP1/SPA}$ complex have been demonstrated. For example, interaction with the MYB-domain transcription factor PRODUCTION OF ANTHOCYANIN PIGMENT2 (PAP2) with both COP1 and SPA1 has been mapped to the WD40-repeat domains of both proteins via the characteristic valine-proline (VP) motif in PAP2 (Maier et al., 2013; Ponnu et al., 2019). To confirm the principal functionality of chimeric COP1/SPA1 proteins, the GAL4 yeast two-hybrid system was

utilized to test whether chimeric COP1/SPA1 proteins retained their interactions with COP1, SPA1 and PAP2. As previously reported, SPA1 fused to the GAL4 activation domain (AD) was able to interact with a BD-COP1 fusion protein (Hoecker and Quail, 2001) (Figure 3.2b). Both chimeric CC1 and 11C proteins interacted with COP1 and SPA1 in this study, confirming that COP1-SPA1 interaction has not been abolished in the domain-swapped proteins. Likewise, AD-PAP2 fusion proteins interacted with COP1, confirming previous results (Ponnu et al., 2019) (Figure 3.2b, interactions of SPA1-CC1, PAP2-COP1 and PAP2-CC1 published in BS.c thesis of Annika Luebbe (Luebbe, 2016)). In a similar fashion, interaction between both chimeric COP1/SPA1 proteins fused to the GAL4-binding domain and AD-PAP2 was detected, demonstrating that these chimeric proteins are functional with respect to the tested interactions. Hence, it is highly unlikely that the swap renders the chimeric proteins non-functional.
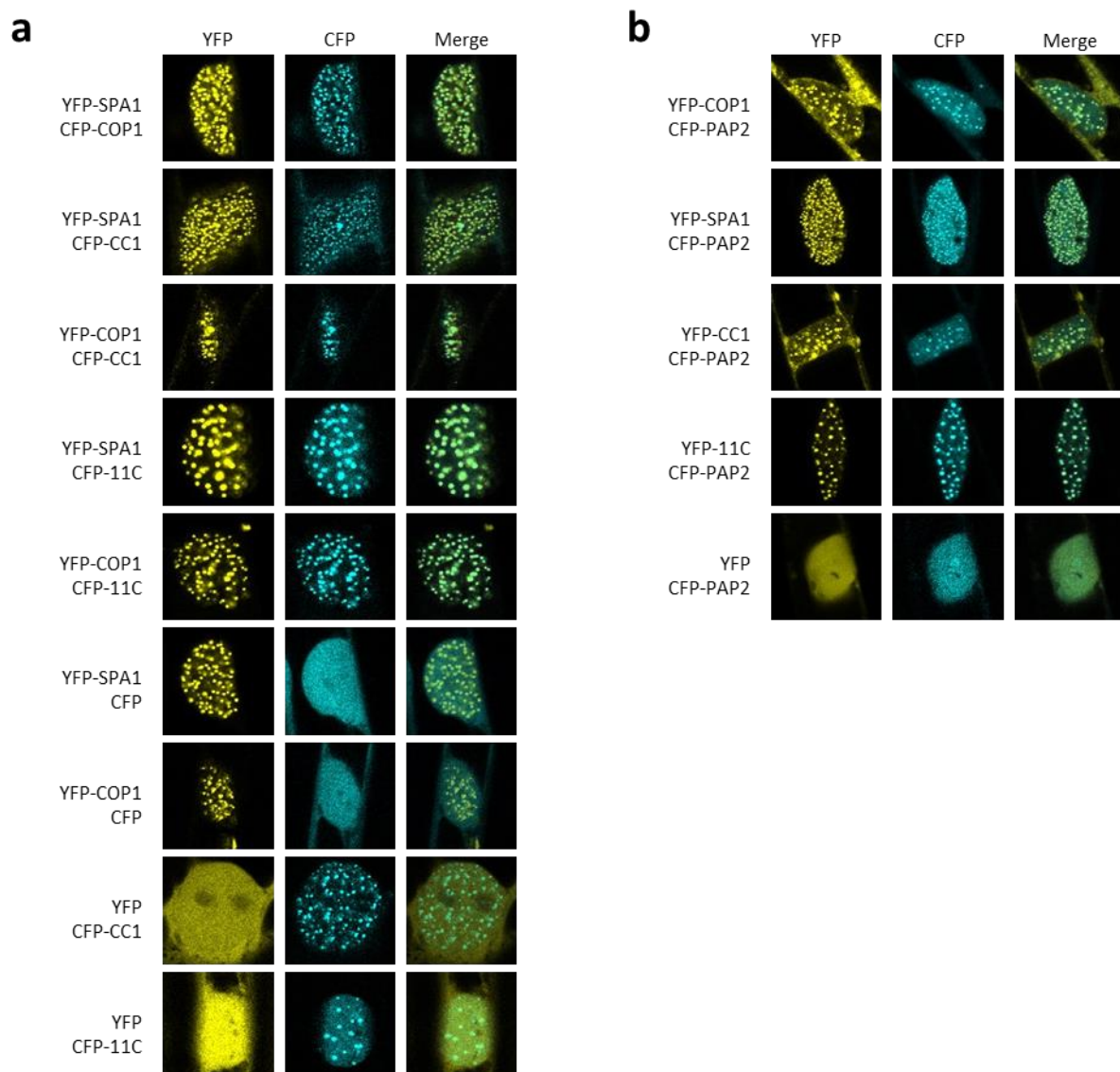
Figure 3.3: Chimeric COP1/SPA1 proteins co-localize into nuclear speckles with full length COP1/SPA1 and PAP2.

(a) Co-localization analysis of chimeric COP1/SPA1 proteins and full-length COP1 and SPA1. Proteins fused to either YFP or CFP were co-expressed in leek epidermal cells and analyzed using confocal laser scanning microscopy. Columns (left to right): Image captured in the YFP channel (YFP); image captured in the CFP channel (CFP); YFP and CFP images layers on top of each other (merge). **(b)** Co-localization analysis of chimeric COP1/SPA1 proteins and PAP2. Proteins fused to either YFP or CFP were co-expressed in leek epidermal cells and analyzed using confocal laser scanning microscopy. Columns (left to right): Image captured in the YFP channel (YFP); image captured in the CFP channel (CFP); YFP and CFP images layers on top of each other (merge).

To confirm the principal functionality of the chimeric proteins *in planta*, protein-protein interactions were examined based on co-localization. The ability of both COP1 and SPA1 to form nuclear bodies (speckles) both in transgenic Arabidopsis and in transient plant expression systems such as tobacco and leek has been widely described (Van Buskirk et al., 2012; Ponnu et al., 2019). In Arabidopsis, both nuclear localization and speckle formation of COP1 is required for COP1 function. Interestingly, some proteins which do not form nuclear speckles on their own, such as the blue-light photoreceptor cry2 or the transcription factor PAP2, can be recruited into speckles by co-expression of either COP1 or SPA1 (Stacey et al., 1999, 2000; Subramanian et al., 2004). The ability of chimeric COP1/SPA1 proteins to form nuclear speckles was tested by generating N-terminal CFP or YFP CC1/11C fusion proteins expressed in leek epidermal cells by particle bombardment. As previously reported, COP1 and SPA1 proteins formed nuclear speckles when expressed on their own and co-localized into nuclear speckles when co-expressed in leek (Figure 3.3a). Similarly, both CC1 and 11C proteins were able to form nuclear speckles when expressed in leek (Figure 3.3a). Moreover, both chimeric proteins colocalized with COP1 and SPA1 when co-expressed, further confirming their functionality. Both COP1 and SPA1, as well as CC1 and 11C were also able to recruit PAP2 proteins into nuclear speckles (Figure 3.3b). Next, speckle co-localization of COP1, SPA1, CC1 and 11C with the photoreceptors phyA, phyB,cry1 and cry2 was tested (Supplemental Figure S 2, S 3, S 4 and S 5). The ability of COP1 and SPA1 to co-localize into nuclear bodies with these photoreceptors when co-expressed in transient plant systems such as tobacco or leek epidermal cells has been previously reported (Zuo et al., 2011; Lian et al., 2011; Sheerin et al., 2015; Van Buskirk et al., 2012). Interestingly, Cryptochrome 2 does not form speckles when expressed alone, but is recruited into nuclear speckles when co-expressed together with COP1 or SPA1. These results could be confirmed, and in addition, the chimeric COP1/SPA1 proteins co-localized with all photoreceptors in a similar fashion to COP1 and SPA1. CC1 and 11C were also able to recruit CRY2 into nuclear speckles when co-expressed. Taken together, these results indicate that the chimeric CC1 and 11C proteins are indistinguishable from COP1 and SPA1 with respect to the tested functions.

3.1.3 Expression of *11C* does not reconstitute *spa* mutant phenotypes, whereas *CC1* reconstitutes *cop1* mutant phenotypes, in the seedling stage

The results above demonstrated that the COP1/SPA1 domain-swap proteins that were generated are likely functional. Thus, these proteins can be used to investigate whether the COP1 and SPA1 WD-repeat domains are functionally interchangeable. The following hypothesis was formulated: If both the COP1 and SPA1 WD-repeat domains were functionally identical, a chimeric protein consisting of the COP1 N-terminal domains and the SPA1 WD-repeat domain expressed in a *cop1* mutant should be able to complement the mutant phenotype. Likewise, the inverse domain-swap protein expressed in higher-order *spa* mutants should be able to complement their mutant phenotypes as well. To test this hypothesis, transgenic plants that expressed either full-length *COP1* or chimeric *CC1* from the *SPA1* promoter in the *cop1-4* mutant background, and transgenic plants that expressed either full-length *SPA1* or *11C* from the *SPA1* promoter in the *spa1 spa2 spa3* triple mutant background, were generated. For subsequent biochemical analysis, a triple hemagglutinin (3xHA) tag was added to the 5' end of the open reading frames of *COP1*, *SPA1*, *11C* and *CC1*. Transgenic plants expressing the same transgenes from the *CaMV-35S* promoter were generated as well; however, none of these transgenic plants complemented either the *cop1-4* or the *spa1 spa2 spa3* mutant phenotypes in the T2 generation, and recombinant protein could not be detected in the same lines. Because results obtained from transgenic lines would be more comparable if all transgenes were expressed from the same promoter, the *SPA1* promoter was used for all transgenic lines.

Both the *cop1-4* mutant and the *spa1 spa2 spa3* triple mutant displayed short hypocotyl and open cotyledons in darkness, and shorter cotyledons in low fluence rates of red light compared to the wild-type. Phenotypic screening of 14-21 independent transgenic lines for each individual genotype in the T2 generation revealed that most transgenic lines expressing either *COP1* or *CC1* were able to complement the *cop1-4* mutant phenotype in darkness, displaying a long hypocotyl and closed cotyledons similar to Col-0 (Supplemental Table S 1). Conversely, while transgenic lines expressing full-length *SPA1* in the *spa1 spa2 spa3* triple mutant were able to complement the mutant phenotype in darkness, transgenic lines expressing *11C* still showed a shorter hypocotyl and open cotyledons similar to the triple mutant.
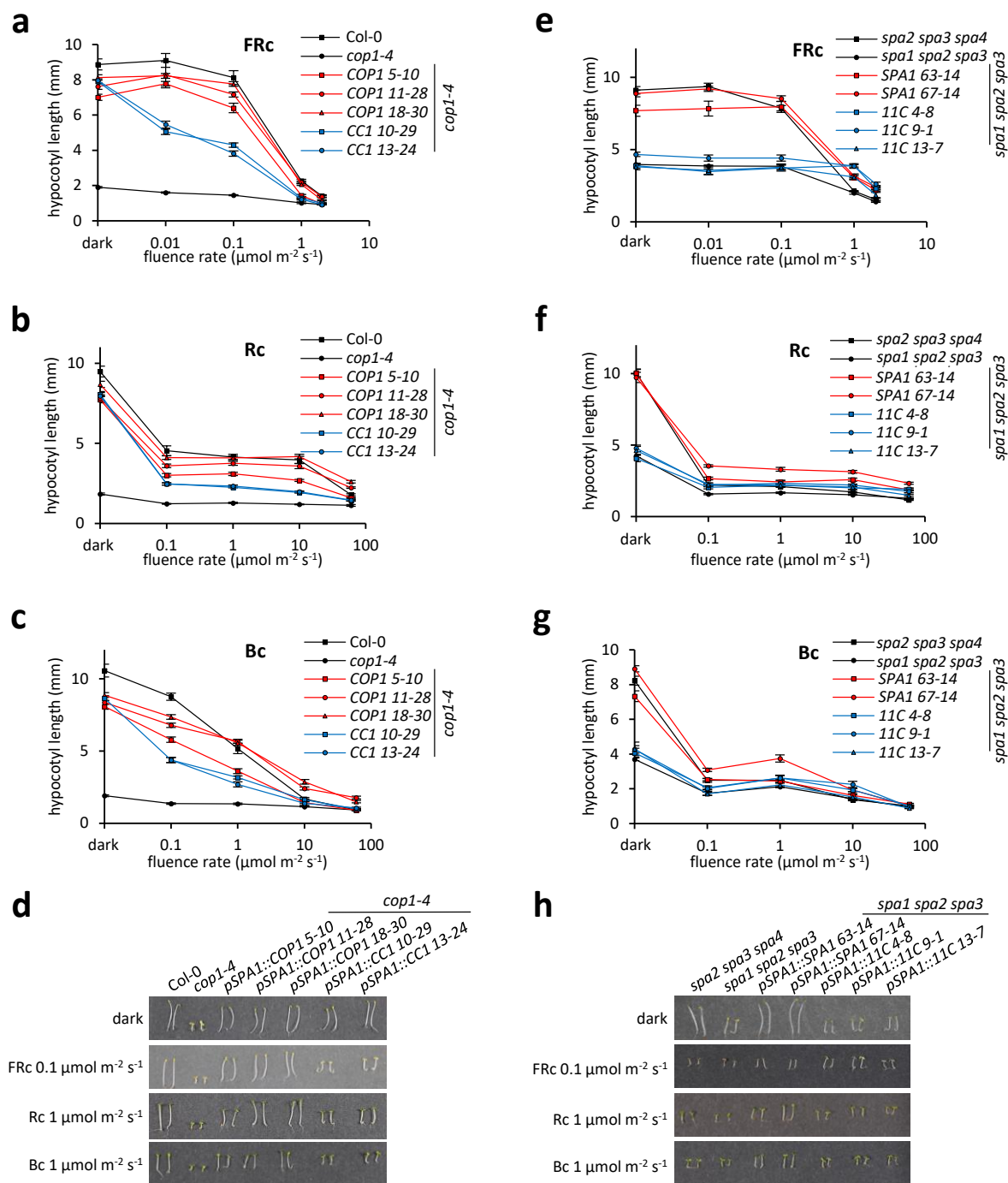
Figure 3.4: Seedling phenotypes of transgenic COP1/SPA1 domain swap lines.

(a-c) Fluence-dose response curves of transgenic lines expressing either full-length COP1 rescue proteins or chimeric COP1 proteins with a SPA1 WD40-repeat domain (CC1). Seedlings were grown for 4 days either in darkness, or various light intensities of far-red (a), red (b) or blue (c) light. Error bars represent standard error of the mean (SEM).

(e-g) Fluence-dose response curves of transgenic lines expressing either full-length SPA1 rescue proteins or chimeric SPA1 proteins with a COP1 WD40-repeat domain (11C). Seedlings were grown either in darkness, or various light intensities of far-red (a), red (b) or blue (c) light for 4 days. Error bars represent standard error of the mean (SEM).

(d+h) Seedling phenotype of transgenic lines expressing either COP1/ chimeric CC1 (d) or SPA1/chimeric 11C proteins (h). Seedlings were grown in either darkness or various fluence rates of far-red, red or blue light for 4 days.

Subsequently, several transgenic lines with representative phenotypes were selected and homozygous plants were isolated in the T3 generation. First, hypocotyl lengths of transgenic seedlings in response to increasing fluence rates of red, far-red, and blue light were analyzed. To this end, seedlings were grown in darkness or increasing fluence rates of monochromatic light. In darkness, hypocotyls of transgenic lines expressing *COP1* in the *cop1-4* mutant background were almost as long as those of wild-type seedlings, indicating a high degree of complementation (Figure 3.4a-d). The slight disparity of hypocotyl length between *COP1* rescue lines and Col-0 seedlings may be due to the lower expression levels of the *SPA1* promoter in darkness (Hoecker et al., 1998; Fittinghoff et al., 2006). Hypocotyls of transgenic lines expressing *CC1* in the *cop1-4* mutant were of the same length as those of *COP1* rescue lines (Figure 3.4a-d), suggesting that the COP1 WD-repeat domain is interchangeable with the SPA1 WD-repeat domain to exert COP1 functions in darkness. In the light, however, transgenic seedlings expressing *CC1* had significantly shorter hypocotyls than seedlings expressing *COP1* in the *cop1-4* background. This was observed for red, far-red, and blue light, ranging from very low to very high fluence rates. This partial complementation of the *cop1-4* mutant phenotype by *CC1* suggests that the COP1 and SPA1 WD-repeat domains are not fully interchangeable in terms of COP1 functions in the light.

As observed in the previous generation, hypocotyls of seedlings expressing *11C* were as short as *spa1 spa2 spa3* triple mutant seedlings in darkness, whereas full length *SPA1* was able to fully rescue the *spa1 spa2 spa3* mutant phenotype in darkness in terms of hypocotyl length (Figure 3.4e-h). Previous studies have demonstrated that hypocotyl length *spa* triple mutants with a *SPA1* wild type allele (*spa2 spa3 spa4* mutants) decreases more rapidly in very low fluence rants of red, far-red or blue light (Laubinger et al., 2004; Ordoñez-Herrera et al., 2015). Since *SPA1*-expressing plants in a *spa1 spa2 spa3* triple mutant background are genetically more similar to *spa* triple mutants with only a functional *SPA1* allele than to the wild type, this triple mutant was used as a positive control for hypocotyl measurements of transgenic *SPA1* or *11C*-expressing plants. Similar to previous studies, hypocotyl length of *spa* triple mutants with only a functional *SPA1* allele displayed characteristically long hypocotyls in darkness, but hypocotyl length rapidly decreased in very low fluence rates of red, blue or far-red light. Transgenic seedlings expressing *SPA1* in the *spa1 spa2 spa3* triple mutant background phenocopied *spa* triple mutants with a *SPA1* wild type allele in terms of hypocotyl length in all fluence rates of red, blue or far-red light with a slight degree of over-complementation, whereas seedlings expressing *11C* phenocopied the *spa1 spa2 spa3* triple mutant (Figure 3.4e-h). Overall, this evidence suggests that the SPA1 WD-repeat domain is indispensable for hypocotyl elongation in darkness and in light *in planta*, and that its functionality cannot be replaced by the COP1 WD-repeat domain.

3.1.4 *CC1* partially reconstitutes adult *cop1* mutant phenotypes

Next, the adult phenotypes of these transgenic plants were analyzed. To this end, wild-type plants, *cop1-4* mutants as well as transgenic plants expressing either *COP1* or *CC1* in the *cop1-4* mutant background were grown in short day conditions. The *cop1-4* mutant displays dwarfism in the adult stage resulting in reduced rosette sizes. Additionally, it flowers early and shows reduced petiole elongation in short-day conditions (McNellis et al., 1994a). Even though leaf shape was affected, transgenic plants expressing *COP1* developed rosettes that were of comparable size to wild-type plants after four weeks in short-day conditions (Figure 3.5a). Interestingly, plants expressing *CC1* developed rosettes of intermediate size, indicating that *CC1* was able to partially complement the mutant phenotype. Plants expressing *COP1* flowered late in short-day both in terms of days after germination and number of leaves, while plants expressing *CC1* showed an intermediate flowering phenotype in short-day, flowering significantly earlier than the wild-type, but later than the *cop1-4* mutant (Figure 3.5b, c, e). Similarly, plants expressing *COP1* showed a comparable degree of petiole elongation in short-day as the wild-type, while plants expressing *CC1* elongated their petioles to a lesser degree than the wild-type, but more than *cop1-4* (Figure 3.5d).
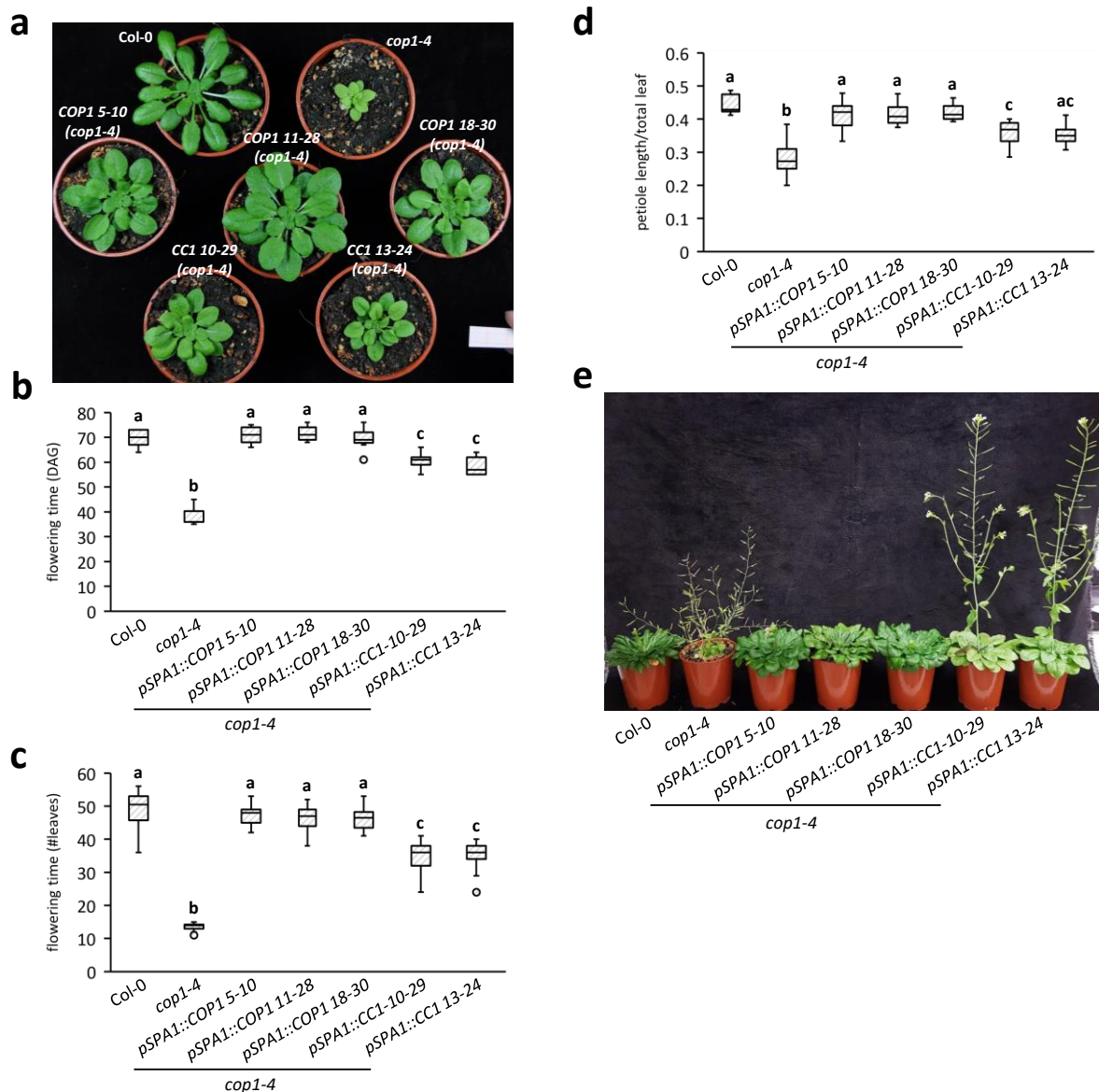
Figure 3.5: Phenotypes of adult transgenic plants expressing chimeric CC1 constructs.

(a) Rosettes of adult transgenic plants expressing either full length COP1 or chimeric COP1 proteins with a SPA1 WD40-repeat domain (CC1). Plants were grown for 2 weeks in short day (SD). **(b-d)** Flowering and petiole length phenotypes of transgenic COP1 rescue lines and chimeric COP1/SPA1 lines. Boxplots display flowering time in terms of days after germination (b) as well as number of leaves (c), and petiole lengths over total leaf length (d) of plants grown in short day (SD). Letters indicate which groups significantly differ from each other; groups marked with the same letter are not significantly different, determined by one-way-ANOVA followed by two-sided Tukey test ($p < 0.05$). **(e)** Representative picture of flowering wild type, *cop1-4* and transgenic plants expressing either full length COP1 or COP1 with a SPA1 WD40-repeat domain (CC1) grown in short day (SD).

3.1.5 *11C* has a dominant negative effect on early flowering of *spa* mutants in short day conditions

SPA proteins also regulate photoperiodic flowering, as evidenced by the fact that *spa1 spa2 spa3 spa4* quadruple null mutants flower significantly earlier than the wild-type both in long day and in short day conditions (Laubinger et al., 2006; Ordoñez-Herrera et al., 2015). The *SPA* quartet acts redundantly in the delay of photoperiodic flowering in short day conditions, but triple mutant analysis demonstrated that *SPA2* and *SPA3* only play minor roles in the delay of photoperiodic flowering in short day conditions, while *SPA1* and *SPA4* delay flowering more effectively. As such, the *spa2 spa3 spa4* triple null mutant flowers almost as late as the wild-type in short day conditions, while the *spa1 spa2 spa3* triple mutant flowers only slightly earlier (Ordoñez-Herrera et al., 2015). For the same reasons specified in **3.1.3**, *spa2 spa3 spa4* (*SPA1* wild type) triple mutants were used as a positive control when scoring flowering time of *SPA1* or *11C*-expressing transgenic plants in the *spa1 spa2 spa3* triple mutant background. Flowering time in short day conditions of transgenic plants expressing either full-length *SPA1* or *11C* in the *spa1 spa2 spa3* triple mutant background was analyzed. *spa1 spa2 spa3* triple mutants flowered significantly earlier than *spa2 spa3 spa4* triple mutants, and transgenic lines expressing full-length *SPA1* flowered as late as *spa2 spa3 spa4* triple mutants, indicating that full-length *SPA1* was able to rescue the early flowering phenotype of *spa1 spa2 spa3* in this experiment (Figure 3.6). Surprisingly, however, transgenic plants expressing *11C* flowered significantly earlier than *spa1 spa2 spa3* triple mutants, with an average flowering time of 17-20 leaves for transgenic *11C* plants and 26 leaves for *spa1 spa2 spa3* triple mutants (Figure 3.6). Thus, given that transgenes were transformed into the *spa1 spa2 spa3* triple mutant, the *11C* transgene has a dominant negative effect on the early flowering phenotype of *spa1 spa2 spa3*. Overall, these data indicate that the SPA1 WD-repeat domain can partially substitute the COP1 WD-repeat domain for COP1-dependent control of flowering time and petiole elongation *in planta*, whereas the COP1 WD-repeat domain cannot substitute its *SPA1* counterpart, and even accelerates flowering of the *spa1 spa2 spa3* triple mutant.
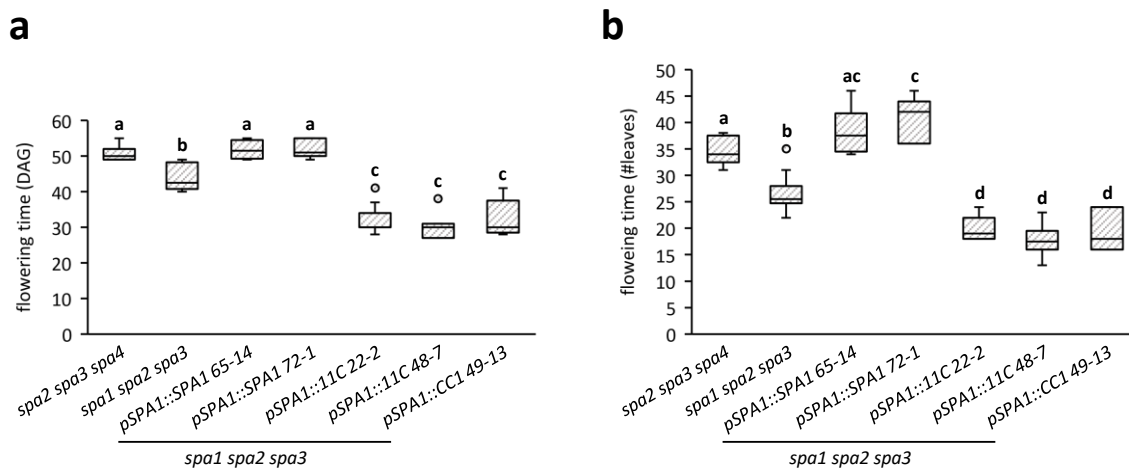
Figure 3.6: Flowering time of transgenic plants expressing chimeric 11C in short day conditions.

Flowering time was scored for *spa2 spa3 spa4* (positive control) and *spa1 spa2 spa3* triple mutants, as well as transgenic plants expressing either full length SPA1 or chimeric 11C proteins in the *spa1 spa2 spa3* triple mutant backgrounds. Boxplots display flowering time expressed in terms of days after germination **(a)** or number of leaves at time of bolting **(b)**. Groups marked with the same letter are not significantly different, as determined by one-way ANOVA followed by two-sided Tukey test ($p < 0.05$).

3.1.6 11C proteins are more stable than full-length SPA1 *in planta*

The transgenic plants expressing chimeric *CC1* or *11C* displayed distinct phenotypes both in the seedling stage and in adult plants compared to control plants expressing either full-length *COP1* or *SPA1*. Photomorphogenesis is a quantitative phenotype that depends on the abundance of light signaling components, including COP1 and SPA1. Therefore, protein levels of transgenic *CC1* or *11C*-expressing plants were analyzed. To this end, plants expressing either full length *COP1* or *CC1* were grown in darkness for four days and protein levels between different transgenic lines were compared. N-terminal 3xHA tags enabled comparison of proteins from different transgenic lines using α-HA antibodies. 3xHA-COP1 or 3xHA-CC1 protein levels were comparable in all lines (Figure 3.7a), suggesting that protein stability of 3xHA-CC1 does not dramatically differ from that of 3xHA-COP1 in darkness. Next, protein levels of transgenic lines expressing *SPA1* or *11C* were analyzed. Surprisingly, dramatically higher protein levels were detected in all lines expressing *11C* compared to lines expressing *SPA1* (Figure 3.7b). To exclude the possibility that this difference in protein levels was only present in the transgenic lines that were selected for further analysis, the protein levels of other transgenic lines in the T2 generation were examined (Supplemental Figure S 6). Much higher protein levels were detected in all transgenic plants expressing *11C* that were analyzed compared to all lines expressing *SPA1*. Therefore, the significantly higher protein levels that were detected in plants expressing *11C* compared to *SPA1* were likely not due to differences in expression levels between

transgenic lines, but rather due to differences in protein stability. Hence, the 11C protein is likely much more stable than the SPA1 protein.
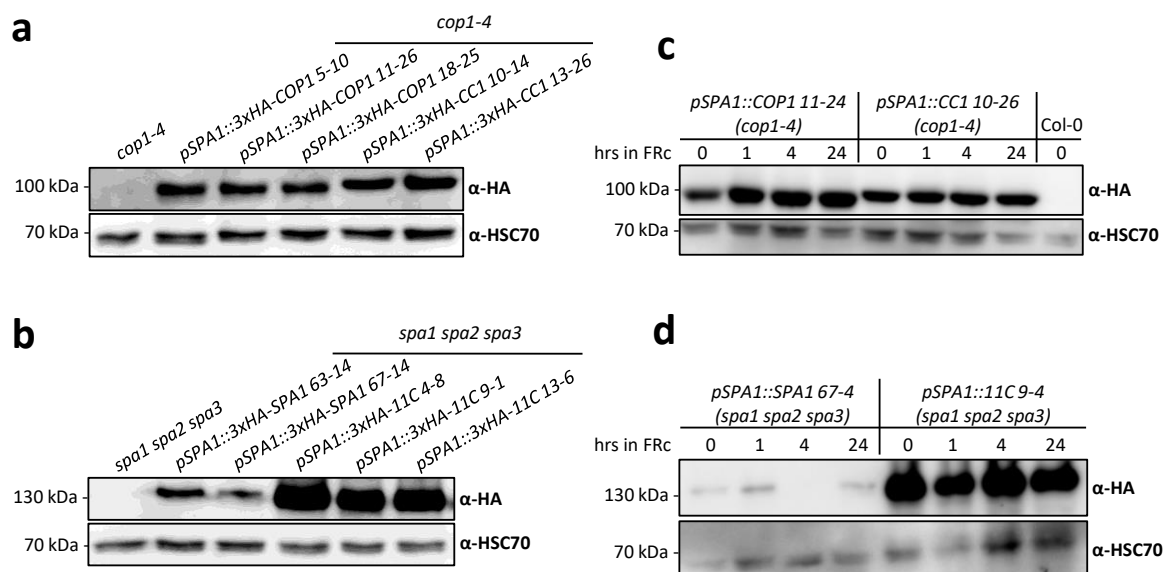
Figure 3.7: Protein levels and dynamics of chimeric COP1/SPA1 transgenic lines.

(a+b) Protein levels of transgenic COP1 rescue lines and chimeric COP1 lines with a SPA1 WD40-repeat domain (CC1) (a), as well as transgenic SPA1 rescue lines and chimeric SPA1 lines with a COP1 WD40-repeat domain (11C) (b). Seedlings were grown for 4 days in darkness. **(c+d)** Protein levels of transgenic lines expressing either COP1/CC1 (c) or SPA1/11C (d) after far-red light exposure. Plants were grown in darkness for 4 days, then shifted to 0.35 µmol m^{-2} s^{-1} far-red light for indicated times.

Previous studies have shown that, while COP1 protein levels are similar in light- and dark-grown seedlings, SPA1 and in particular SPA2 proteins, are rapidly degraded in seedlings upon light exposure (Balcerowicz et al., 2011). Furthermore, domain-swap analyses with SPA1 and SPA2 proteins have demonstrated that the degree to which SPA proteins are degraded in the light is at least in part determined by its WD-repeat domain (Chen et al., 2016). Therefore, the respective WD-repeat domains of SPA1 and COP1 might contribute to the difference in protein stability between SPA1 and COP1. To test this hypothesis, transgenic plants expressing *COP1*, *CC1*, *SPA1* or *11C* were grown in darkness and then exposed to low fluence rates of far-red light for 24 hours (Figure 3.7c, d). While COP1 protein levels increased after 1 hour of far-red light and remained constant for the remaining 23 hours, CC1 protein levels did not change significantly upon exposure to far-red light. The increase in COP1 protein levels is very likely caused by the SPA1 promoter, which is known to increase expression in the light compared to darkness (Hoecker et al., 1998; Fittinghoff et al., 2006). Since the *CC1* construct in the analyzed plants is driven by the same promoter, it is possible that protein levels remain the same upon light exposure because, while expression of the transgene increases, the protein gets partly degraded upon light exposure. Similarly, SPA1 protein levels slightly increased after 1 hour of far-red

light exposure (likely due to an initial boost in expression), but then decreased after 4 hours and returned to their previous levels after 24 hours, while 11C protein levels remained constantly high both in darkness and upon light exposure (Figure 3.7d), indicating that 11C proteins are more stable that SPA1 proteins both in darkness and in FR.

3.1.7   HY5 protein is partially degraded in transgenic *CC1* plants in darkness

The CUL4/DDB1$^{COP1/SPA}$ complex is a major suppressor of photomorphogenesis in darkness. It acts by polyubiquitination of photomorphogenesis-promoting transcription factors such as HY5, thereby targeting them for degradation. Since plants expressing chimeric *CC1* in the *cop1-4* mutant background were able to complement the mutant phenotype in darkness, the question of whether HY5 was as efficiently degraded in dark-grown plants expressing *CC1* as they were in wild-type plants was investigated. Wild-type, *cop1-4* and transgenic plants expressing either *COP1* or *CC1* in the *cop1-4* mutant background were grown in darkness for 4 days and HY5 protein levels were assessed (Figure 3.8a). Interestingly, while HY5 protein accumulated in dark-grown *cop1-4* mutants and was efficiently degraded in dark-grown plants expressing *COP1*, plants expressing *CC1* still accumulated residual levels of HY5, albeit to a significantly lower degree than *cop1-4*. This suggests that, while the CUL4/DDB1$^{COP1/SPA}$ complex is partly functional in darkness when the COP1 WD-repeat domain has been replaced by a SPA1 WD-repeat domain, ubiquitination and subsequent degradation of target proteins is less efficient. Taken together, these findings indicate that the COP1 WD-repeat domain is, at least in part, indispensable for efficient ubiquitination of HY5 in darkness.
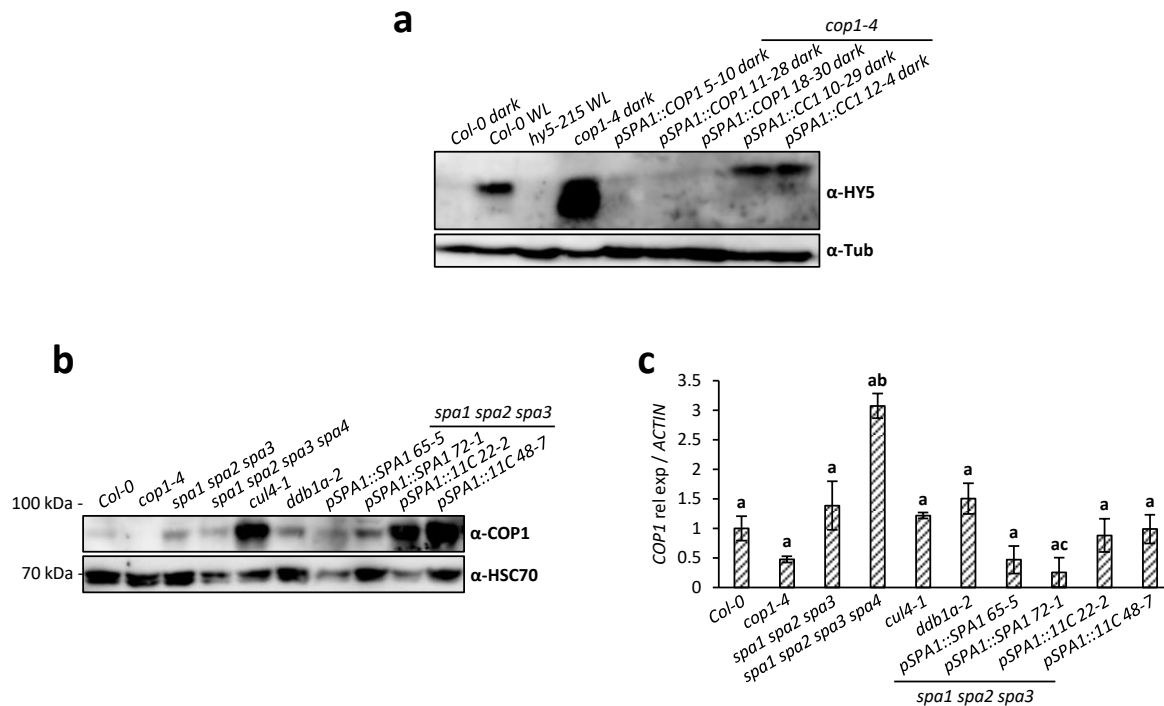
Figure 3.8: Native HY5 protein levels and COP1 protein and expression levels in chimeric COP1/SPA1 transgenic lines.

(a) Immunodetection of HY5 protein levels of transgenic COP1 rescue lines or chimeric COP1 lines with a SPA WD40-repeat domain. Seedlings were grown for 4 days either in continuous white light or darkness. **(b)** Immunodetection of COP1 protein levels of dark-grown wild-type and various mutant seedlings, as well es transgenic SPA1 rescue lines and chimeric 11C lines. **(c)** qRT-PCR evaluating relative expression of *COP1* in dark-grown wild-type and various mutant seedlings, as well as transgenic *SPA1* rescue lines and *11C* lines. Groups marked with the same letter are not significantly different, as determined by one-way ANOVA followed by two-sided Tukey test ($p < 0.05$). Total protein and RNA extracts used (b) and (c) were obtained from seedlings grown on the same plate and harvested at the same time.

3.1.8 Native COP1 hyper-accumulates in dark-grown transgenic seedlings expressing *11C*

Previous studies have shown that COP1 protein levels remain relatively stable in darkness and in light (Zhu et al., 2008; Balcerowicz et al., 2011). Interestingly, however, several mutants with a *cop*-like phenotype such as *cop10-1*, *det1-1* or *cul4-1* are known to hyper-accumulate COP1 protein in dark-grown seedlings compared to the wild-type, suggesting that COP1 is subject to polyubiquitination in darkness (Chen et al., 2010). Since transgenic plants expressing chimeric *11C* did not complement the *spa1 spa2 spa3* triple mutant phenotype in darkness and *spa* mutants do not accumulate COP1 protein, the impact of COP1 and SPA1 WD-repeats on the stability of COP1 in COP1/3xHA-SPA1 and COP1/3xHA-11C complexes was investigated. Surprisingly, plants expressing chimeric *11C* in the *spa1 spa2 spa3* background accumulated high levels of COP1 protein, very similar to other *cop*-like mutants such as *cul4-1*, whereas neither *spa1 spa2 spa3* triple mutants nor *spa1 spa2 spa3 spa4* quadruple

mutants accumulated COP1 protein in darkness, (Figure 3.8b). Additionally, transgenic plants expressing full-length SPA1 in the same genetic background showed no signs of COP1 hyper-accumulation in darkness, and COP1 expression was not dramatically changed in any of the genotypes tested (Figure 3.8c).

In summary, the presented data indicate that the COP1 and SPA1 WD-repeat domains are not interchangeable in terms of CUL4/DDB1$^{COP1/SPA}$ functionality in darkness. SPA1 WD-repeats are able to partially substitute the corresponding COP1 region, but not vice versa. This indicates that the SPA1 WD-repeat domain is indispensable for the function of CUL4-DDB1$^{COP1/SPA}$ complexes.

3.2 SPA PROTEINS AFFECT LIGHT-REGULATED SUBCELLULAR LOCALIZATION OF COP1

Because the COP1/SPA complex acts as a central repressor of photomorphogenesis, precise transduction of light signals requires accurate and efficient inactivation of COP1/SPA in the light. To this end, four currently known mechanisms of COP1/SPA inactivation have evolved (Legris et al., 2019). Among those, nuclear exclusion of COP1 has been proposed as a possible mechanism very early on (Von Arnim and Deng, 1994). Light-dependent nuclear exclusion of COP1 separates COP1 from its nuclear localized substrates, thereby disrupting COP1 activity. However, the precise mechanisms of COP1 nucleocytoplasmic partitioning are not well understood. Moreover, it is not known whether SPA proteins contribute to the light-dependent nuclear exclusion of COP1. Thus, the role of SPA proteins in the light-regulated subcellular localization of COP1 was investigated.

3.2.1 Confocal Laser-Scanning Microscopy enables fluorescence intensity measurement in 3-dimensional bodies

To accurately quantify light-dependent nucleocytoplasmic partitioning of COP1, a precise method of measuring COP1 levels within nuclei is required. The development of fluorescence microscopy has enabled accurate and fast imaging of biological processes and protein dynamics using fluorophore-tagged fusion proteins (Combs and Shroff, 2017). However, since the accurate measurement of fluorescence intensity within 3-dimensional objects such as organelles requires assessment of its volume and shape, the technical limitations of standard, i.e. non-confocal, fluorescence microscopy make it an inaccurate tool for quantification of fluorescence intensity within nuclei (Figure 3.9a). Because of this, Confocal Laser Scanning Microscopy (CLSM) has become a prevalent fluorescence microscopy technique for studies of 3-dimensional biological structures in the last 30 years (Pawley, 2006; Bayguinov et al., 2018). The generation of a conjugate focal pane via the

coincidence of the focal pane of the objective lens and the detector enables isolation of the image plane from adjacent axial planes. This is achieved by the use of a diffraction-limited spot of light which illuminates the sample and an aperture (pinhole) in the collection light path (Bayguinov et al., 2018). Thus, CLSM enables optical sectioning of samples, capturing high-resolution images of multiple axial planes (z-stacks) of a sample in quick succession (Figure 3.9b).
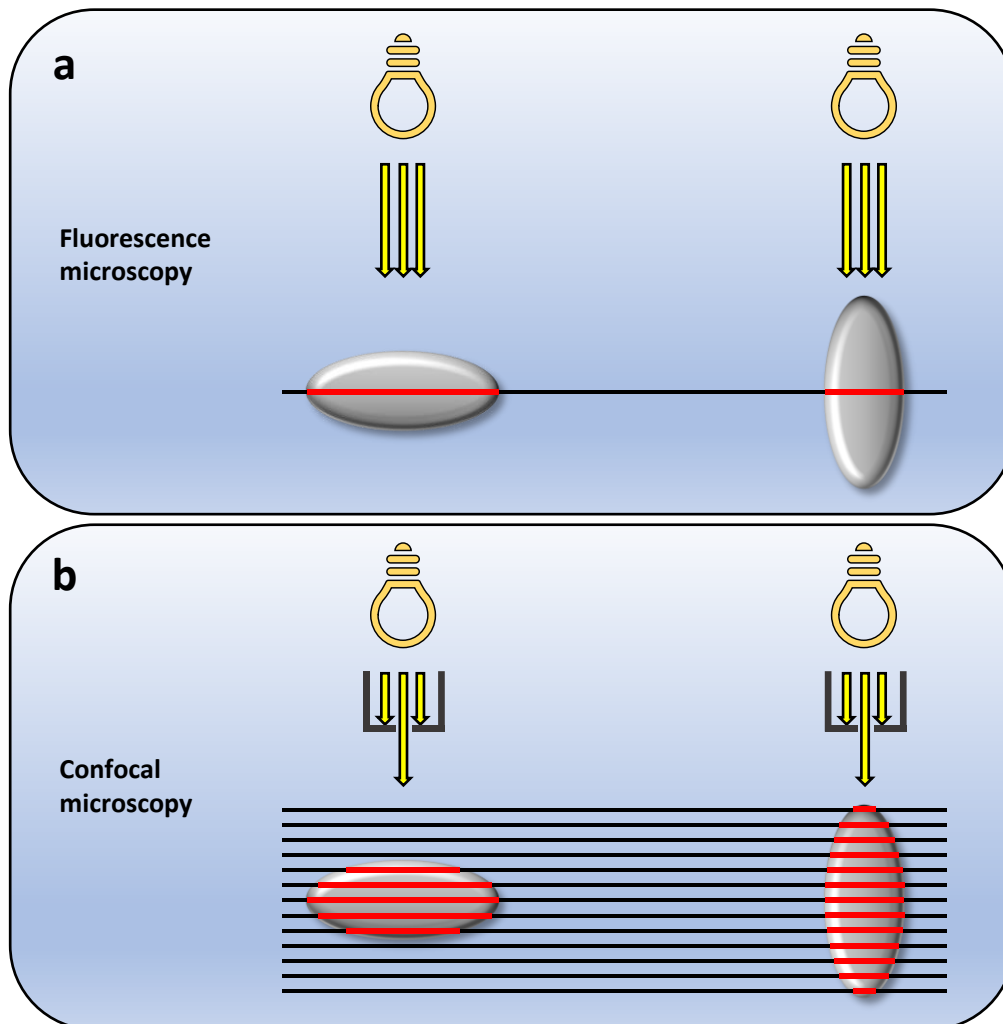
Figure 3.9: Confocal laser scanning microscopy technology provides accurate results for quantitative fluorescence analysis in 3-dimensional objects.

(a) Because classical fluorescence microscopy can only project the wide focal pane onto a 2-dimensional space, it is nearly impossible to evaluate the volume of a 3-dimensional object with this technique. Thus, objects that may have the same volume may appear in different sizes in fluorescence microscopy, and vice versa. **(b)** Due to the utilization of a pinhole which focuses light onto a single focal plane, multiple parallel cross-sections can be generated through an object using Confocal Laser Scanning Microscopy (CLSM). Stacks of multiple cross-sections (z-stacks) can be used to accurately analyze volume of and quantify fluorescence within a 3-dimensional object.

To accurately quantify nuclear-localized YFP-COP1 by measuring nuclear YFP fluorescence, a method for the measurement of volume and fluorescence intensity of 3-dimensional nuclei using CLSM

was developed. First, nuclei of transgenic Arabidopsis seedlings were stained with 4',6-diamidino-2-phenylindole (DAPI). Second, DAPI and YFP fluorescence was captured with CLSM, generating z-stacks with a 1 µm distance between each image plane. Third, the volume of DAPI-stained nuclei was calculated by defining a 3-dimensional region of interest (ROI) within z-stacks. Since the distance between image planes is known, the volume of one pixel (voxel) can thus be defined as the area of one pixel multiplied by its height. Last, fluorescence intensity of each voxel within the previously defined ROI was measured and summed up to calculate the accurate fluorescence intensity within nuclei.

Given that a 3-dimensional object of unknown volume ranges from *a* to *b* in a dimension and *n* cross-sections in a parallel plane are made with the same distance between each cross-section (Figure 3.9), the distance between cross-sections can be defined as

$$\Delta x = \frac{b-a}{n}$$

. Additionally, define that

$$x_i = a + i\Delta x \; for \; i = 1, \dots, n$$

, then Cavalieri's principle can be applied, and the volume (*V*) of the object can be defined as

$$V = \lim_{n \to \infty} \sum_{i=1}^{n} A(x_i)\Delta x = \int_{a}^{b} A(x)dx$$

where *A(x)* is the area of any cross-section *x*. In simpler terms, the volume of a 3-dimensional object is the cumulative sum of the area of all cross-sections multiplied with the increment length between cross-sections. This principle can be applied to z-stacks, in which the area of a ROI can be defined on every slice of that stack. Consequently, the volume of a ROI can be approximated of the cumulative sum of a ROI on each slice multiplied by the increment length.

To gauge the discrepancy between calculations based on the widest area of a nucleus and its true volume, the volumes of ten representative DAPI-stained nuclei from hypocotyls of dark-grown transgenic seedlings expressing YFP-COP1 from the *CaMV::35S* promoter in the *cop1-4* mutant background (Oravecz et al., 2006), as well as the area of each nucleus at its widest position were calculated. As expected, the largest area of a nucleus shows only weak correlation with its true volume (R^2 = 0.2306), demonstrating that area is not a suitable proxy for the volume of a nucleus (Supplemental Figure S 7a). Next, the fluorescence intensity within the same nuclei was measured. Assuming that YFP fluorescence intensity within a nucleus is, at least partly, dependent on its volume, fluorescence intensity of a nucleus is expected to correlate with its volume. Since, as previously shown, the largest area of a nucleus is not an accurate proxy for its volume, correlation between fluorescence

intensity and volume should be higher than between fluorescence intensity and area. Indeed, fluorescence intensity per μm^3 (i.e. volume) measured in ten nuclei shows significantly lower variation than fluorescence intensity per μm^2 (i.e. area) of the same nuclei, with a Coefficient of Variation (CV) of 27.9% for intensity per μm^3 and 53.3% for intensity per μm^2 (Supplemental Figure S 7b). Taken together, 3-dimensional measurements of fluorescence intensity obtained from CLSM imaging can be used as a more accurate measurement for quantification of fluorescence within 3-dimensional objects such as nuclei.

3.2.2 SPA Proteins are not necessary for the nuclear accumulation of COP1 in darkness

SPA proteins are essential for COP1 function in darkness. It is conceivable that this is partly because SPA proteins are needed for the nuclear localization of COP1 in dark-grown Arabidopsis seedlings. In a collaborative work with Dr. Martin Balcerowicz (former Ph.D. student of the Hoecker group), this hypothesis was tested by analyzing nuclear YFP fluorescence in hypocotyl cells of dark- and light-grown transgenic seedlings expressing YFP-COP1 from the constitutive *CaMV-35S* promoter in the *cop1-4* mutant background (Oravecz et al., 2006). Dark-grown seedlings showed distinct nuclear YFP-COP1 photobodies in hypocotyl cells, while no photobodies could be detected in seedlings grown in white light (Figure 3.10a). Light-grown Col-0 seedlings showed YFP fluorescence patterns that were similar to transgenic *YFP-COP1* seedlings, indicating that the circular fluorescent objects in light-grown seedlings are likely not YFP-COP1 signals but rather autofluorescence, likely generated by chloroplasts or similar structures. To exclude the possibility that YFP-COP1 may form no visible photobodies but is still localized in the nucleus in light-grown seedlings, nuclear YFP fluorescence of dark- and light-grown seedlings expressing YFP-COP1 with the above described method. Light grown seedlings showed significantly lower nuclear YFP fluorescence than dark grown seedlings (Figure 3.10b, quantification performed on microscopy pictures generated by Dr. Martin Balcerowicz), indicating that YFP-COP1 is excluded from the nucleus, confirming results from earlier studies (Von Arnim and Deng, 1994; Stacey and Von Arnim, 1999; Pacín et al., 2014).
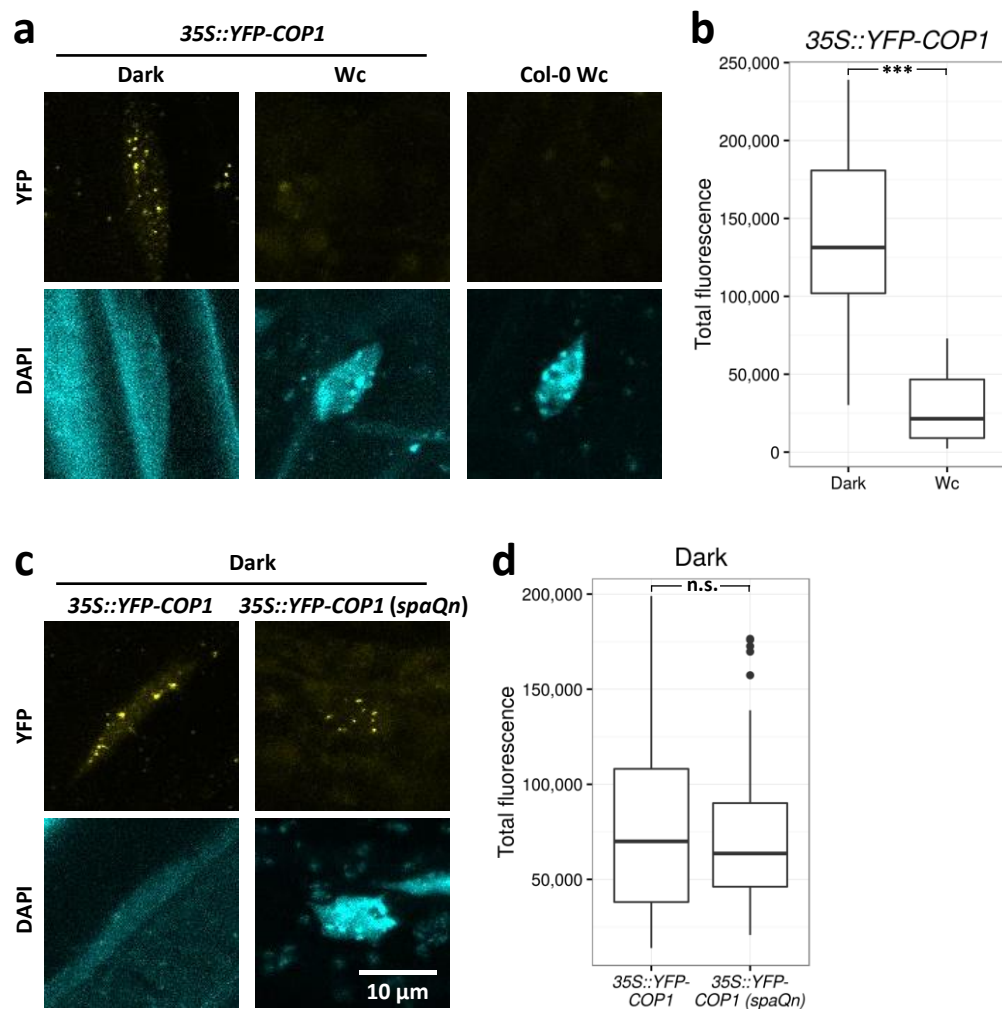
Figure 3.10: SPA proteins are not necessary for the nuclear accumulation of COP1 in darkness.

(a) Representative images of nuclei in hypocotyl cells of transgenic *35S::YFP-COP1* and wild-type seedlings grown in either darkness of 40 µmol m^{-2} s^{-1} of continuous white light for 4 days. **(b)** Nuclear YFP fluorescence of nuclei in hypocotyl cells of transgenic *35S::YFP-COP1* seedlings grown under the same conditions as (a). 20 or 53 nuclear from 8 to 10 different seedlings were analyzed in darkness and continuous white light, respectively. 100% of nuclei in dark-grown seedlings showed speckles, whereas 0% of nuclei in light-grown seedlings showed speckles. quantification performed on microscopy pictures generated by Dr. Martin Balcerowicz. **(c)** Representative images of nuclei in hypocotyl cells of transgenic *35S::YFP-COP1* and *35S::YFP-COP1 (spaQn)* seedlings grown in darkness for 4 days. **(d)** Nuclear YFP fluorescence intensity of the same nuclei depicted in (c). In total, 26 or 60 nuclei from 8 to 10 seedlings of *35S::YFP-COP1* or *35S::YFP-COP1 (spaQn)*, respectively, were analyzed. 85% and 93% of nuclei from *35S::YFP-COP1* and *35S::YFP-COP1 (spaQn)*, respectively, showed speckles. quantification performed on microscopy pictures generated by Dr. Martin Balcerowicz. Upper and lower hinges of boxplots represent the first and third quartiles, respectively. Whiskers extend from the hinges to the highest/lowest value within 1.5 * interquartile range (IQR). Data points which were higher or lower than this range are represented as dots. ***: true difference between means is not equal to 0 at *p < 0.001* in two-sample Student's *t* test. n.s.: not significant at *p = 0.05*.

To investigate the role of SPA proteins in light-dependent nucleocytoplasmic partitioning of COP1, the *35S::YFP-COP1* transgene (Oravecz et al., 2006) was introgressed into the *spa1-100 spa2-2 spa3-1 spa4-3* quadruple null mutant (*spaQn*) (Ordoñez-Herrera et al., 2015) (*35S::YFP-COP1* (*spaQn*) line was generated by Dr. Martin Balcerowicz in previous studies), and nuclear YFP-COP1 fluorescence was analyzed in these lines. As in the *SPA* wild-type background, YFP-COP1 accumulated in the nucleus and formed nuclear photobodies in dark-grown seedlings in the *spaQn* mutant background, indicating that SPA proteins are likely not required for the dark-dependent nuclear localization of COP1 (Figure 3.10c). Quantification of nuclear YFP-fluorescence showed no significant difference between nuclear YFP-COP1 in the *SPA* wild-type and *spaQn* mutant (Figure 3.10d, quantification performed on microscopy pictures generated by Dr. Martin Balcerowicz). Taken together, these results demonstrate that YFP-COP1 is being translocated to the nucleus and forms photobodies in the dark, but SPA proteins are not required for this process.

To evaluate homogeneity within and between datasets, several additional tests were performed (Supplemental Figure S 8). First, because it is reasonable to assume that total fluorescence intensity is somewhat contingent on nuclear volume, the correlation between fluorescence and volume was analyzed. For all four datasets shown in Figure 3.10, total fluorescence of nuclei correlated strongly with nuclear volume, with no R^2 value lower than 0.71. Second, a quantile-quantile plot combined with a Shapiro-Wilk test was utilized to evaluate whether data points followed a normal distribution. Both datasets obtained from dark grown seedlings in the *SPA* wild-type background followed a normal distribution, while datasets from light grown seedlings in the *SPA* wild-type background and dark-grown seedlings in the *spaQn* background may not be normally distributed. Finally, data distribution was visualized in a histogram. In conclusion, strong correlation between nuclear fluorescence and volume provides further evidence that the above described method of YFP-fluorescence quantification yields accurate results; further analysis regarding data distribution might be required, but this is immaterial for the analysis provided.

3.2.3 Light-dependent nuclear exclusion of COP1 requires SPA proteins

Nuclear YFP-COP1 maintains the ability to form nuclear photobodies in dark-grown *spaQn* mutant seedlings. However, it is conceivable that SPA proteins may be required for the nuclear exclusion of YFP-COP1 in the light. To this end, YFP-COP1 fluorescence was investigated in light-grown seedlings in the *SPA* wild-type and the *spaQn* mutant next. As shown above, no speckles could be detected in nuclei of hypocotyl cells of light-grown *SPA* wild-type seedlings. Surprisingly, however, nuclear YFP-COP1 containing photobodies could be detected in light-grown *spaQn* seedlings (Figure 3.11a). Quantification of nuclear YFP fluorescence confirmed that *spaQn* seedlings showed significantly

higher YFP-COP1 fluorescence in light-grown seedlings than the *SPA* wild-type, indicating that YFP-COP1 is retained in the nucleus in the light when SPA proteins are not present (Figure 3.11b, quantification performed on microscopy pictures generated by Dr. Martin Balcerowicz). Additionally, nuclear YFP-COP1 fluorescence of dark-grown *SPA* wild-type seedlings was compared with light-grown *spaQn* seedlings (Figure 3.11c). Quantification of YFP signals revealed that nuclear YFP-COP1 fluorescence intensity was even higher in light-grown *spaQn* seedlings than in dark-grown *SPA* wild-type seedlings, suggesting that YFP-COP1 is retained in nuclear photobodies in the light when SPA proteins are disabled, similar to dark-grown wild-type seedlings (Figure 3.11d, quantification performed on microscopy pictures generated by Dr. Martin Balcerowicz). Taken together, these results indicate that SPA proteins are required for the nuclear exclusion of COP1 in the light.
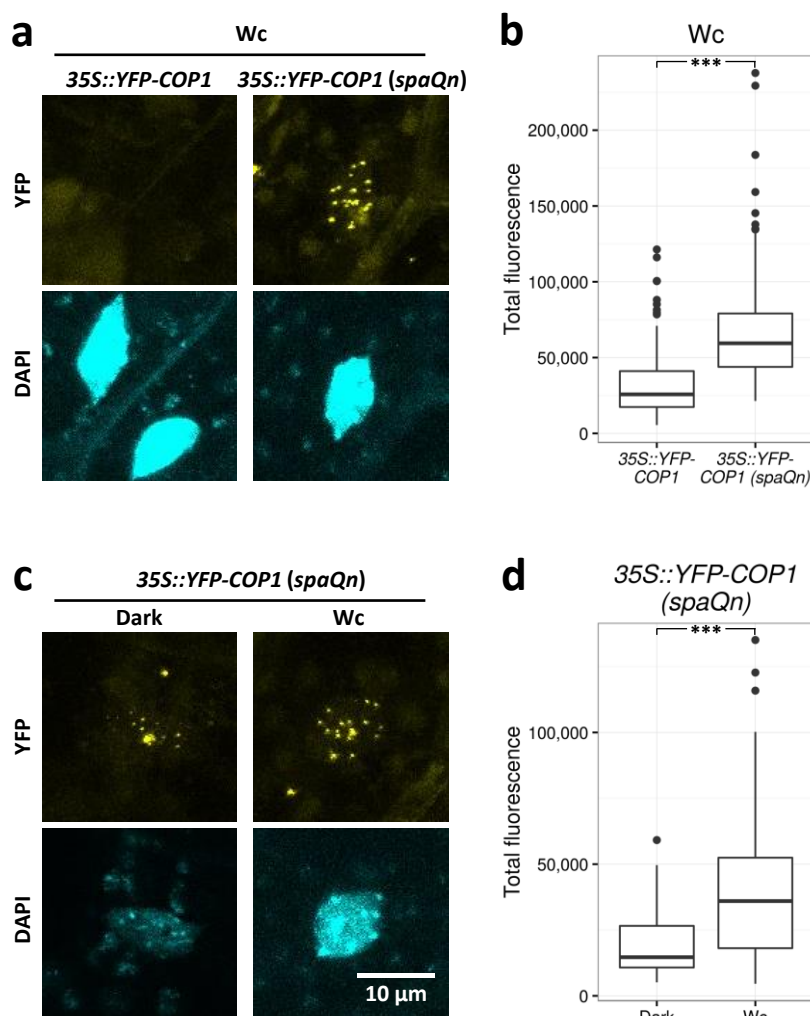
Figure 3.11: Light-dependent nuclear exclusion of COP1 requires SPA proteins.

(a) Representative images of nuclei in hypocotyl cells of transgenic *35S::YFP-COP1* and *35S::YFP-COP1 (spaQn)* seedlings grown in 40 µmol m^{-2} s^{-1} of continuous white light for 4 days. **(b)** Nuclear YFP fluorescence of nuclei in hypocotyl cells of the same genotypes and growth conditions described in (a). 146 or 208 nuclei from 8 to 10 different seedlings were analyzed from *35S::YFP-COP1* and *35S::YFP-*

COP1 (spaQn), respectively. 0% of nuclei in *35S::YFP-COP1* seedlings showed speckles, whereas 97% of nuclei in *35S::YFP-COP1 (spaQn)* seedlings showed speckles. quantification performed on microscopy pictures generated by Dr. Martin Balcerowicz. **(c)** Representative images of nuclei in hypocotyl cells of transgenic *35S::YFP-COP1 (spaQn)* seedlings grown either in darkness or 40 µmol m^{-2} s^{-1} of continuous white light for 4 days. **(d)** Nuclear YFP fluorescence intensity of the same nuclei depicted in (c). In total, 106 or 169 nuclei from 8 to 10 *35S::YFP-COP1 (spaQn)* dark- or light-grown seedlings, respectively, were analyzed. 78% and 97% of nuclei from *35S::YFP-COP1* and *35S::YFP-COP1 (spaQn)*, respectively, showed speckles. quantification performed on microscopy pictures generated by Dr. Martin Balcerowicz. Upper and lower hinges of boxplots represent the first and third quartiles, respectively. Whiskers extend from the hinges to the highest/lowest value within 1.5 * interquartile range (IQR). Data points which were higher or lower than this range are represented as dots. ***: true difference between means is not equal to 0 at *p < 0.001* in two-sample Student's *t* test.

The same tests that were utilized to evaluate data homogeneity for the datasets used in Figure 3.10 was performed for the datasets used in Figure 3.11 (Supplemental Figure S 9). As for the previous datasets, all data showed strong correlation between nuclear YFP-fluorescence and volume, with no R² value lower than 0.86. Only the dataset obtained from light-grown *SPA* wild-type seedlings followed a normal distribution according to Shapiro-Wilk test, while the other three datasets may be distributed otherwise. Strikingly, all datasets obtained from seedlings with a photomorphogenic phenotype (with the only exception of light-grown seedlings in the *SPA* wild type background in the experiment described in Figure 3.11) may or may not follow a normal distribution, while data obtained from seedlings with a skotomorphogenic phenotype are likely normally distributed. Further analysis is necessary to determine whether this may be a causal factor for the lack of normally distributed data in these datasets.

3.2.4 Differential SPA-dependent patterns of nuclear COP1 localization are likely not caused by changes in protein levels

Even though differences in COP1 subcellular localization were observed between the *SPA* wild-type and the *spaQn* mutant, it is possible that this is caused by variations in protein concentration – due to either changes in expression or protein stability -, rather than nucleocytoplasmic partitioning of COP1. YFP-COP1 levels do not significantly differ between light- and dark-grown *35S::YFP-COP1* lines in the *SPA*-wild type or *spaQn* background (Balcerowicz et al., 2017). To confirm that this is not an artifact of this transgenic line, total protein was isolated from light- and dark-grown wild-type and *spaQn* seedlings and native COP1 protein levels were detected. No significant differences in native COP1 protein levels were detected between *spaQn* and wild-type seedlings, irrespective of light condition, indicating that the differences in COP1 photobody formation between wild-type and *spaQn* are likely not due to changes in COP1 protein levels, but rather due to differential nucleocytoplasmic partitioning of COP1 (Figure 3.12).
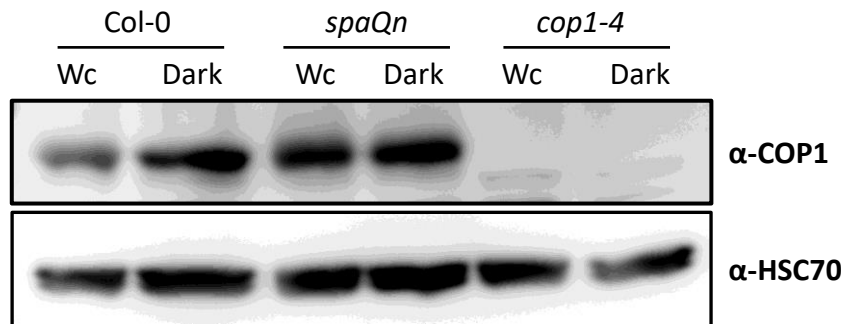
Figure 3.12: Differential SPA-dependent patterns of nuclear COP1 localization are likely not caused by changes in protein levels.

Immunodetection of COP1 protein levels in either wild-type, *spaQn* or *cop1-4* seedlings grown in 40 µmol m^{-2} s^{-1} or darkness for 4 days. HSC70 was used as a loading control. Proteins were detected with anti-COP1 and anti-HSC70 antibodies.

3.2.5 Red, far-red, and blue light differentially affect COP1 nucleocytoplasmic partitioning

The results described above indicate that SPA proteins are required for the nuclear exclusion of YFP-COP1 in white light. Because white light is composed of all visible colors of the light spectrum and thus is perceived by many different photoreceptors in Arabidopsis, it is unclear whether this mechanism is controlled by specific photoreceptors. Previous studies have shown that nucleocytoplasmic partitioning of GUS-COP1 occurs to varying degrees of effectiveness in R, FR and B (Osterlund and Deng, 1998). Thus, in order to investigate the role of SPA proteins of nuclear accumulation of COP1 under monochromatic light, YFP-COP1 photobody formation was investigated in either *SPA* wild-type or *spaQn* seedlings grown in either continuous R, FR, or B (Rc, FRc, Bc, respectively). First, in the *SPA* wild-type background, YFP-COP1 formed nuclear photobodies in dark-grown seedlings, whereas no photobodies were detected in seedlings grown in either FRc or Bc, which is similar to seedlings grown in continuous white light (Figure 3.13a). Surprisingly, however, strong nuclear accumulation of YFP-COP1 into photobodies was detected in *SPA* wild-type seedlings grown in Rc, suggesting that Rc is not sufficient to trigger the light-dependent nuclear exclusion of YFP-COP1 (Figure 3.13a). A fluence rate of Rc emitted from LED lights of 60 µmol m^{-2} s^{-1} was used in this experiment, which should activate phyB molecules sufficiently. Curiously, this suggests that nuclear exclusion of YFP-COP1 may be phyB-independent, at least in this transgenic line.
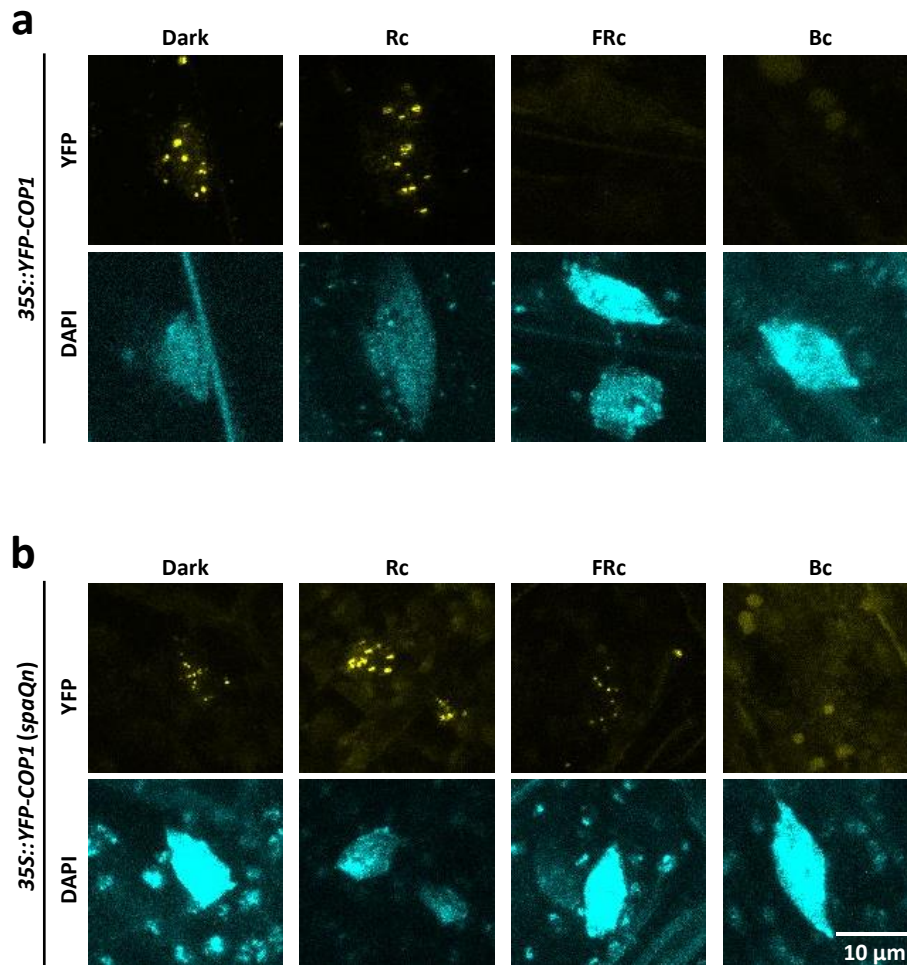
Figure 3.13: Red, far-red and blue light differentially affect COP1 nucleocytoplasmic partitioning.

(a+b) Representative pictures of nuclei from hypocotyl cells of *35S::YFP-COP1* (a) or *35S::YFP-COP1 (spaQn)* (b) seedlings grown either in darkness, 60 µmol m^{-2} s^{-1} Rc, 3 µmol m^{-2} s^{-1} FRc or 50 µmol m^{-2} s^{-1} Bc.

In the *spaQn* background, hypocotyl cells accumulated nuclear YFP-COP1 in seedlings grown in the dark, in Rc and in FRc (Figure 3.13b). This is consistent with previous results which have shown that in the *spaQn* background, YFP-COP1 still accumulated into nuclear speckles in white light. Thus, FRc triggers the nuclear exclusion of YFP-COP1 in a SPA-dependent manner, whereas Rc was not sufficient to cause the nuclear exclusion of YFP-COP1 both in the *SPA* wild-type and the *spaQn* background in this transgenic line. Interestingly, similar to the *SPA* wild-type background, no nuclear YFP-COP1 photobodies were detected in the *spaQn* background, indicating that the Bc-mediated nuclear exclusion of YFP-COP1 may be SPA-independent (Figure 3.13b). This is in contrast to the results obtained from seedlings grown in continuous white light (which contains blue light), in which nuclear YFP-COP1 photobodies were detected in the *spaQn* background, suggesting that nucleocytoplasmic

partitioning of YFP-COP1 in white light may be orchestrated by a complex interplay between different photoreceptors.

3.2.6 Photobody formation of YFP-SPA1 is abolished in Arabidopsis seedlings grown in white light, but not in red, far-red, or blue light

The results described above indicate that SPA proteins are required for the light-induced nuclear exclusion of COP1, at least in white and far-red light. However, light dependent nucleocytoplasmic partitioning of SPA proteins themselves, despite being a topic of scientific discourse, has not been investigated yet (Menon et al., 2016). Notably, the SPA1 peptide sequence contains two nuclear localization signals (NLS), one bipartite NLS in its kinase domain and one SV40-type NLS in the CC domain, but no cytosolic localization signal (CLS) (Hoecker et al., 1999). Nevertheless, light-induced nuclear depletion of SPA1 is still conceivable through other mechanisms such as via light-regulated shuttle proteins.
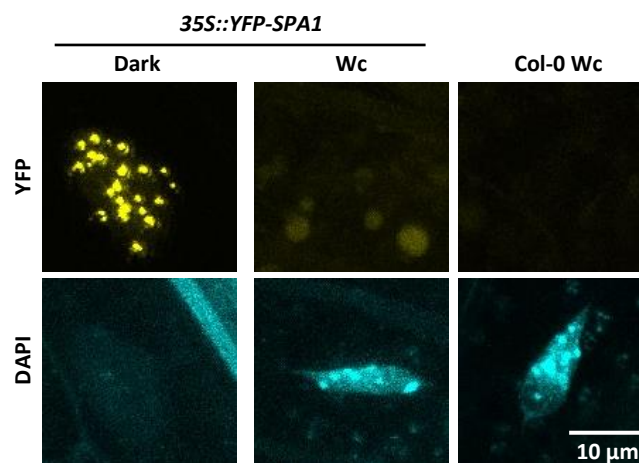
Figure 3.14: Photobody formation of YFP-SPA1 is abolished in seedlings grown in continuous white light.

Representative images of nuclei from hypocotyl cells of *35S::YFP-SPA1 (spa1-7)* or wild-type seedlings grown either in darkness or 40 µmol m^{-2} s^{-1} of continuous white light.

To investigate light-dependent nuclear accumulation of SPA1, a transgenic Arabidopsis line containing a *35S::YFP-SPA1* transgene in the *spa1* mutant background was grown under various light conditions and submitted to microscopic imaging (transgenic line generated by Dr. David Sheerin (Sheerin et al., 2015)). In dark-grown seedlings, nuclear YFP-SPA1 speckles were detected in transgenic hypocotyl cells, confirming that SPA1 accumulates into nuclear photobodies in darkness (Figure 3.14). Interestingly, however, no YFP speckles were detected in white light-grown seedlings (Figure 3.14). Nuclear YFP fluorescence in white light-grown seedlings was indistinguishable from the wild-type

grown in the same light condition, suggesting that YFP-SPA1 may not be localized in the nucleus in this transgenic line. Previous reports have shown that SPA1 is partially degraded in the light (Balcerowicz et al., 2011), however, because nuclear YFP-SPA1 was totally absent in the light, it is conceivable that non-degraded SPA1 is depleted from the nucleus in white light.
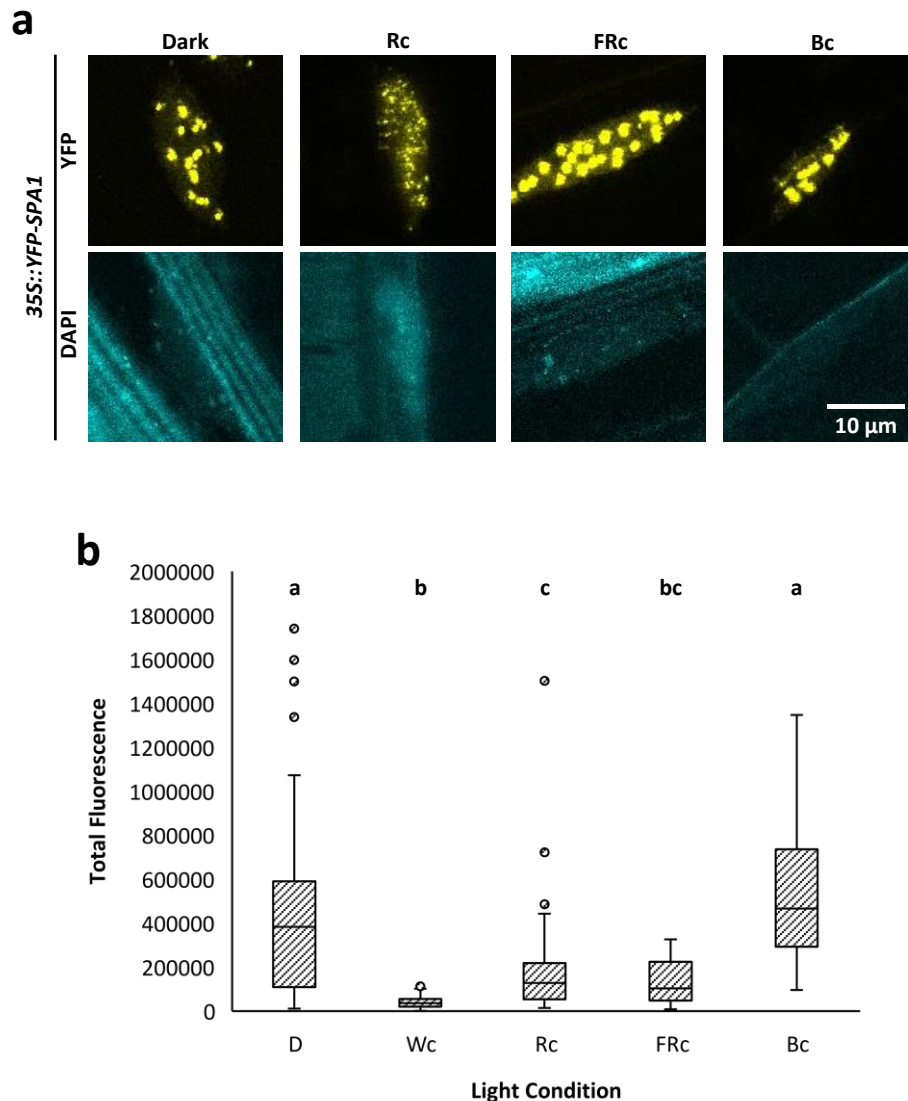
Figure 3.15: Photobody formation of YFP-SPA1 is retained in seedlings grown in Rc, FRc, and Bc.

(a) Representative pictures of nuclei from hypocotyl cells of transgenic *35S::YFP-SPA1 (spa1-7)* seedlings grown in either darkness, 60 µmol m^{-2} s^{-1} Rc, 3 µmol m^{-2} s^{-1} FRc or 50 µmol m^{-2} s^{-1} Bc for 4 days. **(b)** Quantification of nuclear YFP fluorescence in nuclei of hypocotyl cells of transgenic *35S::YFP-SPA1 (spa1-7)* seedlings grown in the same growth conditions described in (a) with the addition of 40 µmol m^{-2} s^{-1} of continuous white light for 4 days. In total, 51, 74, 25, 24 and 17 nuclei from 3 to 14 seedlings were analyzed for seedlings grown in darkness, Wc, Rc, FRc and Bc, respectively. Upper and lower hinges of boxplots represent the first and third quartiles, respectively. Whiskers extend from the hinges to the highest/lowest value within 1.5 * interquartile range (IQR). Data points which were higher or lower than this range are represented as dots. Groups marked with the same letter are not

significantly different, as determined by one-way ANOVA followed by two-sided Tukey test ($p < 0.05$). Data analysis performed by Annika Luebbe (Luebbe, 2016).

Previous results have shown that nuclear YFP-SPA1-containing photobodies are retained in seedlings shifted from darkness to FR for 6 hours or to FR for 6 hours and then to R for an additional 6 hours, indicating that SPA1 is not rapidly depleted from the nucleus upon FR or R exposure (Sheerin et al., 2015). Thus, since seedlings grown in continuous white light do not retain nuclear SPA1 photobodies, nuclear depletion of SPA1, either by degradation or nucleocytoplasmic partitioning, is either a slow process or contingent on other signals besides FR or R. First, to further investigate the mechanisms of light-dependent nuclear depletion of SPA1, transgenic YFP-SPA1 expressing lines were grown in darkness for 4 days and subsequently shifted either to R or FR for 6 hours, or to FR for 6 hours followed by an additional 6 hours of R treatment. Nuclear YFP-SPA1 speckle formation was detected in seedlings grown in all conditions, demonstrating that the results from Sheerin *et al*., 2015 are reproducible (Supplemental Figure S 10). Next, YFP-SPA1 speckle formation in seedlings grown in continuous monochromatic light conditions was investigated. Curiously, YFP-SPA1-containing speckles were detected in hypocotyl cells of transgenic seedlings grown in Rc, FRc and Bc, indicating that light-dependent nuclear depletion of SPA1 may not be contingent on the length of light exposure (Figure 3.15a). To investigate whether continuous treatment of monochromatic light induced quantitative instead of qualitative changes in nuclear YFP-SPA1 fluorescence, YFP fluorescence in DAPI-stained nuclei of seedlings grown in either darkness, Rc, FRc, Bc or continuous white light was measured. As expected, nuclear YFP fluorescence was significantly reduced in seedlings grown in continuous white light when compared to dark-grown seedlings (Figure 3.15b, data analyses performed by Annika Luebbe (Luebbe, 2016)). Intriguingly, nuclear YFP fluorescence was also significantly reduced in seedlings grown in Rc and FRc, contrary to the finding that nuclear speckles were detected in these conditions. Nuclear YFP fluorescence in seedlings grown in Rc was lower than in darkness, but still significantly higher than in white light, while fluorescence in seedlings grown in FRc was as low as in white light. In contrast, YFP-fluorescence in seedlings grown in Bc was as high as in dark-grown seedlings, which is consistent with the retention of YFP-containing nuclear speckles in seedlings grown in Bc. Taken together, these results suggest that nuclear exclusion of YFP-SPA1 may be controlled by a complex interplay between photoreceptors. Further analysis is required to determine whether this process involves SPA1 degradation, nucleocytoplasmic partitioning, a combination of both or other mechanisms.

4 DISCUSSION

4.1 STRUCTURAL AND FUNCTIONAL DIVERGENCE OF THE COP1 AND SPA1 WD-REPEAT DOMAIN.

In this study, both theoretical and experimental evidence was provided to support the hypothesis that the Arabidopsis COP1 and SPA1 WD-repeat domain possess both structural and functional differences. SPA proteins have partially redundant and partially distinct functions (Laubinger et al., 2004). Additionally, the WD-repeat domains of SPA proteins are, at least in terms of sequence homology, more similar to each other than they are to COP1, whereas SPA1 is the most similar to COP1 out of the four SPAs. Therefore, to reduce redundant work, only the SPA1 WD-repeat domain was analyzed for comparative studies with COP1.

4.1.1 The SPA1 WD-repeat domain may contain structural differences to COP1.

The SPA1 WD-repeat domain is very similar to COP1 in terms of sequence homology (45% sequence identity, Figure 3.1a). Earlier studies have described X-ray structure of the COP1 WD-repeat domain in great detail and found that it is comprised of a seven-bladed propeller with four β-sheet structures connected by loops comprising each propeller blade (Uljon et al., 2016; Lau et al., 2019). The interaction between human and Arabidopsis COP1 and Trib1 was also described in one of these studies, including residues within the COP1 WD-repeat domain which contribute to COP1-Trib1 binding (Uljon et al., 2016). To identify potential differences in the function of the COP1 and SPA1 WD-repeat domain, the conservation of all residues which contribute to COP1-Trib1 binding, including residues which have not been described in previous publication, was investigated in SPA1 (Table 3.1). Four residues which were not conserved in SPA1 were identified. Out of these, COP1 H528 (homologous to SPA1 Y873) has been reported to form a salt bridge to HY5 E45 in COP1-HY5 co-crystals (Lau et al., 2019), which may potentially result in differential interaction dynamics of COP1-HY5 and SPA1-HY5. Interestingly, COP1 H528 has not been reported to be essential for the interaction between Arabidopsis COP1 and Trib1. Thus, although the VP motif required for COP1 interaction is relatively conserved among most known COP1 substrates and other interacting proteins, it is possible that different COP1-interacting proteins may 1) have different interaction dynamics among each other, and 2) show different affinities to the COP1 and SPA1 WD-repeat domains. The hypothesis that VP motifs contained within different COP1 and SPA1-interacting proteins may have differential binding affinities is further substantiated by the finding that the light-activated photoreceptors cry1 and UVR8 are able to disrupt the interaction between COP1 and the substrates PAP2 and HY5, respectively (Ponnu et al., 2019; Lau et al., 2019). UV-B activated UVR8 especially has been shown to fully disrupt the COP1-HY5 interaction in yeast 3-hybrid assays, which demonstrates that activated UVR8 may have a higher binding affinity to COP1 than HY5, at least *in vitro*. Similarly, considering that some COP1 residues

which contribute to COP1-ligand binding are not conserved in SPA1, it is possible that VP-containing peptides may have differential binding affinities to COP1 and SPA1, potentially altering precise functions of its WD-repeat domains.

To analyze possible structural differences between the COP1 and SPA1 WD-repeat domains, a homology model of the SPA1 WD-repeat domain was generated in this study. The homology model was based of the structural data of the COP1 WD-repeat domain from Uljon *et al.*, 2016. As expected, the homology model predicts that the SPA1 WD-repeat domain also forms a seven bladed β-propeller structure (Figure 3.1c) that is very similar to COP1. However, when comparing the COP1 X-ray structure with the SPA1 homology model, two types of structural differences were identified: First, two residues that likely contribute to COP1-TRIB1 binding are positioned slightly different in the SPA1 homology model. Notably, among those is the residue COP1 H528/SPA1 Y873, which has been shown to contribute to COP1-HY5 binding, providing further evidence that binding properties of the COP1 and SPA1 WD-repeat domain may differ depending on the substrate. Second, two major structural differences have been identified, labeled indel1 and indel2 (Figure 3.1a, c and e).

Indel1 is a stretch of 8 amino acids absent in COP1, which forms an unstructured loop at the bottom face of the propeller structure. Since the VP-binding pocket is on the top face, it is unlikely, although not impossible, that this structural difference may lead to differential binding properties between COP1 and SPA1. However, it is worth noting that some proteins may not interact on the top surface of the propeller structure. The proteins DDB1A and DDB1B, for example, whose interaction with COP1 is essential for COP1 function, are comprised of three WD-repeat domains (BPA, BPB and BPC). While it is currently unclear which domain is essential for the interaction with COP1 and SPA1, point mutations in the BPB region have been shown to reduce COP1-DDB1B interaction strength *in vivo* (Chen et al., 2010). Notably, the BPB motif does not contain any VP motifs. Furthermore, since the COP1-DDB1 interaction is essential for COP1 activity, and active COP1 binds its targets at its VP-binding pocket (i.e. both interactions need to occur simultaneously), it is unlikely that DDB1 interacts with COP1 via the same mechanism as COP1 substrates. It has previously been proposed that COP1 and SPAs interact with DDB1 via a WDxR motif which is conserved in many DCAFs (Chen et al., 2006; Zhang et al., 2008; Chen et al., 2010), however, this view has recently been challenged because X-ray analysis has shown that this motif is not on the surface of the COP1 WD-repeat structure (Uljon et al., 2016). Therefore, the exact mechanisms of COP1-DDB1 and SPA-DDB1 binding are currently unclear, and the elucidation of these via COP1-DDB1 co-crystals would be a worthwhile investigation. Indel1 may therefore differentially affect binding affinities of COP1 and SPA1 with proteins which interact with their WD-repeat domains via mechanisms other than VP-motif interaction.

Indel2 is a small disordered stretch on the top-face of the propeller comprised of three residues which are not conserved in Arabidopsis COP1. This region is not part of the COP1 VP-binding pocket. However, X-ray structural studies have so far only used small VP-containing peptides of COP1 substrates for co-crystallization analysis. Thus, because proteins which interact with COP1 and SPA1 are considerably larger *in vivo*, even structural changes at the top-face of the propeller that are not in direct proximity to the VP-binding pocket can differentially affect binding affinity to other proteins. Furthermore, the finding that indel2 is conserved in human COP1 and Arabidopsis SPA1, but not in Arabidopsis COP1, may provide further insights about the evolutionary history of SPA proteins. Notably, whereas COP1 is conserved in humans and most other eucaryotes, SPA proteins are specific to the green lineage and therefore do not exist in humans. Given that SPA proteins show high degrees of conservation even in early diverging land plants such as *Physcomitrium patens*, the origins of *SPAs* are yet to be elucidated (Ranjan et al., 2014; Artz et al., 2019). Taken together, structural differences between the COP1 X-ray model and the homology model of the SPA1 WD-repeat domain demonstrate the potential basis for functional divergence between the two domains.

4.1.2 The SPA1 WD-repeat domain is essential for COP1/SPA function in darkness

To delineate functional differences between the COP1 and SPA1 WD-repeat domains *in vivo*, chimeric COP1/SPA1 proteins that had their respective WD-repeat domains swapped with each other were expressed in either Arabidopsis *cop1* single or *spa1 spa2 spa3* triple mutants. Similar experimental setups have previously provided insights on the functional divergence of cryptochromes, BBX proteins as well as SPA1 and SPA2 (Ahmad et al., 1998a; Job et al., 2018; Chen et al., 2016). This experimental approach provided a unique possibility of studying function of the COP1 and SPA1 WD-repeat domains in isolation *in vivo*. Assuming that the model that COP1 and SPA form a tetrameric complex consisting of two COP1 and two SPA proteins by interaction via their CC domains is correct (Zhu et al., 2008), the expression of chimeric hybrids which still possess the CC domain of the original protein in *cop1* or *spa* mutants yields a scenario where a typical tetrameric COP1/SPA complex can still be formed with the respective native proteins, but each tetrameric complex contains only one type of WD-repeat domain (Figure 4.1). In other terms, CC1 proteins expressed in the *cop1-4* mutant may form a tetrameric complex with native SPA proteins containing only SPA WD-repeat domains, whereas 11C proteins expressed in *spa1 spa2 spa3* triple mutants can hypothetically form a tetrameric complex with native COP1 containing only COP1 WD-repeat domains. It still remains to be tested experimentally whether these tetrameric complexes do indeed assemble as expected in transgenic plants; nevertheless, this experimental approach likely provides the opportunity to study the mode of action of singular functional WD-repeat domains *in vivo*.
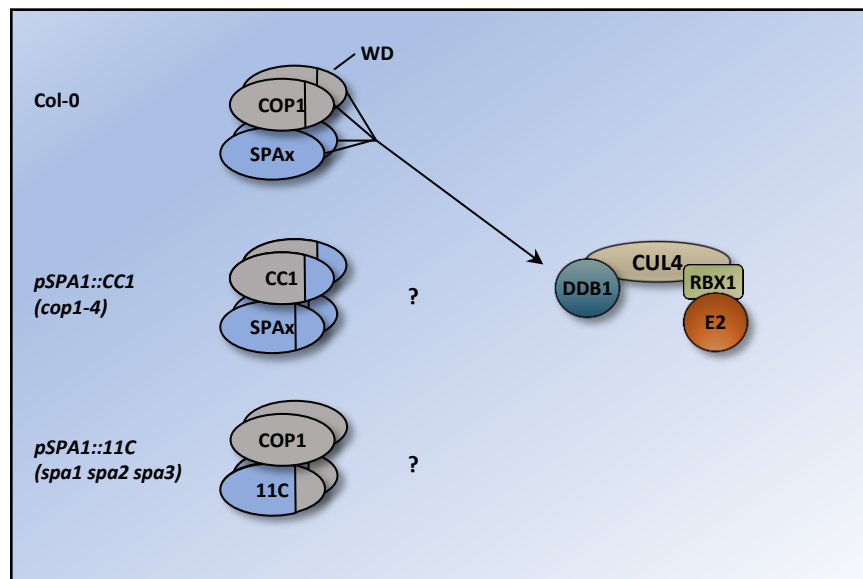
Figure 4.1: Model for the types of configurations of COP1/SPA complexes in transgenic plants expressing chimeric COP1/SPA1 domain-swap proteins.

COP1 and SPA proteins are assumed to form tetrameric complexes containing two COP1 proteins and two SPA proteins of any combination between the four SPA homologs (SPAx) with their respective CC domains in darkness (Chen et al., 2010). In the wild-type, tetrameric COP1/SPA complexes therefore contain two COP1 and two SPAx WD-repeat domains. In this configuration, COP1/SPA interacts with the bridging protein DDB1 to form the higher order CUL4-DDB1COP1/SPA E3 ligase complex by DDB1 association with the COP1 and SPA WD-repeat domains. Although both WD-repeat domains physically interact with DDB1 *in vitro*, it is unclear whether the COP1/SPA complex requires both types of WD-repeat domains to associate with DDB1 and thereby act as a substrate recognition module for CRL4 complexes *in vivo*. In transgenic plants expressing *CC1* in a *cop1* mutant background, endogenous COP1 is replaced by COP1 containing SPA1 WD-repeat domains. Therefore, tetrameric COP1/SPA complexes still assemble by physical interaction of COP1 and SPA CC domains, but only contain SPAx WD-repeat domains. Since expression of *CC1* rescues the short hypocotyl phenotype of *cop1* mutants in darkness, CC1/SPA complexes seem to be functional with regards to suppression of photomorphogenesis in darkness. In transgenic plants expressing *11C* in a *spa1 spa2 spa3* triple mutant background, endogenous SPAs (except for SPA4) are replaced by SPA1 containing COP1 WD-repeat domains. Therefore, tetrameric COP1/SPA complexes assemble as normal, but contain only COP1 WD-repeat domains. Since expression of *11C* does not rescue the short hypocotyl phenotype of *spa1 spa2 spa3* triple mutants in darkness, COP1/11C complexes do not seem to be functional.

Whereas COP1 proteins with a SPA1 WD-repeat domain showed a high degree of complementation of the *cop1-4* mutant phenotype in dark-grown seedlings, the inverse chimeric protein did not complement the mutant phenotype of dark-grown *spa1 spa2 spa3* seedlings (Figure 3.4). This indicates that the SPA1, but not the COP1 WD-repeat domain, is indispensable for function of the COP1/SPA complex in darkness. This result provides further proof for the hypothesis that the COP1 and SPA1 WD-repeat domains are, although structurally similar, functionally divergent. Furthermore, differential functions of the COP1 and SPA1 WD-repeat domains could provide insights into the question of how SPA proteins enhance COP1 activity. Since SPA proteins are required for COP1 function, a prevalent theory is that SPA proteins are COP1 enhancer proteins, but the exact mechanism

for such a model is currently unknown (Lau and Deng, 2012). One possibility is that, although most proteins that physically interact with the COP1 WD-repeat domain also interact with the SPA1 WD-repeat domain *in vitro*, SPA proteins may be required for certain interactions to occur *in vivo*. Further studies utilizing the transgenic lines generated in this study could investigate this hypothesis.

In the light, transgenic lines expressing *CC1* only partially recover the *cop1* mutant phenotype, whereas plants expressing *11C* do not complement the *spa1 spa2 spa3* triple mutant phenotype. Strikingly, this is true for seedlings grown in Rc, FRc and Bc, indicating that the observed responses are likely not contingent on specific photoreceptors (Figure 3.4). Given that all tested photoreceptor signaling pathways are affected to roughly equal amounts in domain-swap lines, it is likely that COP1/SPA-photoreceptor interactions are not affected by swapping of WD-repeat domains. This is substantiated by the finding that both chimeric proteins still co-localize into nuclear speckles with phyA, phyB, cry1 and cry2 to similar degrees as full-length COP1 and SPA1 (Supplemental Figure S 2, S 3, S 4 and S 5). However, it remains to be tested whether photoreceptors in fact do interact with chimeric proteins *in vivo* as well. Thus, disruption of interactions other than with photoreceptors are more likely the cause of the phenotypes observed in transgenic domain-swap lines, since they would affect photomorphogenic growth independent of light color. To this end, it is possible that the interaction of COP1 and SPA1 with the linker protein DDB1 or with specific downstream targets of the COP1/SPA complex may be differentially affected in domain-swap lines; however, further studies are required in order to elucidate which interactions are specifically affected *in vivo*. In conclusion, the SPA1 WD-repeat domain's essential function in the suppression of photomorphogenesis both in darkness and in light is likely independent of specific photoreceptors in the seedling stage.

4.1.3 Adult phenotypes of transgenic domain-swap lines show an essential function of the SPA1 WD-repeat domain in the suppression of photoperiodic flowering

Transgenic plants expressing chimeric *CC1* showed partial complementation of *cop1* mutant phenotypes in the adult stage, such as early flowering and reduced petiole elongation in short day conditions and reduced rosette sizes (Figure 3.5). This is consistent with phenotypic data obtained from seedlings, which showed only partial complementation in the light as well. Thus, the SPA1 WD-repeat domain can, at least partly, replace the function of the COP1 WD-repeat domain in terms of photoperiodic flowering, petiole elongation and leaf growth, indicating again that the two domains are not interchangeable with regards to certain functions. The COP1/SPA complex mainly regulates photoperiodic flowering by targeting the inducer of flowering CO for degradation in short photocycles (Jang et al., 2008; Liu et al., 2008b). Both COP1 and SPA1 can physically interact with CO *in vitro*, and both are required for the targeted destabilization of CO *in vivo*, evidenced by the fact that expression

of the florigen *FLOWERING LOCUS T* (*FT*) is induced both in *cop1-4* mutants as well as in higher order *spa* mutants in short day (Jang et al., 2008; Liu et al., 2008b; Laubinger et al., 2006). It is unclear why COP1/SPA complexes containing only SPA1 WD-repeat domains cannot fully rescue the early flowering phenotypes of *cop1* mutants, given that both WD-repeat domains are able to interact with CO. One possible explanation is that the combination of COP1 and SPA1 WD-repeat domains within the COP1/SPA complex create a cooperative binding effect to certain substrates such as CO, possibly by creating an additional binding surface which only exists if both WD-repeat domains are present. Such a cooperative binding model would explain why the SPA1 WD-repeat domain by itself is unable to fully complement the function of the corresponding COP1 domain in terms of control of photoperiodic flowering. Future studies may be able to elucidate differential binding affinities of the COP1 and SPA1 WD-repeat domain to CO, as well as potential evidence of cooperative binding, by utilizing transgenic COP1/SPA1 domain-swapped lines.

Curiously, plants expressing chimeric *11C* in *spa1 spa2 spa3* triple mutants were not only unable to complement the early flowering mutant phenotype in short day, but rather flowered even earlier than the mutant (Figure 3.6). This dominant negative effect was only visible in the adult stage. Whereas *11C* was unable to complement the mutant phenotype of *spa1 spa2 spa3* triple mutant seedlings in darkness and in the light, no degree of dominant negative effect could be observed. *spa1 spa2 spa3* triple mutant seedlings are not fully de-etiolated in darkness and do not flower as early as *spa1 spa2 spa3 spa4* quadruple mutant in short day (Ordoñez-Herrera et al., 2015). This indicates that, despite the capacity for a dominant negative effect to show in this line, no such effect manifested in the seedling stage. This disparity may possibly be explained by the activity of SPA4, which has been shown to play a dominant role in the adult stage rather than the seedling stage (Laubinger et al., 2004). Notably, *spa1 spa2 spa3* triple mutants flower considerably later in short day conditions than *spa1 spa2 spa3 spa4* quadruple mutants, which illustrates the role of *SPA4* in the regulation of photoperiodic flowering. Assuming that 11C is a non-functional version of SPA1 because the COP1 WD-repeat domain cannot replace some functions of the SPA1 WD-repeat domain, it is possible that 11C evicts SPA4 from COP1/SPA complexes, thereby disrupting SPA4-mediated suppression of photoperiodic flowering. This does not, however, explain why 11C is unable to suppress the slightly elongated hypocotyl phenotype of *spa1 spa2 spa3* triple mutants in dark-grown seedlings. If 11C were to interfere with the activity of SPA4 in general, a similar dominant negative effect would be expected to manifest in dark-grown seedlings. 11C may therefore a) interfere specifically with the functions of SPA4 which only affect the regulation of photoperiodic flowering or other phenotypes in the adult stage (e.g. by specifically interfering with the ability of SPA4 to target CO for degradation), or b) interfere specifically with mechanisms of regulating photoperiodic flowering that are independent of SPA4. A conceivable way of testing this hypothesis is to introgress the *11C* transgene into the *spa1*

spa2 spa3 spa4 quadruple mutant background. If no similar dominant negative effect of *11C* can be observed in this background, 11C likely specifically disrupts the ability of SPA4 to regulate photoperiodic flowering. Nevertheless, the finding that transgenic plants expressing *11C* in higher order *spa* mutant backgrounds are unable to complement the early flowering phenotype in short day conditions provides further evidence for the functional divergence of the COP1 and SPA1 WD-repeat domain.

4.1.4 Accumulation of native HY5 and COP1 demonstrates that domain swap proteins partially disrupt molecular functions of the COP1/SPA complex

Dark-grown transgenic seedlings expressing *CC1* in the *cop1* mutant background accumulate native HY5 protein almost to a similar degree as light-grown wild-type seedlings (Figure 3.8a). However, this accumulation of HY5 does not seem to be sufficient to promote de-etiolated growth in darkness in these transgenic lines. Thus, although *CC1* seems to fully complement the *cop1* mutant phenotype in dark-grown seedlings, it does not seem to do so on the molecular level. This is interesting because many hypocotyl elongation responses seem to be dosage-dependent. For example, hypocotyl length is directly dependent on light intensity in wild-type seedlings, and the degree of COP1 overexpression strongly correlates with hypocotyl length in in seedlings grown in FRc or Rc (McNellis et al., 1994b). Thus, it is curious that dark-grown transgenic seedlings expressing full-length *COP1* show the same degree of hypocotyl elongation as dark-grown seedlings expressing *CC1*, whereas both lines accumulate HY5 protein to different degrees. It is possible that this is because accumulated HY5 does not reach a threshold to activate photomorphogenic growth responses, however there is no evidence that such a threshold exists. More likely, this discrepancy occurs because suppression of photomorphogenic growth in darkness is achieved by the targeted degradation of multiple photomorphogenesis-promoting transcription factors, HY5 being only one of them. Beyond HY5, the COP1/SPA complex also targets HYH, LAF1 and HFR1, all of which are positive regulators of photomorphogenesis (Osterlund et al., 2000; Holm et al., 2002; Seo et al., 2003a). The cumulative effect of partial destabilization of multiple photomorphogenesis-promoting transcription factors may result in a total loss of de-etiolated growth in dark-grown seedlings expressing *CC1*. Moreover, it is possible that HY5 specifically is more stable in seedlings expressing *CC1* because these plants exclusively contain SPA WD-repeat domains. As discussed in previous chapters, the residue COP1 H528, which is partly responsible for COP1-HY5 interaction by forming a salt-bridge with HY5 E45, is not conserved in SPA1. Assuming that this may result in a weaker affinity of HY5 to the SPA1 WD-repeat domain than to the homologous region of COP1, targeted destabilization of HY5 in transgenic *CC1* lines may be specifically affected. Thus, although a partial accumulation of HY5 can be detected,

de-etiolation responses may not be visible because other photomorphogenesis-promoting transcription factors might still be efficiently degraded. More extensive studies on the stability of these transcription factors in transgenic plants expressing chimeric COP1/SPA1 domain swap proteins are required to further elucidate the basis of this discrepancy.

Native COP1 protein was found to accumulate in dark-grown transgenic seedlings expressing *11C* (Figure 3.8b). Interestingly, COP1 does not accumulate in *spa1 spa2 spa3* triple mutant and *spa1 spa2 spa3 spa4* quadruple mutant seedlings, indicating that COP1 accumulation is not a result of missing SPA proteins. Rather, similar to the effect of *11C* on flowering time, the 11C protein seems to enact a dominant negative effect on COP1 accumulation. It is worth noting that the antibody used for COP1 immunodetection was raised against the N-terminal region of COP1 (Balcerowicz et al., 2011). Therefore, it is unlikely that COP1 immunodetection is increased because the COP1 antibody also detects degradation products of 11C, since only the C-terminal domain of COP1 is contained within this chimeric protein. Furthermore, qRT-PCR analysis demonstrated that the increase in COP1 protein abundance is not due to increased *COP1* expression. Thus, COP1 accumulation is likely the result of changes in post-translational mechanisms affecting COP1 protein stability, although the exact mechanism for 11C-dependent accumulation of COP1 is currently unknown. One possible explanation might be that COP1 autoubiquitination is disrupted by 11C. Autoubiquitination is a common characteristic of RING-based E3 ligases, although autoubiquitination and subsequent degradation of COP1 has not been demonstrated yet (Yang and Xiaodan, 2003; Wang et al., 2018b). If COP1 does indeed show autoubiquitination, it is likely that only enzymatically active COP1, i.e. COP1 molecules that are part of a functional higher order CUL4-DDB1$^{COP1/SPA}$ ligase complex, would ubiquitinate and therefore mark itself for degradation, whereas the pool of inactive COP1 molecules that exist within a given cell might accumulate. COP1 protein might be inactive if either a) COP1 is dissociated from the higher order CUL4-DDB1$^{COP1/SPA}$ complex, e.g. by light-regulated nucleocytoplasmic partitioning of COP1, or b) COP1 associates with non-functional CUL4-DDB1$^{COP1/SPA}$ complexes. This hypothetical is consistent with the finding that *cul4-1* mutants also accumulate native COP1 protein, since active CUL4-DDB1COP1/SPA complexes cannot be formed in this mutant. COP1 is therefore part of inactive COP1/SPA complexes and does not have autoubiquitination activity. Similarly, 11C might trap COP1 proteins in inactive COP1/11C complexes, which causes COP1 to accumulate in transgenic lines expressing this chimeric protein. However, this model does not explain why *spa1 spa2 spa3 spa4* quadruple mutants do not accumulate native COP1 protein. Since SPA proteins are essential for COP1 activity (Zhang et al., 2008), COP1 is not incorporated in active COP1/SPA complexes in the *spa1 spa2 spa3 spa4* quadruple mutant, which would increase the pool of inactive COP1 molecules and should therefore cause COP1 to accumulate. A possible explanation for this is that COP1 accumulates only when it is contained within inactive COP1/SPA complexes, which is likely the case both in the *cul4-1*

mutant and transgenic *11C* lines. In this case, however, the question of why inactive COP1 still has autoubiquitination activity in *spa1 spa2 spa3 spa4* quadruple mutants remains unanswered. Future investigations that study the autoubiquitination activity of COP1 in wild-type, *cul4-1*, *11C* transgenic plants and *spa1 spa2 spa3 spa4* quadruple mutants are required to fully understand the accumulation of COP1 protein in certain mutants.

In conclusion, both structural and functional analysis of the COP1 and SPA1 WD-repeat domains demonstrates that the COP1 and SPA1 WD-repeat domains are neither structurally identical nor functionally interchangeable, the SPA1 WD-repeat domain is essential for the suppression of photomorphogenesis in darkness, whereas the COP1 WD-repeat domain can be partially replaced by the homologous region of SPA1, and expression of *11C* in a higher order *spa* mutant background triggers dominant negative effects such as the acceleration of photoperiodic flowering in short day conditions, and the accumulation of native COP1 proteins in dark-grown seedlings. These results provide useful information on the unique function of SPA1 as an enhancer of COP1 activity. Further studies are required to determine the mechanistic basis for the requirement of the SPA1 WD-repeat domain in the suppression of photomorphogenesis.

4.2   Nucleocytoplasmic partitioning of COP1 and SPA1

The strong constitutive photomorphogenic phenotypes of *cop1* and higher order *spa* mutants clearly illustrate that both COP1 and SPAs are required for the suppression of photomorphogenesis in darkness mediated by activity of the COP1/SPA complex (Deng et al., 1991; Laubinger et al., 2004; Ordoñez-Herrera et al., 2015). But, whereas the role of COP1 as a RING-based E3 ubiquitin ligase is well established, the precise function of SPA proteins within the COP1/SPA complex remains unknown. Borne out of the observation that both the CLS and the SPA1-interacting region of COP1 map to the COP1 CC domain, the question was raised whether SPA proteins are required for the nuclear accumulation of COP1 (Stacey et al., 1999; Hoecker and Quail, 2001; Laubinger and Hoecker, 2003; Saijo et al., 2003; Chen et al., 2016). COP1 nucleocytoplasmic partitioning is a well-characterized mechanism for the regulation of COP1 activity (Osterlund and Deng, 1998; Pacín et al., 2014). Since COP1 activity is dependent on its localization in the nucleus (Stacey et al., 2000; Subramanian et al., 2004), nuclear export of COP1 rapidly decreases COP1 activity. To investigate whether SPA proteins are required for the nuclear accumulation of COP1, a YFP-transgene was introgressed into the *spaQn* mutant in previous studies (performed by Dr. Martin Balcerowicz). This enabled the analysis of the subcellular localization of YFP-COP1 in the absence of SPA proteins *in vivo*. While the mechanism of COP1 nucleocytoplasmic partitioning is well known, the light-dependent subcellular localization of SPA

proteins has not been thoroughly investigated yet (Menon et al., 2016). Since SPA proteins have partially distinct, but also partially redundant functions (Laubinger et al., 2004), the subcellular localization of SPA1 was investigated rather than all four SPAs. To this end, a transgenic line constitutively expressing *YFP-SPA1* in a *spa1* mutant background was utilized to study the subcellular localization of SPA1 in both light- and dark-grown seedlings.

4.2.1 SPA proteins are not required for the nuclear accumulation of COP1 in darkness

Interestingly, YFP-COP1 accumulated both in dark-grown *SPA* wild-type seedlings and in *spaQn* seedlings (Figure 3.10a, b), indicating that nuclear import and accumulation of COP1 is not dependent SPA proteins. Furthermore, photobody formation of YFP-COP1 was not visibly reduced in the *spaQn* mutant background. Thus, SPA proteins are likely not required for the nuclear translocation and photobody formation of COP1. This demonstrates that either the COP1 NLS is sufficient for the nuclear import of COP1 in darkness by overcoming COP1 nuclear export signals from the CLS, or other proteins regulate COP1 nucleocytoplasmic partitioning by currently unknown mechanisms. Since COP1 possesses both a CLS and an NLS, it is unlikely that the two signals regulate light-dependent nucleocytoplasmic partitioning autonomously. COP1 activity is not known to be regulated by light directly, which makes it unlikely that COP1 nucleocytoplasmic partitioning is regulated by COP1 itself. There is, however, evidence that other proteins besides SPAs can regulate the nuclear accumulation of COP1: One study has found that GUS-COP1 is not localized in the nucleus in *csn* mutants, and the CSN subunit CSN1 promotes the nuclear accumulation of COP1 (Wang et al., 2009). Thus, nuclear accumulation and photobody formation of COP1 is likely regulated by COP1-interacting proteins apart from SPAs.

4.2.2 Retention of nuclear COP1 in *spaQn* reveals disparity between photobody formation and activity of COP1

Light exposure triggers the nuclear exclusion of COP1. In early studies, this process was believed to be slow, but more recent studies have demonstrated that nuclear exclusion of COP1 occurs within several hours (Von Arnim and Deng, 1994; Pacín et al., 2014). Data obtained in this study demonstrated that both light-dependent nuclear exclusion of COP1 and dissolution of COP1-containing photobodies are strongly impaired in the *spaQn* mutant. The finding that COP1 subcellular localization is not responsive to light in the absence of SPA proteins indicates that SPA proteins are required for the nuclear exclusion of COP1 in continuous white light. The mechanism behind the SPA-dependent nucleocytoplasmic partitioning is currently unknown. One possible explanation may be that SPA proteins are required for the interaction of light-activated photoreceptors with the COP1/SPA

complex *in vivo*. Although photoreceptors physically interact with both COP1 and SPA1 *in vitro* it is possible that the association of COP1 and SPA proteins is required for the association of photoreceptors with COP1/SPA in plant cells. Another possibility is that SPA proteins do not directly regulate the subcellular localization of COP1, but rather affect the nuclear export of COP1 indirectly via currently unknown feedback mechanisms. Such negative feedback regulation has been shown to occur for other light-signaling components. For example, the interaction of PIF proteins with phyB facilitates nuclear import of light activated phytochromes (Pfeiffer et al., 2012). Nuclear phyB subsequently causes destabilization of PIFs (Leivar and Quail, 2011), thereby downregulating nuclear import of light-activated phyB by PIFs. Similarly, active phyA is imported into the nucleus by the shuttle proteins FHY1 and FHL (Hiltbrunner et al., 2005, 2006), but in the nucleus, phyA suppresses *FHY1* and *FHL* expression, thereby negatively affecting nuclear import of active phyA (Li et al., 2010).

Interestingly, transgenic plants expressing *35S::YFP-COP1* in the *spaQn* mutant still display a constitutively photomorphogenic phenotype both in the seedling and the adult stage. Hence, since YFP-COP1 speckles are retained in these plants both in darkness and in white light, YFP-COP1 formation of photobodies does not correlate with COP1 activity in this case. This demonstrates that nuclear COP1 in *spaQn* mutants is still inactive. Thus, SPA proteins seem to have at least a dual role in the control of COP1 activity. First, SPA proteins are required for light-responsiveness in the COP1/SPA complex in seedlings grown in continuous white light, and second, they are required for COP1 function in darkness. Based on studies on chimeric COP1/SPA1 proteins, it is possible that WD-repeat domains of both COP1 and SPA1 are required for activity of the COP1/SPA complex, but many other mechanisms might be involved. Native COP1 did not accumulate in dark-grown *spaQn* mutants, indicating that although nuclear localized COP1 is largely inactive in the absence of SPA proteins, there does not seem to be any change in the degree of autoubiquitination in any direction. However, the hypothesis that SPA1 proteins facilitate the nuclear localization of COP1 in darkness can be rejected on the basis of this study. The exact molecular mechanisms of SPA-dependent nuclear exclusion in light-grown seedlings remain to be elucidated.

4.2.3 Subcellular localization is controlled by a complex interplay of phytochromes and cryptochromes

Continuous white light activates a variety of photoreceptors. To investigate the effect on specific subgroups of photoreceptors on COP1 subcellular localization, YFP-COP1 photobody formation was also analyzed in seedlings grown in Rc, FRc and Bc. Seedlings grown in FRc displayed similar dynamics of COP1 subcellular localization as seedlings grown in continuous white light; nuclear exclusion of YFP-COP1 was FRc-dependent. Previous studies have obtained similar results, indicating

that phyA is sufficient for the nuclear export of YFP-COP1 (Osterlund and Deng, 1998). FRc-dependent nuclear exclusion of YFP-COP1 was also contingent on SPA activity, indicating that SPAs are required for the phyA-dependent nuclear exclusion of YFP-COP1. In contrast, YFP-COP1 remained localized in the nucleus in seedlings grown in Rc, which disagrees with previous studies (Osterlund and Deng, 1998). The reason for this discrepancy is currently unknown. It is possible that the epitope tag used in both studies (YFP or GUS) differentially affects nucleocytoplasmic partitioning in R due to size differences of the two tags (Pacín et al., 2014). Furthermore, in a study investigating endogenous nuclear and cytoplasmic COP1, no difference in terms of COP1 localization was detectable between seedlings grown in darkness and seedlings shifted to R for 24 hours (Jang et al., 2010), which is consistent with the results obtained in this study. Since no change in YFP-COP1 localization was detected between the *SPA* wild-type and *spaQn* mutant background, no further conclusions can be drawn about the role of SPA proteins in the R-controlled subcellular localization of YFP-COP1. In seedlings grown in Bc, YFP-COP1 was excluded from the nucleus, which is consistent with the results obtained in continuous white light. However, in contrast to white light, the B-induced nuclear exclusion of YFP-COP1 was not SPA-dependent. This indicated that SPA proteins are likely not required for the nuclear exclusion of COP1 mediated by cryptochromes. In total these results suggest that nucleocytoplasmic partitioning of COP1 is controlled by a complex, non-additive interplay of phytochromes and cryptochromes in continuous white light which is not replicable by the activation of individual subgroups of photoreceptors.

4.2.4 The light-regulated subcellular localization of SPA proteins remains unclear

Lastly, the subcellular localization of YFP-SPA1 in dark- and light-grown seedlings was analyzed as well. This investigation was motivated by the finding that SPA proteins are required for the light-induced nuclear exclusion of YFP-COP1. SPA peptide sequences contain only NLS and no CLS. Nevertheless, white light-grown transgenic *35S::YFP-SPA1* seedlings did not form YFP-SPA1-containing speckles. This difference in nuclear speckle formation was qualitative of nature, as 0 photobody-containing nuclei could be found in *YFP-SPA1*-expressing seedlings grown in continuous white light. SPA1 is known to be partially degraded in the light (Balcerowicz et al., 2011). Remaining SPA1 therefore seems unable to form nuclear speckles in continuous white light. However, it is also possible that YFP-SPA1 is fully degraded in this particular transgenic line. It is also feasible that remaining, non-degraded SPA1 is evicted from nuclear photobodies, but not excluded from the nucleus in white light. Additional studies on the subcellular localization and total protein levels of dark- and light-grown seedlings expressing *35S::YFP-SPA1* are required to conclusively answer these questions. Strikingly, YFP-SPA1 was not excluded from nuclear speckles in seedlings grown in Rc, FRc or Bc. Thus, in contrast to YFP-

COP1, light-activated photoreceptors may additively contribute to the nuclear exclusion (either by degradation or nucleocytoplasmic partitioning) in continuous white light. Since SPA proteins are involved in the nuclear exclusion of COP1, it is possible that co-shuttling of COP1 and SPA proteins occurs in the light as well. However, light-activated phytochromes and cry1 induce the dissociation of COP1 and SPA proteins in yeast three-hybrid experiments and to a weaker extent *in planta* (Sheerin et al., 2015; Lian et al., 2011; Lu et al., 2015; Liu et al., 2011). Disruption of COP1-SPA1 interaction may also trigger the exclusion of SPA1 from nuclear photobodies. Moreover, if SPA1 is indeed excluded from the nucleus in continuous white light, the question remains of whether COP1 is required for the nuclear exclusion of SPA1. Thus, the exclusion of YFP-SPA1 from nuclear photobodies in continuous white light may be caused either by nucleocytoplasmic partitioning of SPA1, dissociation from COP1 and subsequent eviction from photobodies, light-induced SPA1 degradation, or a combination of these factors.

In summary, the results obtained in this study clearly demonstrate that SPA proteins are required for the nuclear exclusion of COP1 in continuous white light, as well as COP1 function in general. Photoreceptors seem to trigger COP1 nuclear exclusion by complex, non-additive interplays between phytochromes and cryptochromes, but cryptochrome-induced nuclear export of COP1 is not dependent on SPA proteins. Lastly, YFP-SPA1 does not form nuclear speckles in hypocotyl cells of seedlings grown in continuous white light. This nuclear exclusion of YFP-SPA1 may be controlled by various mechanisms such as degradation or nucleocytoplasmic partitioning of SPA1. These results provide vital insights into the role of SPA proteins in the regulation of COP1 activity.

5 MATERIALS AND METHODS

5.1 MATERIALS

5.1.1 Chemicals

Chemicals in research were purchased from AppliChem GmbH (Darmstadt, Germany), BD Biosciences (Heidelberg, Germany), Bio-Rad Laboratories GmbH (Munich, Germany), Calbiochem (Darmstadt, Germany), Carl Roth GmbH (Karlsruhe, Germany), Colgate-Palmolive GmbH (Hamburg, Germany), Duchefa Biochemie B.V. (Haarlem, Netherlands), Honeywell Riedel-de-haen Specialty Chemicals Seelze GmbH (Seelze, Germany), Life Technologies GmbH (Karlsruhe, Germany), Merck KGaA (Darmstadt, Germany), Miltenyi Biotec (Bergisch Gladbach, Germany), p.j.k. GmbH (Kleinblittersdorf, Germany), Promega (Mannheim, Germany), Roche Diagnostics GmbH (Mannheim, Germany), SERVA Electrophoresis GmbH (Heidelberg, Germany), Sigma Aldrich Chemie GmbH (Munich, Germany), Thermo Fisher Scientific (Schwerte, Germany) and VWR International GmbH (Darmstadt, Germany).

5.1.2 Buffers

All buffers and solutions were prepared with double-distilled water if not otherwise stated. Buffers and solutions that do not represent a simple solution or dilution of a single stock chemical are listed in Table 5.1. Unless otherwise stated, buffers were stored at room temperature (RT).

Table 5.1: Buffers and solutions

Buffer/Solution	Components
10 x Carbonate blotting buffer	0.31% (w/v) Na_2CO_3
	0.84% (w/v) $NaHCO_3$
	0.08% (w/v) SDS
Coomassie staining solution	0.25% (w/v) Coomassie Brilliant Blue R250
	50% (v/v) MeOH
	7% (v/v) glacial acetic acid
Coomassie destaining solution	50% (v/v) MeOH
	7% (v/v) glacial acetic acid

Continued on next page

Table 5.1: Buffers and solutions (continued)

Buffer/Solution	Components
DNA extraction buffer	200 mM Tris/HCl pH 7.5
	250 mM NaCl
	25 mM EDTA
	0.5% (w/v) SDS
DNA loading dye	0.25 (W/v) Bromophenol Blue
	30% (v/v) glycerol
5 x Laemmli buffer[a]	310 mM Tris/HCl pH 6.8
	10% (w/v) SDS
	50% (v/v) glycerol
	0.25% (w/v) Bromophenol Blue
	500 mM DTT
PCR reaction buffer	100 mM Tris/HCl pH 9.0
	500 mM KCl
	15 mM MgCl2
Protein extraction buffer	50 mM Tris/HCl pH 7.5
	150 mM NaCl
	1 mM EDTA
	10% (v/v) glycerol
	0.1% (v/v) Triton™ X-100
	5 mM DTT (added freshly)
	1 x protease inhibitor cocktail (added freshly)
	10 µM MG132 (added freshly)
2 x SDS protein extraction buffer	125 mM Tris/HCl pH 6.8
	4% (w/v) SDS
	20% (v/v) glycerol
	1 x protease inhibitor cocktail (added freshly)
	1 mM PMSF (added freshly)

Continued on next page

Table 5.1: Buffers and solutions (continued)

Buffer/Solution	Components
SDS-PAGE separating gel	7.5-15% (w/v) acrylamide
	375 mM Tris/HCl pH 8.8
	0.1% (w/v) SDS
	0.08% (w/v) APS (added before pouring)
	0.08% (v/v) TEMED (added before pouring)
SDS-PAGE stacking gel	5% (w/v) acrylamide
	125 mM Tris/HCl pH 6.8
	0.1% (w/v) SDS
	0.08% (w/v) APS (added before pouring)
	0.08% (v/v) TEMED (added before pouring)
10 x SDS running buffer	1.9 M Glycine
	240 mM Tris
	1% (w/v) SDS
Seed sterilization solution	70% (v/v) Ethanol
	0.05% (v/v) Tween® 20
50 x TAE buffer	50 mM EDTA
	2 M Tris
	1 M glacial acetic acid
TB buffer[b]	10 mM PIPES/KOH pH 6.7
	15 mM $CaCl_2$
	55 mM KCl
	55 mM $MnCl_2$ (added after pH adjustment)
10 x TBS buffer	200 mM Tris/HCl pH 7.5
	1.37 M NaCl
TBS-T buffer	0.1% (v/v) Tween® 20
	in 1 x TBS
TE buffer	10 mM Tris/HCl pH 8.0
	1 mM EDTA

[a] Solution was stored at -20 °C.

[b] Solution was filter-sterilized after preparation.

5.1.3 Antibiotics and growth regulators

Antibiotics and growth regulators used in this study are listed in Table 5.2. Stock solutions were filter-sterilized and stored at -20 °C, unless otherwise stated.

Table 5.2: Antibiotics and growth regultors

Chemical	Solvent	Working concentration	Manufacturer
Ampicillin	ddH_2O	100 µg/µl	Duchefa (Haarlem, Netherlands)
Gentamycin	ddH_2O	25 µg/ml	Duchefa (Haarlem, Netherlands)
Hygromycin[a]	ddH_2O	50 µg/ml	Life Technologies (Karlsruhe, Germany)
Kanamycin	ddH_2O	50 µg/ml	Duchefa (Haarlem, Netherlands)
MG132	DMSO	30 µM	Sigma-Aldrich (Munich, Germany)
Rifampicin[b]	DMSO	25 µg/ml	Duchefa (Haarlem, Netherlands)
Spectinomycin	ddH_2O	10 µg/ml	Duchefa (Haarlem, Netherlands)

[a] Solution was stored at 4 °C.

[b] Solution was stored at RT.

5.1.4 Growth media

Media for bacteria, yeast cells and plant seedling growth used in this study are listed in Table 5.3. Solid LB media contains 1.5% agar, while solid MS media contains 1% agar. All media were autoclaved prior to usage. Antibiotics were added after media was autoclaved and cooled down to approximately 60 °C. All media except liquid LB were stored at 4 °C.

Table 5.3: Growth media

Medium	Components
Luria-Bertani (LB) broth medium	10 g/L Tryptone
	5 g/L Yeast extract
	10 g/L NaCl
Murashige and Skoog (MS) medium	4.44 g/L MS salts
	pH adjusted to 5.8
Yeast extract broth (YEB) medium	5 g/L Peptone
	5 g/L Beef extract
	5 g/L Yeast extract
	5 g/L Sucrose
	2 mM MgSO$_4$
Yeast extract peptone dextrose (YPD) medium	20 g/L Peptone
	10 g/L Yeast extract
	100 mg/L Adenine hemisulfate
	pH adjusted to 5.8
	50 ml/L 40% glucose added after autoclaving
Synthetic "drop-out" medium	6.7 g/L nitrogen base without amino acids
	40 mg/L adenine hemisulfate
	x g/L drop-out supplement (according to manufacturer's instructions)
	pH adjusted to 5.8
	50 ml/L 40% glucose added after autoclaving

5.1.5 Antibodies

Antibodies used in this study are listed in Table 5.4. Primary antibodies were diluted in TBS containing 2% (w/v) milk powder. Horseradish peroxidase (HRP)-coupled secondary antibodies, as well as α-HA antibody conjugated with HRP, were diluted in TBS containing 5% (w/v) milk powder.

Table 5.4:Antibodies

Antibody	Host	Dilution	Manufacturer
α-COP1	rabbit	1:250	Balcerowicz et al., 2011
α-HA-HRP (Cat: 12013819001)	rat	1:1,000	Roche Diagnostics (Mannheim, Germany)
α-HSC70 (Cat: SPA-817)	mouse	1:10,000	Stressgen Biotechnologies (San Diego, USA)
α-HY5	rabbit	1:1,000	Osterlund et al., 2000
α-mouse IgG-HRP	goat	1:50,000	Sigma-Aldrich (Munich, Germany)
α-rabbit IgG-HRP	goat	1:50,000	Sigma-Aldrich (Munich, Germany)
α-Tubulin (Cat: T5168)	rabbit	1:10,000	Sigma-Aldrich (Munich, Germany)

5.1.6 Enzymes

Enzymes used in this study are listed in Table 5.5. All enzymes were stored on -20 °C unless otherwise stated.

Table 5.5: Enzymes

Enzyme	Manufacturer
Calf Intestine Phosphatase	New England Biolabs (Frankfurt, Germany)
Gateway® BP Clonase® Mix[a]	Life Technologies (Karlsruhe, Germany)
Gateway® LR Clonase® Mix[a]	Life Technologies (Karlsruhe, Germany)
GoTaq® G2 Hot Start Green Master Mix	Promega (Mannheim, Germany)
KAPA[TM]SYBR® FAST qPCR Master Mix	PEQLAB Biotechnologie (Erlangen, Germany)
Q5® High-Fidelity DNA polymerase	New England Biolabs (Frankfurt, Germany)
Restriction endonucleases	Thermo Fisher Scientific (Schwerte, Germany)
RevertAidTMH Minus Rev Transcriptase	Thermo Fisher Scientific (Schwerte, Germany)
T4 DNA Ligase	Thermo Fisher Scientific (Schwerte, Germany)
Taq DNA polymerase	purified from *E. coli*
TURBO[TM] DNase	Life Technologies (Karlsruhe, Germany)

[a] Enzyme was stored at -80 °C

5.1.7 Kits for molecular biology

Kits used in this study are listed in Table 5.6.

Table 5.6: Kits for molecular biology

Kit	Manufacturer
Pierce^{TM} BCA^{TM} Protein-Assay Kit (Cat: 23225)	Thermo Fisher Scientific (Schwerte, Germany)
CloneJET PCR Cloning Kit (Cat: K1232)	Thermo Fisher Scientific (Schwerte, Germany)
Frozen-EZ Yeast Transformation II Kit	Zymo Research (Freiburg, Germany)
NucleoSpin® Gel and PCR Clean-up Kit (Cat: 740609250)	Macherey Nagel (Düren, Germany)
NucleoSpin® Plasmid Purification Kit (Cat: 740588250)	Macherey Nagel (Düren, Germany)
Plasmid Plus Midi Kit (Cat: 12941)	Qiagen (Hilden, Germany)
RNeasy® Plant Mini Kit (Cat: 74904)	Qiagen (Hilden, Germany)

5.1.8   Primers

Primers used in this study are listed in Table 5.7. Primers were synthesized by Life Technologies (Karlsruhe, Germany).

Table 5.7: Primers

ID	Primer	Sequence 5' --> 3'	Reference
cloning			
ol-0007	DSC1_COP1_attB1_ApaI_F_001	GGGGACAAGTTTGTACAAAAAAGCAGGCTT AGGGCCCATGGAAGAGATTTCGACGGATC	this study
ol-0008	DSC1_COP1_NotI_attB2_R_001	GGGGACCACTTTGTACAAGAAAGCTGGGT AGCGGCCGCTCACGCAGCGAGTACCAGAA	this study
ol-0009	DSC1_CCX_R_001	TCCCACAGGTTCTTAGACGACTGTAGCGA GTG	this study
ol-0012	DSC1_XXC_F_001	CAAGTTCGAAGTTATAGCAGAAATCCGGCA TG	this study
ol-0013	DSC1_SPA1_attB1_ApaI_F_001	GGGGACAAGTTTGTACAAAAAAGCAGGCTT AGGGCCCATGCCTGTTATGGAAAGAGT	this study
ol-0014	DSC1_SPA1_attB2_NotI_R_001	GGGGACCACTTTGTACAAGAAAGCTGGGT AGCGGCCGCTCAAACAAGTTTTAGTAGCTT CA	this study

Continued on next page

Table 5.7: Primers (continued)

ID	Primer	Sequence 5' --> 3'	Reference
ol-0016	DSC1_11X_R_001	CTGCTATAACTTCGAACTTGCTATACCGAGC	this study
ol-0018	DSC1_XX1_F_001	TCGTCTAAGAACCTGTGGGACAATAAGAAGTG	this study
ol-0019	DSC1_ApaI_ATG_3xHA_F_001	GGGCCCATGTACCCATATGACGTTCCAGACT	this study
ol-0020	DSC1_ApaI_ATG_3xHA_R_001	GGGCCCAGCGTAGTCAGGTACGTCGT	this study
ol-0061	attL1_F_001	GGGCCCCAAATAATGATTTTATTT	this study
ol-0062	attL2_R_001	CAGCTGGATGGCAAATAATGA	this study
genotyping			
ol-0021	spa1-100 WT F1	CATTCATAATACTATTCTCACCAGC	Ordoñez-Herrera et al., 2015
ol-0022	spa1-100 WT R1	GATTTAAGGTATGGAGGCTGTAG	Ordoñez-Herrera et al., 2015
ol-0023	SPA2 geno F2	GGGAAAATGTCTTTGCCTGA	Ordoñez-Herrera et al., 2015
ol-0024	SPA2 geno R2	AGCACGGCAAACCATCATA	Ordoñez-Herrera et al., 2015
ol-0025	SPA3-F2	TTCGGACTCTGGCTCTGATTCCTTG	Ordoñez-Herrera et al., 2015
ol-0026	SPA3-R4	GTCCTCATTGATGGTCGACAAGTT	Ordoñez-Herrera et al., 2015
ol-0027	SPA4 geno F1	GGTCAAGAAGCTTCCTCGTG	Ordoñez-Herrera et al., 2015

Continued on next page

Table 5.7: Primers (continued)

ID	Primer	Sequence 5' --> 3'	Reference
ol-0028	SPA4 geno R1	TCATCATCAAGTCCTCCCAAG	Ordoñez-Herrera et al., 2015
ol-0029	LB-SAIL	TAGCATCTGAATTTCATAACCA	Ordoñez-Herrera et al., 2015
ol-0030	FISH geno1	CTGGGAATGGCGAAATCAAG	Ordoñez-Herrera et al., 2015
qRT-PCR			
ol-1323	ACTIN_qPCR_XWD12_F_001	CAAGGCCGAGTATGATGAGG	Huang et al., 2012
ol-1324	ACTIN_qPCR_XWD12_R_001	GAAACGCAGACGTAAGTAAAAAC	Huang et al., 2012
ol-1327	COP1_qPCR_XWD12_exon5_F_001	AAGAGTGTAGTACGGAGGGAAGG	Huang et al., 2012
ol-1328	COP1_qPCR_XWD12_exon5_R_001	TAGACGACTGTAGCGAGTGAAGG	Huang et al., 2012

5.1.9 Molecular weight markers

Molecular weight markers used in this study are listed in Table 5.8.

Table 5.8: Molecular weight markers

Molecular marker	Manufacturer
GeneRuler™ 1kb DNA Ladder	Thermo Fisher Scientific (Schwerte, Germany)
GeneRuler™ Low Range DNA Ladder	Thermo Fisher Scientific (Schwerte, Germany)
PageRuler™ Prestained Protein Ladder	Thermo Fisher Scientific (Schwerte, Germany)

5.1.10 Plasmids

Plasmids used in this study are listed in Table 5.9.

Table 5.9: Plasmids

Vector	Desciption	Resistance	Reference
pACT-GW	Gateway® Destination vector for yeast two-hybrid analysis. Contains GAL4-activating domain	Amp	Clontech™, modified by Hülskamp laboratory, unpublished
pACT-COP1	Gateway® Destination vector for yeast two-hybrid analysis. GAL4-activating domain fused to COP1 CDS	Amp	Provided by Krzysztof Klaczynski, Hoecker laboratory, unpublished
pACT-SPA1	Gateway® Destination vector for yeast two-hybrid analysis. GAL4-activating domain fused to SPA1 CDS	Amp	Provided by Krzysztof Klaczynski, Hoecker laboratory, unpublished
pACT-CC1	Gateway® Destination vector for yeast two-hybrid analysis. GAL4-activating domain fused to CC1 domain swap CDS	Amp	this study
pACT-11C	Gateway® Destination vector for yeast two-hybrid analysis. GAL4-activating domain fused to 11C domain swap CDS	Amp	this study
pACT-PAP2	Gateway® Destination vector for yeast two-hybrid analysis. GAL4-activating domain fused to PAP2 CDS	Amp	Provided by Krzysztof Klaczynski, Hoecker laboratory, unpublished

Continued on next page

Table 5.9: Plasmids (continued)

Vector	Desciption	Resistance	Reference
pAS-GW	Gateway® Destination vector for yeast two-hybrid analysis. Contains GAL4-binding domain	Amp	Clontech™, modified by Hülskamp laboratory, unpublished
pAS-COP1	Gateway® Destination vector for yeast two-hybrid analysis. GAL4-binding domain fused to COP1 CDS	Amp	Provided by Krzysztof Klaczynski, Hoecker laboratory, unpublished
pAS-CC1	Gateway® Destination vector for yeast two-hybrid analysis. GAL4-binding domain fused to CC1 domain swap CDS	Amp	this study
pAS-11C	Gateway® Destination vector for yeast two-hybrid analysis. GAL4-binding domain fused to 11C domain swap CDS	Amp	this study
pBS-SK+-pSPA1-SPA1-HA_SPA1-3'	pBS vector carrying SPA1 5', the *SPA1* CDS fused to the HA-tag repetitions, and SPA1 3' genomic regions. Used to amplify 3xHA with a start codon.	Amp	Balcerowicz et al., 2011
pBS-SK+_pSPA1_SPA1-3'	pBS vector carrying SPA1 5' and SPA1 3' genomic regions	Amp	Balcerowicz et al., 2011
pBS_pSPA1-3xHA-SPA1_SPA1-3'	pBS vector carrying SPA1 5', HA-tag repetitions fused to the SPA1 CDS, followed SPA1 3' genomic regions	Amp	this study

Continued on next page

Table 5.9: Plasmids (continued)

Vector	Desciption	Resistance	Reference
pBS_pSPA1-3xHA-COP1_SPA1-3'	pBS vector carrying SPA1 5', HA-tag repetitions fused to the COP1 CDS, followed SPA1 3' genomic regions	Amp	this study
pBS_pSPA1-3xHA-CC1_SPA1-3'	pBS vector carrying SPA1 5', HA-tag repetitions fused to the COP1 CDS with the SPA1 WD-repeat domain swapped, followed *SPA1 3'* genomic regions	Amp	this study
pBS_pSPA1-3xHA-11C_SPA1-3'	pBS vector carrying SPA1 5', HA-tag repetitions fused to the SPA1 CDS with the COP1 WD-repeat domain swapped, followed *SPA1 3'* genomic regions	Amp	this study
pJHA212-nptII_pSPA1::3xHA-SPA1	pJHA212 with the cloned-in SPA1 ORF under the control of the SPA1 5' and SPA1 3' regulatory sequences. Backbone carries kanamycin resistance gene NPTII for selection in plants	Spec	this study
pJHA212-nptII_pSPA1::3xHA-COP1	pJHA212 with the cloned-in COP1 ORF under the control of the SPA1 5' and SPA1 3' regulatory sequences. Backbone carries kanamycin resistance gene NPTII for selection in plants	Spec	this study
pJHA212-nptII_pSPA1::3xHA-CC1	pJHA212 with the cloned-in COP1 ORF (SPA1 WD-repeat domain swapped) under the control of the SPA1 5' and *SPA1* 3' regulatory sequences. Backbone carries kanamycin resistance gene NPTII for selection in plants	Spec	this study

Table 5.9: Plasmids (continued)

Vector	Desciption	Resistance	Reference
pJHA212-nptII_pSPA1::3xHA-11C	pJHA212 with the cloned-in SPA1 ORF (COP1 WD-repeat domain swapped) under the control of the SPA1 5' and *SPA1* 3' regulatory sequences. Backbone carries kanamycin resistance gene NPTII for selection in plants	Spec	this study
pENTR™ 3C-SPA1	Gateway® entry vector. Contains full-length SPA1 cDNA	Kan	(Holtkotte, 2014)
pENSG-CFP	Gateway® destination vector; 35S promoter, NT-CFP	Amp	Laubinger et al., 2006
pENSG-CFP-COP1	Gateway® expression vector for expression of CFP-COP1 in leek cells; 35S promoter, NT-CFP	Amp	(Holtkotte, 2014)
pENSG-CFP-SPA1	Gateway® expression vector for expression of CFP-SPA1 in leek cells; 35S promoter, NT-CFP	Amp	(Holtkotte, 2014)
pENSG-CFP-CC1	Gateway® expression vector for expression of CFP-CC1 in leek cells; 35S promoter, NT-CFP	Amp	This study
pENSG-CFP-11C	Gateway® expression vector for expression of CFP-11C in leek cells; 35S promoter, NT-CFP	Amp	This study
pENSG-CFP-PAP2	Gateway® expression vector for expression of CFP-PAP2 in leek cells; 35S promoter, NT-CFP	Amp	Provided by Krzysztof Klaczynski, Hoecker laboratory, unpublished

Continued on next page

Table 5.9: Plasmids (continued)

Vector	Desciption	Resistance	Reference
pENSG-YFP	Gateway® destination vector; 35S promoter, NT-YFP	Amp	Laubinger et al., 2006
pENSG-YFP-COP1	Gateway® expression vector for expression of YFP-COP1 in leek cells; 35S promoter, NT-YFP	Amp	Ordoñez-Herrera et al., 2018
pENSG-YFP-SPA1	Gateway® expression vector for expression of YFP-SPA1 in leek cells; 35S promoter, NT-YFP	Amp	Ordoñez-Herrera et al., 2018
pENSG-YFP-CC1	Gateway® expression vector for expression of YFP-CC1 in leek cells; 35S promoter, NT-YFP	Amp	This study
pENSG-YFP-11C	Gateway® expression vector for expression of YFP-11C in leek cells; 35S promoter, NT-YFP	Amp	This study
pENSG-YFP-PHYA	Gateway® expression vector for expression of YFP-PHYA in leek cells; 35S promoter, NT-YFP	Amp	Provided by Xu Holtkotte, Hoecker laboratory, unpublished
pENSG-YFP-PHYB	Gateway® expression vector for expression of YFP-PHYB in leek cells; 35S promoter, NT-YFP	Amp	Provided by Xu Holtkotte, Hoecker laboratory, unpublished
pENSG-YFP-CRY1	Gateway® expression vector for expression of YFP-CRY1 in leek cells; 35S promoter, NT-YFP	Amp	Provided by Jathish Ponnu, Hoecker laboratory, unpublished

Table 5.9: Plasmids (continued)

Vector	Desciption	Resistance	Reference
pENSG-YFP-CRY2	Gateway® expression vector for expression of YFP-CRY2 in leek cells; 35S promoter, NT-YFP	Amp	Provided by Jathish Ponnu, Hoecker laboratory, unpublished
pDONR221-CC1	Gateway® entry clone; contains COP1 cDNA (SPA1 WD-repeat domain swapped)	Kan	this study
pJET-attL-11C	pJET® pre-cloning vector; contains SPA1 cDNA (COP1 WD-repeat domain swapped), flanked by Gateway® attL cloning sites	Kan	this study
pJET1.2-3xHA	pJET® pre-cloning vector; contains triple HA tag preceded by a start codon (ATG) and flanked by ApaI restriction sites on both sides.	Amp	this study

5.1.11 Bacterial and yeast strains

The *E. coli* strain DH5α was used for standard cloning. The ccdB-resistant *E. coli* strain DB3.1 was used for propagating empty Gateway® vectors (Life Technologies, Karlsruhe, Germany). For plant transformation, *Agrobacterium tumefaciens* strain GV3101 (pMP90RK) was used. The yeast strain AH109 was used for yeast two-hybrid assays.

5.1.12 Plant material

Arabidopsis mutant lines used in this study are listed in Table 5.10. Transgenic lines used in this study are listed in Table 5.11.

Table 5.10: Arabidopsis mutants

Mutant	Background	Mutagen	Reference
cop1-4	Col-0	EMS	McNellis *et al.*, 1994
hy5-215	Col-0	EMS	Oyama *et al.*, 1997

Table 5.11: Arabidopsis transgenic lines

Line	Background	Reference
35S::YFP-COP1 cop1-4	Col-0	Oravecz et al., 2006
35S::YFP-COP1 spaQn	Col-0	Balcerowicz et al., 2017
spa1-100 spa2-2 spa3-1 spa4-3 (spaQn)	Col-0	Ordoñez-Herrera et al*.,* 2015
spa1-100 spa2-2 spa3-1 (spa1 spa2 spa3)	Col-0	Ordoñez-Herrera et al*.,* 2015
spa2-2 spa3-1 spa4-3 (spa2 spa3 spa4)	Col-0	Ordoñez-Herrera et al*.,* 2015
pSPA1::3xHA-COP1 cop1-4	Col-0	this study
pSPA1::3xHA-CC1 cop1-4	Col-0	this study
pSPA1::3xHA-SPA1 spa1 spa2 spa3	Col-0	this study
pSPA1::3xHA-11C spa1 spa2 spa3	Col-0	this study

5.2 METHODS FOR PLANT GROWTH

5.2.1 Seed sterilization

For axenic growth of Arabidopsis seedlings on MS plates, seeds were surface-sterilized prior to plating. For liquid sterilization, seeds were incubated in seed sterilization solution for 10 min, rinsed in 100% ethanol and then dried on sterile paper. For dry sterilization, seeds were incubated in a chlorine gas atmosphere (produced by adding 2.5 ml 37% HCl to 80 ml NaClO) for 3 h. Chlorine gas was subsequently evaporated in a sterile hood for 1 h.

5.2.2 Conditions and methods for plant growth

For growth on soil, seeds were sowed on soil and stratified at 4 °C for 3 days. Soil was prepared as a mixture of three parts soil and one part vermiculite. For propagation, plants were grown in the greenhouse under long day conditions (16 h light, 8 h darkness) at approximately 40% humidity and a temperature cycle of 21 °C during the day and 18 °C during the night. For phenotypic analysis, plants

were grown in walk-in growth chambers (Johnson Controls, Milwaukee, WI, USA) under short day conditions (8 h light, 16 h darkness) at 21 °C and 60% humidity. Light intensities of approximately 100 µmol m^{-2} s^{-1} generated by Lumilux L36W/840 cool white fluorescent tubes (Osram, Munich, Germany).

For sterile growth, prior sterilized seeds were plated on MS medium without sucrose. Seeds plated on MS medium were stratified at 4 °C for 3 days before germination was induced by 3 h of treatment with white light (approximately 40 µmol m^{-2} s^{-1}). Plates were then either kept in white light, moved to continuous darkness or incubated in the dark for 21 hours before being shifted to monochromatic R, FR or B. In each case, plates were incubated in reach-in growth chambers (CLF Plant Climatics, Wertingen, Germany) at 21 °C- Fluora L58W/77 fluorescent tubes (Osram, Munich, Germany) was used to produce white light while LED light sources (Quantum Devices, Barneveld, WI, USA) were used to produce monochromatic R, FR and B.

5.3   METHODS FOR PHENOTYPIC ANALYSIS

5.3.1   Measurement of hypocotyl length

To measure hypocotyl length, 4 days-old seedlings were pressed lengthwise on MS plates on which they were grown and subsequently documented with a digital camera. Measurements of hypocotyl length were performed on digital images using Fiji (Schindelin et al., 2012). At least 15 seedlings were measured per genotype.

5.3.2   Measurement of flowering time and leaf/petiole length

Flowering time under short day conditions was measured by counting the numbers of rosette leaves at the day when the first inflorescence was visible by eye. 10 to 15 plants were analyzed for each genotype.

Four-week-old plants grown in short day conditions were used to determine leaf length by measuring the petiole length and total length (including petiole) of the longest leaf.

5.4 MOLECULAR BIOLOGY METHODS

5.4.1 Agarose gel electrophoresis

Agarose gel electrophoresis in 1 x TAE buffer was used for DNA separation according to standard protocols (Sambrook and Russell, 2001). 0.25 µg/ml ethidium bromide was added in agarose gels for visualization of DNA bands on a GEL Stick "Touch" imager (INTAS Science Imaging Instruments, Goettingen, Germany).

5.4.2 Polymerase chain reaction (PCR)

Standard PCR was performed in a 20 µl reaction system with 1 µl *Taq* DNA polymerase, 1 x PCR reaction buffer, 0.1 µM forward and reverse primers and 125 µM dNTPs. 1 µl of genomic DNA extract was used as DNA template. Standard PCRs were performed as follows: 2 min initial denaturation at 95 °C, 40 cycles of 30 s denaturation at 95 °C, 30 s annealing at 55 °C and 1 min per kb elongation at 72 °C, followed by a final elongation step of 10 min at 72 °C. For colony PCR, a small portion of a bacterial colony was used as template. Cloning PCRs were performed in a 50 µl system using Q5® High-Fidelity DNA polymerase (New England Biolabs, Frankfurt, Germany) according to the manufacturer's instructions.

5.4.3 DNA sequencing

DNA sequences were determined by GATC biotech (Konstanz, Germany) or Eurofins Genomics (Ebersberg, Germany). All sequences were analyzed with the software Geneious R9.1.8 (https://www.geneious.com).

5.4.4 Cloning

For conventional cloning, restriction digestion, DNA fragment dephosphorylation and ligation were performed according to standard protocols (Sambrook and Russell, 2001). For Gateway® cloning, BP and LR reactions were performed in reaction systems scaled down to a total volume of 5 µl and proportionally added components according to the manufacturer's instructions. PCR products and digested DNA fragments used for cloning were purified from agarose gels using NucleoSpin® Gel and PCR Clean-up Kit (Macherey Nagel, Düren, Germany). Positive clones were selected by colony PCR and DNA sequences were verified by restriction digestion and sequencing. For plasmid isolation, either NucleoSpin® Plasmid Purification Kit (Macherey Nagel, Düren, Germany) or Plasmid Plus Midi Kit (Qiagen, Hilden, Germany) were used.

5.4.5 Cloning strategy for *CC1* or *11C* constructs into entry clones

DNA fragments of chimeric *COP1/SPA1* domain swap constructs were generated by overhang-extension PCR. For *CC1*, a 5' *attB1* sequence and ApaI restriction site and a 3' overhang to the *SPA1* CDS were attached to the 1-1071 bp region of the *COP1* CDS by PCR amplification using ol-0007 and ol-0009 as forward and reverse primers, respectively, and pENSG-YFP-COP1 as template. Next, a 5' overhang to the previously amplified COP1 fragment and a 3' *attB2* sequence and a NotI restriction site were attached to the 2107-3090 bp region of the *SPA1* CDS by PCR amplification using ol-0018 and ol-0008 as forward and reverse primers, respectively, and pENSG-YFP-SPA1 as template. Both fragments were then fused in an overhang-extension PCR by adding both fragments in one reaction as templates and ol-0007 and ol-0008 as primers. The PCR product, a chimeric sequence of the *COP1* CDS with a *SPA1* WD-repeat domain, flanked by *attB* sites, was used in a BP reaction together with pDONR™ 221 to generated pDONR™ 221-CC1. For *11C*, the 1-2106 bp region of the *SPA1* CDS, including the 5' *attL1* site, was amplified with a 10 bp 3' overhang to the *COP1* CDS from pENTR™ 3C-SPA1 using ol-0061 and ol-0016 as forward and reverse primers, respectively. Next, the 1072-2028 bp region of the *COP1* CDS, including the 3' *attL2* site, was amplified with a 10 bp 5' overhang to the previously generated fragment of the 1-2106 bp region of the *SPA1* CDS from pDONR™ 221-COP1 using ol-0012 and ol-0062 as forward and reverse primers, respectively. Both fragments were subsequently fused at their overlapping region in an overhang extension PCR by adding both fragments in one PCR reaction as templates and ol-0061 and ol-0062 as primers. The PCR product, which contained a chimeric sequence of the *SPA1* CDS with a *COP1* WD-repeat domain, flanked by *attL* sites, was then ligated into pJET using CloneJET PCR Cloning Kit (Thermo Fisher Scientific, Schwerte, Germany) to generated pJET-attL-11C.

5.4.6 Cloning strategy for binary vectors containing *3xHA-COP1*, *3xHA-SPA1*, *3xHA-CC1* or *3xHA-11C* constructs with the *SPA1* 5' and 3' regulatory regions

A pBlueScript SK+ vector containing the *SPA1* 5' and 3' regulatory sequences with a multiple cloning site with one ApaI and one NotI restriction site between both sequences (pBS-SK+_pSPA1_SPA1-3') has been generated previously (Balcerowicz et al., 2011). 5' ApaI and a 3' NotI restriction sites were fused to both the *COP1* and *SPA1* CDS by PCR with primers ol-0007 and ol-0008 for *COP1* and primers ol-0013 and ol-0014 for *SPA1*. A PCR fragment of a chimeric *COP1* CDS with a *SPA1* WD-repeat domain (*CC1*) has been generated in **5.4.5**. For *11C*, an overhang extension PCR was performed again by first generating overlapping fragments of the 1-2106 bp region of the *SPA1* CDS and the 1072-2028 bp region of the *COP1* CDS flanked by a 5' ApaI restriction site and a 3' NotI

restriction site by using the primers ol-0013 and ol-0016 in a PCR with the *SPA1* CDS and the primers ol-0012 and ol-0008 in a PCR with the *COP1* CDS, followed by an overhang-extension PCR with both fragments and primers ol-0013 and ol-0008. ApaI and NotI restriction sites were used to ligate *COP1*, *SPA1*, *CC1* and *11C* fragments into pBS-SK+_pSPA1_SPA1-3' to create intermediate vectors pBS_pSPA1-COP1_SPA1-3', pBS_pSPA1-SPA1_SPA1-3', pBS_pSPA1-CC1_SPA1-3' and pBS_pSPA1-11C_SPA1-3', respectively. Next, a 3xHA fragment with an ATG start codon and flanked by ApaI restriction sites on both ends was produced by amplifying a 3xHA sequence from a previously generated pBS-SK+-pSPA1-SPA1-HA_SPA1-3' (Balcerowicz et al., 2011) with primers ol-0019 and ol-0020, and the fragment was ligated into pJET with the CloneJET PCR Cloning Kit (Thermo Fisher Scientific, Schwerte, Germany) to generate pJET1.2-3xHA. The ATG-3xHA fragment was then ligated into the previously generated intermediate vectors pBS_pSPA1-COP1_SPA1-3', pBS_pSPA1-SPA1_SPA1-3', pBS_pSPA1-CC1_SPA1-3' and pBS_pSPA1-11C_SPA1-3' to generate pBS_pSPA1-3xHA-COP1_SPA1-3', pBS_pSPA1-3xHA-SPA1_SPA1-3', pBS_pSPA1-3xHA-CC1_SPA1-3' and pBS_pSPA1-3xHA-11C_SPA1-3', respectively. Finally, the KpnI restriction sites flanking the 5' end of the *SPA1* 5' regulatory sequence and the 3' end of the *SPA1* 3' regulatory sequence in all four vectors were used to ligate the *pSPA1-3xHA-COP1-SPA1-3'*, *pSPA1-3xHA-SPA1-SPA1-3'*, *pSPA1-3xHA-CC1-SPA1-3'* and *pSPA1-3xHA-11C-SPA1-3'* sequences into the binary pJHA212-nptII vector to generate pJHA212-nptII_pSPA1::3xHA-COP1, pJHA212-nptII_pSPA1::3xHA-SPA1, pJHA212-nptII_pSPA1::3xHA-CC1 and pJHA212-nptII_pSPA1::3xHA-11C, respectively.

5.4.7 Cloning of Expression vectors

For expression of proteins in yeast cells, entry vector pDONR^{TM} 221-CC1 was used to perform LR reaction with destination vectors pAS-GW and pACT-GW to generate expression vectors pAS-CC1 and pACT-CC1, respectively. pJET-attL-11C was used to perform LR reaction with destination vectors pAS-GW and pACT-GW to generate expression vectors pAS-11C and pACT-11C, respectively.

For expression of fluorescent-tagged proteins in leek epidermal cells, entry vector pDONR^{TM} 221-CC1 was used to perform LR reaction with destination vectors pENSG-CFP and pENSG-YFP to generate expression vectors pENSG-CFP-CC1 and pENSG-YFP-11C, respectively. pJET-attL-11C was used to perform LR reaction with destination vectors pENSG-CFP and pENSG-YFP to generate expression vectors pENSG-CFP-11C and pENSG-YFP-11C, respectively.

5.4.8   Transformation of chemically competent *E. coli*

To prepare chemically competent *E. coli* cells, a single colony was inoculated in a 250 ml LB culture. The culture was grown at 18 °C until reaching an OD600 of 0.6 and subsequently centrifuged for 10 min at 250 g and 4 °C. After removing the supernatant, the pellet was resuspended in 80 ml ice-cold TB buffer and incubated on ice for 10 min. The suspension was centrifuged again for 10 min at 2500 g and 4 °C and the pellet was subsequently resuspended in 20 ml of ice-cold TB buffer. DMSO was added to a final concentration of 7% (v/v) and the mixture was incubated on ice for 10 min. The cell suspension was then split into 50 µl aliquots that were snap-frozen in liquid nitrogen and stored at -80 °C.

For transformation, a 50 µl aliquot of chemically competent *E. coli* cells was thawed on ice, mixed with 50-100 ng of plasmid DNA and then heat-shocked at 42 °C for 90 s, and immediately cooled on ice. After that, 200 µl LB medium were added and the mixture was incubated at 37 °C for 45-60 min before being plated on solid LB medium containing the appropriate antibiotics for selection of transformed cells.

5.4.9   Transformation of electrocompetent *Agrobacterium tumefaciens*

For preparation of electrocompetent *Agrobacterium tumefaciens* cells, three single colonies were used to inoculate a 250 ml culture. The culture was grown at 28°C until an OD600 of 0.5 was reached and then centrifuged for 10 min at 4000 g and 4 °C. After removal of the supernatant, the pellet was resuspended in 300 ml ice-cold water and centrifuged again for 10 min at 4000 g and 4 °C. The supernatant was removed again and the pellet was rinsed with 300 ml ice-cold 10% (v/v) glycerol and centrifuged again for 10 min at 4000 g and 4 °C. This wash step was repeated twice before the pellet was resuspended in 1-2 ml 10% (v/v) glycerol. The cell suspension was split into 40 µl aliquots and snap-frozen in liquid nitrogen. Aliquots were stored at -80 °C.

For transformation, a 40 µl aliquot of electrocompetent *Agrobacterium tumefaciens* cells was mixed with 20 ng plasmid, incubated for 30 min on ice and then electroporated using the Micro-Pulser^TM electroporator (Bio-Rad Laboratories, Munich, Germany) according to the manufacturer's instructions. Transformed cells were cooled on ice and mixed with 500 µl YEB medium and incubated at 28 °C for 3 h before being plated on solid LB medium containing appropriate antibiotics for selection of transformed cells.

5.4.10   Stable transformation of Arabidopsis by floral dipping

Arabidopsis plants were stably transformed using the floral-dip method (Clough and Bent, 1998). A 5 ml LB pre-culture of agrobacteria containing the plasmid with the T-DNA to be transformed was used to inoculate a 250 ml LB culture and grown for 8-10 h at 28 °C. The culture was then centrifuged at 4000 g for 20 min, the supernatant was discarded, and the pellet was resuspended in 200 ml 5% (w/v) sucrose solution. Immediately before dipping, Silwet L77 was added to a final concentration of 0.05% (v/v) and the suspension was transferred to a container with a wide opening. Inflorescences of plants were submerged into the solution for 1 min. Dipped plants were kept in low light and high humidity for 24 h.

5.4.11   Isolation of genomic DNA from

For preparation of genomic DNA, single leaves were snap-frozen in liquid nitrogen, ground to a powder and suspended in 400 µl DNA extraction buffer. Samples were then centrifuged at 20,000 g for 3 min. 300 µl of the supernatant were transferred to a new tube, mixed with 300 µl isopropanol, incubated at RT for 5 min and centrifuged again at 20,000 g for 10 min. After removing the supernatant, the DNA pellets were air-dried and then resuspended in 50 µl TE buffer. DNA was kept at 4 °C or 20 °C for long-term storage.

5.4.12   Screening of transgenic plants

Agrobacterium tumefaciens GV3101 strains carrying *pJHA212-nptII_pSPA1::3xHA-COP1* or *pJHA212-nptII_pSPA1::3xHA-CC1* constructs were used to transform *cop1-4* mutant plants. *Agrobacterium tumefaciens GV3101* strains carrying *pJHA212-nptII_pSPA1::3xHA-SPA1* or *pJHA212-nptII_pSPA1::3xHA-11C* constructs were used to transform the progeny of a segregating *spa1-100 spa2-2 spa3-1 SPA4+/-* mutant plant which contained *spa1-100 spa2-2 spa3-1 SPA4* or *spa1-100 spa2-2 spa3-1 SPA4+/-* separately. Prior to transformation, the segregating plant was genotyped for the *spa1-100*, *spa2-2*, *spa3-1* and *spa4-3* loci with primer combinations specified in Table 5.12. T1 seeds from all transformed plants were plated on 1 x MS plates containing 50 µg/ml kanamycin (Duchefa, Haarlem, Netherlands). Seedlings which formed true leaves on selection media were transferred to soil. Adult T1 plants from *3xHA-SPA1* and *3xHA-11C* transgenic lines were again genotyped for the *spa4-3* locus. Lines that maintained the *SPA4+/-* genotype and all selected *3xHA-COP1* and *3xHA-CC1* lines were propagated to the T2 generation. T2 seeds were sowed on 1 x MS plates containing kanamycin and the segregation ratio of resistant to susceptible offspring was analyzed to calculate the number of insertions of each transgenic line. Lines that had only one insertion (segregation ratio of 3:1) were transferred to soil. Adult plants from transgenic *3xHA-SPA1* and *3xHA-11C* lines were

genotyped for the *spa4-3* locus, and plants which were homozygous for the *SPA4* wild type allele, as well as all *3xHA-COP1* and *3xHA-CC1* transgenic lines were propagated to the T3 generation. To find homozygous transgenic lines, T3 seeds from all transgenic lines were plated on 1 x MS plates containing kanamycin. Lines in which all seedlings were resistant were considered homozygous transgenic lines. These lines were used for detailed phenotypic and biochemical analysis.

5.4.13   Primer combinations used for genotyping of T-DNA insertion mutants

For confirmation of T-DNA insertion mutants by genotyping, genomic DNA was prepared from leaves of adult Arabidopsis plants. Two separate PCR reactions were prepared with genomic DNA as template: One reaction with two wild-type specific primers and another reaction with one wild-type specific primer and one T-DNA-specific primer. Primer combinations used for genotyping of T-DNA insertion mutants are listed in Table 5.12.

Table 5.12: Primer combinations used for genotyping of T-DNA insertion mutants

Mutant	Primer combination	Product size
spa1-100	wt: spa1-100-WT_F1 + spa1-100-WT_R1	700 bp
	spa1-100: spa1-100-WT_R1 + LB-SAIL	ca. 550 bp
spa2-2	wt: SPA2-geno_F2 + SPA2-geno_R2	360 bp
	spa2-2: SPA2-geno_F2 + FISH-geno1	ca. 600 bp
spa3-1	wt: SPA3-F2 + SPA3-R4	600 bp
	spa3-1: SPA3-F2 + LB-SAIL	ca. 400 bp
spa4-3	wt: SPA4-geno_F1 + SPA4-geno_R1	380 bp
	spa4-3: SPA4-geno_F1 + FISH-geno1	ca. 380 bp

5.4.14   Isolation of total RNA from Arabidopsis

Total RNA was isolated from 50-100 mg of snap-frozen seedlings with the RNeasy® Plant Mini Kit (Qiagen, Hilden, Germany) according to the manufacturer's instructions. RNA concentrations were measured using a Nanodrop® ND-1000 spectrophotometer (Thermo Fisher Scientific, Schwerte, Germany). RNA integrity was assessed on a 1% agarose gel by checking the presence and integrity of 28S and 18S rRNA bands. RNA samples were stored on -80 °C.

5.4.15 DNase treatment of RNA

DNA contamination of RNA samples was removed by incubating 1 µl of RNA with 1 µl TURBO^TM DNase (Life Technologies, Karlsruhe, Germany) in a 20 µl reaction containing 1 x TURBO^TM DNase buffer at 37 °C for 1 h. Then, DNase was inactivated by adding 2 µl 50 mM EDTA and an incubation at 75 °C for 10 min.

5.4.16 Reverse transcription of RNA to cDNA

1 µl DNase-treated RNA was incubated with 2 µl 10µM oligo(dT)$_{18}$ primers in a 20 µl reaction system at 65 °C for 5 min and immediately cooled down to 4 °C for 2 min. Then, 4 µl 10 mM dNTPs, 8 µl 5 x RevertAid^TM buffer and 1 µl RevertAid^TM H Minues M-MuLV Reverse Transcriptase (Thermo Fisher Scientific, Schwerte, Germany) were added to the reaction mix and the reaction was incubated at 37 °C for 5 min, 42 °C for 60 min and 70 °C for 5 min. cDNA was stored at -20 °C.

5.4.17 Quantitative real-time PCR

1 µl of gDNA-free cDNA was used as a template in a 10 µl reaction system containing 125 nM forward and reverse primers and 1 x KAPA^TMSYBR® FAST qPCR Mastermix (PEQLAB Biotechnologie, Erlangen, Germany). The Applied Biosystems® 7300 Real-time PCR system (Life Technologies, Karlsruhe, Germany) was used for thermocycling and measurements. For thermocycling, a program of an initial denaturation step at 95 °C for 2 min, followed by 40 cycles of 95 °C for 2 s and 60 °C for 30 s was used. Amplicon dissociation was tested by two cycles for 60 °C for 15 s and 95 °C for 15 s at the end of the run. Relative transcript levels were determined by the $2^{-\Delta\Delta CT}$ method (Livak and Schmittgen, 2001). Quantitative real-time PCR was performed on 3 biological and 2 technical replicates on a QuantStudio 5 Real-Time PCR System (Thermo Fisher Scientific, Schwerte, Germany).

5.5 BIOCHEMICAL METHODS

5.5.1 Isolation of total protein from Arabidopsis seedlings

For extraction of total proteins from Arabidopsis seedlings, 200 mg tissue were snap-frozen in liquid nitrogen and ground to a fine powder with mortar and pestle. Ground powder was mixed with 300 µl protein extraction buffer 2x SDS protein extraction buffer (for blot in Figure 3.8c) until fully thawed. Extracts mixed with protein extraction buffer were centrifuged at 20,000 g and 4 °C for 15 min and the supernatant was transferred to a new tube. Part of the supernatant was used for quantification

of protein concentration by Bradford assay, and the remainder was supplemented with Laemmli buffer (Laemmli, 1970) and incubated at 65 °C for 10 min. Extracts mixed with 2 x SDS protein extraction buffer were incubated at 65 °C for 10 min immediately after buffer was added to the powder, centrifuged at 20,000 g and RT for 15 min and the supernatant was transferred to a new tube. Part of the supernatant was used for quantification of protein concentration by BCA assay, while the remainder was supplemented with Laemmli buffer. Samples were stored at -20 °C.

5.5.2   Bradford assay

Protein concentration in total protein extracts with protein extraction buffer was determined by Bradford Assay (Bio-Rad Laboratories, Munich, Germany) prior to addition of Laemmli buffer. Extracts were diluted at 1:5 or 1:10 and 10 µl of the diluted extracts were mixed with 190 µl 1:5 diluted Bradford reagent (Bio-Rad Laboratories, Munich, Germany). Samples were incubated for 5 min at RT and then the OD595 was measured in an Infinite® M200 plate reader (Tecan, Männedorf, Switzerland). Protein concentration was calculated from the OD595 using a calibration curve from samples containing bovine serum albumin (BSA).

5.5.3   BCA assay

Protein concentration in total protein extracts with 2 x SDS protein extraction buffer was determined with Pierce™ BCA™ Protein-Assay Kit according to the manufacturer's instructions prior to addition of Laemmli buffer. Extracts were diluted 1:10 and 25 µl of the diluted extracts were mixed with 200 µl of the pre-mixed Working Reagent (WR). Reaction mixes were mixed thoroughly and incubated at 37 °C for 30 min. Absorbance at 562 nm was measured on an Infinite ® M200 plate reader (Tecan, Männedorf, Switzerland). Protein concentration was calculated from the absorbance at 562 nm using a calibration curve from samples containing bovine serum albumin (BSA).

5.5.4   SDS polyacrylamide gel electrophoresis (SDS-PAGE)

SDS-PAGE was performed in the Mini PROTEAN® Tetra electrophoresis system (Bio-Rad Laboratories, Munich, Germany). Protein samples were separated in a discontinuous gel system (Laemmli, 1970). A 5% acrylamide concentration was used for stacking gels, and concentrations of 7.5%, 10%, 12.5% or 15% acrylamide were used for resolving gels.

5.5.5 Western blotting

For western blotting, polyvinylidene difluoride (PVDF) membranes were activated in MeOH for 10 s. Proteins separated by SDS-PAGE were then blotted on (PVDF) membranes in carbonate blotting buffer at a current of 0.35 mA cm^{-2} for 120 min using the Mini PROTEAN® Tetra cell wet blot system (Bio-Rad Laboratories, Munich, Germany). After transfer, membranes were blocked by incubation in Roti®- Block (Roth, Karlsruhe, Germany) for 1 h at RT.

5.5.6 Immunodetection of blotted proteins

Membranes were incubated in TBS buffer supplemented with milk powder and containing the appropriate concentration of primary antibody for 1 h at RT or at least 12 h at 4 °C and washed three times in TBS-T buffer for 10 min. Afterward, membranes were incubated with HRP-coupled secondary antibody in TBS buffer supplemented with milk powder for 45 min and washed again three times in TBS-T for 5 min. HRP activity was detected with ECL PLUS^{TM} Western Blotting kit (GE Healthcare, Piscataway, USA) or the SuperSignal® west Femto Maximum Sensitivity kit (Thermo Fisher Scientific, Schwerte, Germany, according to the manufacturer's instructions and visualized on an ImageQuant^{TM} LAS 4000 mini imaging system (GE Healthcare, Piscataway, USA).

5.6 PROTEIN-PROTEIN INTERACTION METHODS

5.6.1 Colocalization of fluorescent-tagged proteins in leek epidermal cells

For colocalization studies in leek epidermal cells, leek cells were transiently transformed with plasmids expressing fluorescent-tagged proteins by biolistic transformation with DNA-coated gold particles. First, gold particle solution was prepared by adding 1 ml 70% ethanol to 30 mg gold particles with a diameter of 1 µm. The mixture was then vortexed and incubated at RT for 15 min. Particles were pulse-centrifuged and washed in 1 ml sterile water twice. Lastly, gold particles were resuspended in 1 ml sterile water, mixed and split into 50 µl aliquots while vortexing. Gold particles were stored at 20 °C for long-term storage. For each transformation, 5 µl gold particles were mixed with 400 ng of each plasmid required for the colocalization study, as well as 10 µl 2.5 M CaCl$_2$ and 4 µl 0.1 M spermidine and incubated for 15 min at RT with intermitted vortexing. Gold particles were pelleted by pulse centrifugation and the supernatant was discarded. Next, the gold particle pellet was washed in 100 µl 70% (v/v) ethanol and 50 µl 100% (v/v) ethanol, and then resuspended in 12 µl 100% (v/v) ethanol. Gold particle solution was transferred to the middle of a microcarrier (Bio-Rad Laboratories, Munich, Germany) and particle bombardment was performed with a Helios gun (Bio-Rad Laboratories, Munich,

Germany) according to the manufacturer's instruction. The second to fourth layers of the lower white part of a fresh leek stalk were used for transformation. Transformed samples were incubated at RT and in darkness for at least 12 h. Fluorescent proteins were detected using a DM5000 B fluorescent microscope (Leica Microsystems, Wetzlar, Germany) for Supplemental Figure S 2, Supplemental Figure S 4 and Supplemental Figure S 5, or a SP8 confocal laser scanning microscope (Leica Microsystems, Wetzlar, Germany) for Figure 3.3 and Supplemental Figure S 3. Detailed information of fluorescence filters used in standard fluorescence microscopy is summarized in Table 5.13. For confocal laser scanning microscopy, YFP was excited with an argon laser at 561 nm and detected at 525-600 nm by a HyD (Leica Microsystems, Wetzlar, Germany), and CFP was excited by an argon laser at 458 nm and detected at 465-505 nm by a HyD.

Table 5.13: Fluorescence filter information

Filter	Excitation filter	Dichroic mirror	Suppression filter
CFP	436/20 nm	455 nm	BP 480/40 nm
YFP	500/20 nm	515 nm	BP 535/30 nm

5.6.2 Yeast two-hybrid

For transformation of *Saccharomyces cerevisiae* cells, the strain AH109 was used. The Frozen-EZ Yeast Transformation II Kit (Zymo Research, Freiburg, Germany) was used both for preparation of chemically competent cells and yeast transformation.

For preparation of chemically competent cells, a single colony was used to inoculate a 100 ml YPD culture and incubated at 30 °C until an OD600 of 0.8 was reached. Yeast cells were pelleted by centrifugation at 3000 g and RT for 4 min. The supernatant was removed, and the pellet was washed in 10 ml EZ 1 solution (Zymo Research, Freiburg, Germany). Cells were pelleted again at 3000 g and RT for 4 min, the supernatant was removed, and the pellet was resuspended in 2 ml EZ 2 solution (Zymo Research, Freiburg, Germany). Cell suspension was immediately divided in 50 µl aliquots, wrapped in 7 layers of tissue paper and frozen slowly in pre-cooled paper boxes at -80 °C. Competent cell aliquots were stored at -80 °C.

For transformation of chemically competent yeast cells, 1 µg of both bait- and prey-encoding plasmids were added to 10 µl of competent yeast cell suspension. Afterward, 100 µl of EZ 3 solution (Zymo Research, Freiburg, Germany) was added to the mix and the suspension was incubated at 28 °C for 90 min, with brief vortexing steps every 30 min. The entire mix was plated on SD medium containing drop-out supplement lacking either leucin and tryptophane (-L/-W) or leucin, tryptophane and

histidine (-L/-W/-H) and incubated at 30 °C for 4 days. For each transformed combination of bait and prey, 10 colonies were pooled in sterile water and the OD600 was adjusted to 1, 0.1 and 0.01. 10 µl of each cell suspension was dropped on SD medium containing drop-out supplement lacking either leucin and tryptophane (-L/-W) or leucin, tryptophane and histidine (-L/-W/-H) and incubated at 30 °C for 2 days.

5.7   IMAGING AND QUANTIFICATION OF YFP FLUORESCENCE INTENSITY

For Imaging of YFP fluorescence in stable transgenic lines expressing *35S::YFP-COP1* or *35S::YFP-SPA1*, seedlings were grown for 4 days in respective light conditions. For visualization of nuclei, seedlings were incubated in 1 µg/ml DAPI solution for 20 min at room temperature, washed in 70% (v/v) ethanol and submerged and mounted in water. Nuclei of hypocotyl cells were analyzed with a Leica SP8 confocal laser-scanning microscope (Leica Microsystems, Wetzlar, Germany). DAPI fluorescence was excited with a Diode 405 laser and detected at 443-448 nm by a HyD (Leica Microsystems, Wetzlar, Germany), and YFP fluorescence was excited with an Argon 514 laser and detected at 520-580 nm by a HyD.

For Quantification of nuclear YFP fluorescence, hyperstacks obtained from confocal laser-scanning microscopy were analyzed in 3D-ImageJ Suite (Schindelin et al., 2012, 2015; Ollion et al., 2013). First, 3D thresholding of DAPI z-stacks was performed with the tool "3D Hysteresis Thresholding". Thresholded images were then segmented with the tool "3D segmentation". Nuclear volume was then measured by capturing the volume of segmented ROIs with "Measure 3D". Lastly, ROIs obtained from DAPI z-stacks were superimposed on 3D-filtered YFP z-stacks to capture fluorescence intensity of nuclei with "Quantif 3D". Since fluorescence intensities differed significantly between experiments performed on separate days, only fluorescence values obtained from the same experiment were directly compared.

6 REFERENCES

Ahmad, M. and Cashmore, A.R. (1993). HY4 gene of A. thaliana encodes a protein with characteristics of a blue-light photoreceptor. Nature **366**: 162–166.

Ahmad, M., Jarillo, J.A., and Cashmore, A.R. (1998a). Chimeric proteins between cry1 and cry2 Arabidopsis blue light photoreceptors indicate overlapping functions and varying protein stability. Plant Cell **10**: 197–207.

Ahmad, M., Jarillo, J.A., Smirnova, O., and Cashmore, A.R. (1998b). The CRY1 blue light photoreceptor of Arabidopsis interacts with phytochrome a in vitro. Mol. Cell **1**: 939–948.

Al-Sady, B., Ni, W., Kircher, S., Schäfer, E., and Quail, P.H. (2006). Photoactivated Phytochrome Induces Rapid PIF3 Phosphorylation Prior to Proteasome-Mediated Degradation. Mol. Cell **23**: 439–446.

Ang, L.H., Chattopadhyay, S., Wei, N., Oyama, T., Okada, K., Batschauer, A., and Deng, X.W. (1998). Molecular interaction between COP1 and HY5 defines a regulatory switch for light control of Arabidopsis development. Mol. Cell **1**: 213–222.

Angers, S., Li, T., Yi, X., MacCoss, M.J., Moon, R.T., and Zheng, N. (2006). Molecular architecture and assembly of the DDB1-CUL4A ubiquitin ligase machinery. Nature **443**: 590–593.

Von Arnim, A.G. and Deng, X.-W. (1994). Light inactivation of Arabidopsis Photomorphogenic Repressor COP1 Involves a Cell-Specific Regulation of Its Nucleocytoplasmic Partitioning.

Arongaus, A.B., Chen, S., Pireyre, M., Glöckner, N., Galvão, V.C., Albert, A., Winkler, J.B., Fankhauser, C., Harter, K., and Ulm, R. (2018). Arabidopsis RUP2 represses UVR8-mediated flowering in noninductive photoperiods. Genes Dev. **32**: 1332–1343.

Artz, O., Dickopf, S., Ranjan, A., Kreiss, M., Abraham, E.T., Boll, V., Rensing, S.A., and Hoecker, U. (2019). Characterization of *spa* mutants in the moss *Physcomitrella* provides evidence for functional divergence of SPA genes during the evolution of land plants. New Phytol. **224**: 1613–1626.

Balcerowicz, M., Fittinghoff, K., Wirthmueller, L., Maier, A., Fackendahl, P., Fiene, G., Koncz, C., and Hoecker, U. (2011). Light exposure of arabidopsis seedlings causes rapid de-stabilization as well as selective post-translational inactivation of the repressor of photomorphogenesis SPA2. Plant J. **65**: 712–723.

Balcerowicz, M., Kerner, K., Schenkel, C., and Hoecker, U. (2017). SPA proteins affect the subcellular localization of COP1 in the COP1/SPA ubiquitin ligase complex during photomorphogenesis. Plant Physiol. **174**: 1314–1321.

Banerjee, R., Schleicher, E., Meier, S., Viana, R.M., Pokorny, R., Ahmad, M., Bittl, R., and Batschauer, A. (2007). The signaling state of Arabidopsis cryptochrome 2 contains flavin semiquinone. J. Biol. Chem. **282**: 14916–14922.

Baudry, A., Ito, S., Song, Y.H., Strait, A.A., Kiba, T., Lu, S., Henriques, R., Pruneda-Paz, J.L., Chua, N.H., Tobin, E.M., Kay, S.A., and Imaizumi, T. (2010). F-Box proteins FKF1 and LKP2 act in concert with ZEITLUPE to control Arabidopsis clock progression. Plant Cell **22**: 606–622.

Bayguinov, P.O., Oakley, D.M., Shih, C.-C., Geanon, D.J., Joens, M.S., and Fitzpatrick, J.A.J. (2018). Modern Laser Scanning Confocal Microscopy. Curr. Protoc. Cytom. **85**: e39.

Bernhardt, A., Lechner, E., Hano, P., Schade, V., Dieterle, M., Anders, M., Dubin, M.J., Benvenuto, G., Bowler, C., Genschik, P., and Hellmann, H. (2006). CUL4 associates with DDB1 and DET1 and its downregulation affects diverse aspects of development in *Arabidopsis thaliana*. Plant J. **47**: 591–603.

Biedermann, S. and Hellmann, H. (2011). WD40 and CUL4-based E3 ligases: Lubricating all aspects of life. Trends Plant Sci. **16**: 38–46.

Brown, B.A., Cloix, C., Jiang, G.H., Kaiserli, E., Herzyk, P., Kliebenstein, D.J., and Jenkins, G.I. (2005). A UV-B-specific signaling component orchestrates plant UV protection. Proc. Natl. Acad. Sci. U. S. A. **102**: 18225–18230.

Van Buskirk, E.K., Decker, P. V., and Chen, M. (2012). Photobodies in Light Signaling. Plant Physiol. **158**: 52–60.

de Carbonnel, M., Davis, P., Roelfsema, M.R.G., Inoue, S.I., Schepens, I., Lariguet, P., Geisler, M., Shimazaki, K.I., Hangarter, R., and Fankhauser, C. (2010). The Arabidopsis PHYTOCHROME KINASE SUBSTRATE2 protein is a phototropin signaling element that regulates leaf flattening and leaf positioning. Plant Physiol. **152**: 1391–1405.

Casal, J.J., Cerdán, P.D., Staneloni, R.J., and Cattaneo, L. (1998). Different Phototransduction Kinetics of Phytochrome A and Phytochrome B in Arabidopsis thaliana. Plant Physiol. **116**: 1533–1538.

Catalá, R., Medina, J., and Salinas, J. (2011). Integration of low temperature and light signaling during cold acclimation response in Arabidopsis. Proc. Natl. Acad. Sci. U. S. A. **108**: 16475–16480.

Chen, H., Huang, X., Gusmaroli, G., Terzaghi, W., Lau, O.S., Yanagawa, Y., Zhang, Y., Li, J., Lee, J.-H.H., Zhu, D., Deng, X.W., and Denga, X.W. (2010). Arabidopsis CULLIN4-damaged DNA binding protein 1 interacts with CONSTITUTIVELY PHOTOMORPHOGENIC1-SUPPRESSOR OF PHYA complexes to regulate photomorphogenesis and flowering time. Plant Cell **22**: 108–23.

Chen, H., Shen, Y., Tang, X., Yu, L., Wang, J., Guo, L., Zhang, Y., Zhang, H., Feng, S., Strickland, E., Zheng, N., and Deng, X.W. (2006). Arabidopsis CULLIN4 Forms an E3 Ubiquitin Ligase with RBX1 and the CDD Complex in Mediating Light Control of Development. Plant Cell **18**: 1991–2004.

Chen, M. and Chory, J. (2011). Phytochrome signaling mechanisms and the control of plant development. Trends Cell Biol. **21**: 664–671.

Chen, M., Schwab, R., and Chory, J. (2003). Characterization of the requirements for localization of phytochrome B to nuclear bodies. Proc. Natl. Acad. Sci. U. S. A. **100**: 14493–14498.

Chen, S., Lory, N., Stauber, J., and Hoecker, U. (2015). Photoreceptor Specificity in the Light-Induced and COP1-Mediated Rapid Degradation of the Repressor of Photomorphogenesis SPA2 in Arabidopsis. PLoS Genet. **11**: e1005516.

Chen, S., Wirthmueller, L., Stauber, J., Lory, N., Holtkotte, X., Leson, L., Schenkel, C., Ahmad, M., and Hoecker, U. (2016). The functional divergence between SPA1 and SPA2 in Arabidopsis photomorphogenesis maps primarily to the respective N-terminal kinase-like domain. BMC Plant Biol. **16**: 165.

Chory, J., Peto, C., Feinbaum, R., Pratt, L., and Ausubel, F. (1989). Arabidopsis thaliana mutant that develops as a light-grown plant in the absence of light. Cell **58**: 991–999.

Christie, J.M., Arvai, A.S., Baxter, K.J., Heilmann, M., Pratt, A.J., O'Hara, A., Kelly, S.M., Hothorn, M., Smith, B.O., Hitomi, K., Jenkins, G.I., and Getzoff, E.D. (2012). Plant UVR8 photoreceptor senses UV-B by tryptophan-mediated disruption of cross-dimer salt bridges. Science (80-.). **335**: 1492–1496.

Christie, J.M., Blackwood, L., Petersen, J., and Sullivan, S. (2015). Plant flavoprotein photoreceptors. Plant Cell Physiol. **56**: 401–413.

Christie, J.M., Reymond, P., Powell, G.K., Bernasconi, P., Raibekas, A.A., Liscum, E., and Briggs, W.R. (1998). Arabidopsis NPH1: A flavoprotein with the properties of a photoreceptor for phototropism. Science (80-.). **282**: 1698–1701.

Christie, J.M., Salomon, M., Nozue, K., Wada, M., and Briggs, W.R. (1999). LOV (light, oxygen, or voltage) domains of the blue-light photoreceptor phototropin (nph1): Binding sites for the

chromophore flavin mononucleotide. Proc. Natl. Acad. Sci. U. S. A. **96**: 8779–8783.

Clack, T., Mathews, S., and Sharrock, R.A. (1994). The phytochrome apoprotein family in Arabidopsis is encoded by five genes: the sequences and expression of PHYD and PHYE. Plant Mol. Biol. **25**: 413–427.

Cloix, C., Kaiserli, E., Heilmann, M., Baxter, K.J., Brown, B.A., O'Hara, A., Smith, B.O., Christie, J.M., and Jenkins, G.I. (2012). C-terminal region of the UV-B photoreceptor UVR8 initiates signaling through interaction with the COP1 protein. Proc. Natl. Acad. Sci. U. S. A. **109**: 16366–16370.

Clough, R.C. and Vierstra, R.D. (1997). Phytochrome degradation. Plant, Cell Environ. **20**: 713–721.

Clough, S.J. and Bent, A.F. (1998). Floral dip: A simplified method for Agrobacterium-mediated transformation of Arabidopsis thaliana. Plant J. **16**: 735–743.

Combs, C.A. and Shroff, H. (2017). Fluorescence microscopy: A concise guide to current imaging methods. Curr. Protoc. Neurosci. **2017**: 2.1.1-2.1.25.

Cope, G.A., Suh, G.S.B., Aravind, L., Schwarz, S.E., Zipursky, S.L., Koonin, E. V., and Deshaies, R.J. (2002). Role of predicted metalloprotease motif of Jab1/Csn5 in cleavage of Nedd8 from Cul1. Science (80-.). **298**: 608–611.

Crocco, C.D., Holm, M., Yanovsky, M.J., and Botto, J.F. (2010). AtBBX21 and COP1 genetically interact in the regulation of shade avoidance. Plant J. **64**: 551–562.

Datta, S., Johansson, H., Hettiarachchi, C., Irigoyen, M.L., Desai, M., Rubio, V., and Holm, M. (2008). LZF1/salt tolerance HOMOLOG3, an Arabidopsis B-box protein involved in light-dependent development and gene expression, undergoes COP1-mediated ubiquitination. Plant Cell **20**: 2324–2338.

Davey, M.P., Susanti, N.I., Wargent, J.J., Findlay, J.E., Paul Quick, W., Paul, N.D., and Jenkins, G.I. (2012). The UV-B photoreceptor UVR8 promotes photosynthetic efficiency in Arabidopsis thaliana exposed to elevated levels of UV-B. Photosynth. Res. **114**: 121–131.

Dehesh, K., Franci, C., Parks, B.M., Seeley, K.A., Short, T.W., Tepperman, J.M., and Quail, P.H. (1993). Arabidopsis HY8 locus encodes phytochrome A. Plant Cell **5**: 1081–1088.

Deng, X.W., Caspar, T., and Quail, P.H. (1991). cop1: A regulatory locus involved in light-controlled development and gene expression in Arabidopsis. Genes Dev. **5**: 1172–1182.

Deng, X.W., Matsui, M., Wei, N., Wagner, D., Chu, A.M., Feldmann, K.A., and Quail, P.H. (1992). COP1, an arabidopsis regulatory gene, encodes a protein with both a zinc-binding motif and a G?? homologous domain. Cell **71**: 791–801.

Deshaies, R.J. and Joazeiro, C.A.P. (2009). RING domain E3 ubiquitin ligases. Annu. Rev. Biochem. **78**: 399–434.

Devlin, P.F. and Kay, S.A. (2000). Cryptochromes are required for phytochrome signaling to the circadian clock but not for rhythmicity. Plant Cell **12**: 2499–2509.

Duek, P.D., Elmer, M. V., Van Oosten, V.R., and Fankhauser, C. (2004). The degradation of HFR1, a putative bHLH class transcription factor involved in light signaling, is regulated by phosphorylation and requires COP1. Curr. Biol. **14**: 2296–2301.

Duek, P.D. and Fankhauser, C. (2003). HFR1, a putative bHLH transcription factor, mediates both phytochrome A and cryptochrome signalling. Plant J. **34**: 827–836.

El-Din El-Assal, S., Alonso-Blanco, C., Peeters, A.J.M., Raz, V., and Koornneef, M. (2001). A QTL for flowering time in Arabidopsis reveals a novel allele of CRY2. Nat. Genet. **29**: 435–440.

Fankhauser, C. and Christie, J.M. (2015). Plant phototropic growth. Curr. Biol. **25**: R384–R389.

Fankhauser, C. and Ulm, R. (2011). Light-regulated interactions with spa proteins underlie cryptochrome-mediated gene expression. Genes Dev. **25**: 1004–1009.

Favory, J.-J.J. et al. (2009). Interaction of COP1 and UVR8 regulates UV-B-induced photomorphogenesis and stress acclimation in Arabidopsis. **28**: 591–601.

Fittinghoff, K., Laubinger, S., Nixdorf, M., Fackendahl, P., Baumgardt, R.L., Batschauer, A., and Hoecker, U. (2006). Functional and expression analysis of Arabidopsis SPA genes during seedling photomorphogenesis and adult growth. Plant J. **47**: 577–590.

Fonseca, S. and Rubio, V. (2019). Arabidopsis CRL4 Complexes: Surveying Chromatin States and Gene Expression. Front. Plant Sci. **10**.

Franklin, K.A., Davis, S.J., Stoddart, W.M., Vierstra, R.D., and Whitelam, G.C. (2003a). Mutant analyses define multiple roles for phytochrome C in Arabidopsis photomorphogenesis. Plant Cell **15**: 1981–1989.

Franklin, K.A., Praekelt, U., Stoddart, W.M., Billingham, O.E., Halliday, K.J., and Whitelam, G.C. (2003b). Phytochromes B, D, and E act redundantly to control multiple physiological responses in arabidopsis. Plant Physiol. **131**: 1340–1346.

Franklin, K.A. and Quail, P.H. (2010). Phytochrome functions in Arabidopsis development. J. Exp. Bot. **61**: 11–24.

Fraser, D.P., Hayes, S., and Franklin, K.A. (2016). Photoreceptor crosstalk in shade avoidance. Curr.

Opin. Plant Biol. **33**: 1–7.

Fujimori, T., Yamashino, T., Kato, T., and Mizuno, T. (2004). Circadian-controlled basic/helix-loop-helix factor, PIL6, implicated in light-signal transduction in Arabidopsis thaliana. Plant Cell Physiol. **45**: 1078–1086.

Genoud, T., Schweizer, F., Tscheuschler, A., Debrieux, D., Casal, J.J., Schäfer, E., Hiltbrunner, A., and Fankhauser, C. (2008). FHY1 mediates nuclear import of the light-activated phytochrome A photoreceptor. PLoS Genet. **4**.

Gruber, H., Heijde, M., Heller, W., Albert, A., Seidlitz, H.K., and Ulm, R. (2010). Negative feedback regulation of UV-B-induced photomorphogenesis and stress acclimation in Arabidopsis. Proc. Natl. Acad. Sci. U. S. A. **107**: 20132–20137.

Gu, N.N., Zhang, Y.C., and Yang, H.Q. (2012). Substitution of a conserved glycine in the PHR domain of arabidopsis CRYPTOCHROME 1 confers a constitutive light response. Mol. Plant **5**: 85–97.

Guo, H., Duong, H., Ma, N., and Lin, C. (1999). The Arabidopsis blue light receptor cryptochrome 2 is a nuclear protein regulated by a blue light-dependent post-transcriptional mechanism. Plant J. **19**: 279–287.

Guo, H., Yang, H., Mockler, T.C., and Lin, C. (1998). Regulation of flowering time by Arabidopsis photoreceptors. Science (80-.). **279**: 1360–1363.

He, Y.J., McCall, C.M., Hu, J., Zeng, Y., and Xiong, Y. (2006). DDB1 functions as a linker to recruit receptor WD40 proteins to CUL4-ROC1 ubiquitin ligases. Genes Dev. **20**: 2949–2954.

Heijde, M. and Ulm, R. (2013). Reversion of the Arabidopsis UV-B photoreceptor UVR8 to the homodimeric ground state. Proc. Natl. Acad. Sci. U. S. A. **110**: 1113–1118.

Heilmann, M., Christie, J.M., Kennis, J.T.M., Jenkins, G.I., and Mathes, T. (2015). Photoinduced transformation of UVR8 monitored by vibrational and fluorescence spectroscopy. Photochem. Photobiol. Sci. **14**: 252–257.

Heilmann, M., Velanis, C.N., Cloix, C., Smith, B.O., Christie, J.M., and Jenkins, G.I. (2016). Dimer/monomer status and *in vivo* function of salt-bridge mutants of the plant UV-B photoreceptor UVR8. Plant J. **88**: 71–81.

Hennig, L., Buche, C., and Schafer, E. (2000). Degradation of phytochrome A and the high irradiance response in Arabidopsis: a kinetic analysis. Plant, Cell Environ. **23**: 727–734.

Hennig, L., Stoddart, W.M., Dieterle, M., Whitelam, G.C., and Scháfer, E. (2002). Phytochrome E controls light-induced germination of arabidopsis. Plant Physiol. **128**: 194–200.

Higa, L. and Zhang, H. (2007). Stealing the spotlight: CUL4-DDB1 ubiquitin ligase docks WD40-repeat proteins to destroy. Cell Div. **2**.

Hiltbrunner, A., Tscheuschler, A., Andra´s, A., Viczia´n, V., Kunkel, T., Kircher, S., and Scha¨fer, E.S. (2006). Rapid Paper FHY1 and FHL Act Together to Mediate Nuclear Accumulation of the Phytochrome A Photoreceptor. Plant Cell Physiol. **47**: 1023–1034.

Hiltbrunner, A., Viczián, A., Bury, E., Tscheuschler, A., Kircher, S., Tóth, R., Honsberger, A., Nagy, F., Fankhauser, C., and Schäfer, E. (2005). Nuclear accumulation of the phytochrome A photoreceptor requires FHY1. Curr. Biol. **15**: 2125–2130.

Hoecker, U. (2005). Regulated proteolysis in light signaling. Curr. Opin. Plant Biol. **8**: 469–476.

Hoecker, U. (2017). The activities of the E3 ubiquitin ligase COP1/SPA, a key repressor in light signaling. Curr. Opin. Plant Biol. **37**: 63–69.

Hoecker, U. and Quail, P.H. (2001). The Phytochrome A-specific Signaling Intermediate SPA1 Interacts Directly with COP1, a Constitutive Repressor of Light Signaling in Arabidopsis. J. Biol. Chem. **276**: 38173–38178.

Hoecker, U., Tepperman, J.M., and Quail, P.H. (1999). SPA1, a WD-repeat protein specific to phytochrome A signal transduction. Science (80-.). **284**: 496–499.

Hoecker, U., Xu, Y., and Quail, P.H. (1998). SPA1 : A New Genetic Locus Involved in Phytochrome A-Specific Signal Transduction.

Holm, M., Hardtke, C.S., Gaudet, R., and Deng, X.W. (2001). Identification of a structural motif that confers specific interaction with the WD40 repeat domain of Arabidopsis COP1. EMBO J. **20**: 118–127.

Holm, M., Ma, L.G., Qu, L.J., and Deng, X.W. (2002). Two interacting bZIP proteins are direct targets of COP1-mediated control of light-dependent gene expression in Arabidopsis. Genes Dev. **16**: 1247–1259.

Holtkotte, X. (2014). Genetic and Biochemical Investigation of Light Signaling Components in Arabidopsis thaliana. *Ph.D. thesis*, Universität zu Köln.

Holtkotte, X., Dieterle, S., Kokkelink, L., Artz, O., Leson, L., Fittinghoff, K., Hayama, R., Ahmad, M., and Hoecker, U. (2016). Mutations in the N-terminal kinase-like domain of the repressor of photomorphogenesis SPA1 severely impair SPA1 function but not light responsiveness in Arabidopsis. Plant J. **88**: 205–218.

Holtkotte, X., Ponnu, J., Ahmad, M., and Hoecker, U. (2017). The blue light-induced interaction of

cryptochrome 1 with COP1 requires SPA proteins during Arabidopsis light signaling. PLoS Genet. **13**: e1007044.

Huang, X., Ouyang, X., and Deng, X.W. (2014). Beyond repression of photomorphogenesis: Role switching of COP/DET/FUS in light signaling. Curr. Opin. Plant Biol. **21**: 96–103.

Huang, X., Ouyang, X., Yang, P., Lau, O.S., Chen, L., Wei, N., and Deng, X.W. (2013). Conversion from CUL4-based COP1-SPA E3 apparatus to UVR8-COP1-SPA complexes underlies a distinct biochemical function of COP1 under UV-B. Proc. Natl. Acad. Sci. U. S. A. **110**: 16669–16674.

Huang, X., Ouyang, X., Yang, P., Lau, O.S., Li, G., Li, J., Chen, H., and Deng, X.W. (2012). Arabidopsis FHY3 and HY5 positively mediate induction of COP1 transcription in response to photomorphogenic UV-B light. Plant Cell **24**: 4590–4607.

Hughes, R.M., Vrana, J.D., Song, J., and Tucker, C.L. (2012). Light-dependent, dark-promoted interaction between arabidopsis cryptochrome 1 and phytochrome b proteins. J. Biol. Chem. **287**: 22165–22172.

Huq, E. and Quail, P.H. (2002). PIF4, a phytochrome-interacting bHLH factor, functions as a negative regulator of phytochrome B signaling in Arabidopsis. EMBO J. **21**: 2441–2450.

Imaizumi, T., Tran, H.G., Swartz, T.E., Briggs, W.R., and Kay, S.A. (2003). FKF1 is essential for photoperiodic-specific light signalling in Arabidopsis. Nature **426**: 302–306.

Irigoyen, M.L. et al. (2014). Targeted degradation of abscisic acid receptors is mediated by the ubiquitin ligase substrate adaptor DDA1 in Arabidopsis. Plant Cell **26**: 712–728.

Ito, S., Song, Y.H., and Imaizumi, T. (2012). LOV domain-containing F-box proteins: Light-dependent protein degradation modules in Arabidopsis. Mol. Plant **5**: 573–582.

Jackson, S. and Xiong, Y. (2009). CRL4s: the CUL4-RING E3 ubiquitin ligases. Trends Biochem. Sci. **34**: 562–570.

Jang, I.C., Henriques, R., Seo, H.S., Nagatani, A., and Chua, N.H. (2010). Arabidopsis PHYTOCHROME INTERACTING FACTOR proteins promote phytochrome B polyubiquitination by COP1 E3 ligase in the nucleus. Plant Cell **22**: 2370–2383.

Jang, I.C., Yang, J.Y., Seo, H.S., and Chua, N.H. (2005). HFR1 is targeted by COP1 E3 ligase for post-translational proteolysis during phytochrome A signaling. Genes Dev. **19**: 593–602.

Jang, S., Marchal, V., Panigrahi, K.C.S., Wenkel, S., Soppe, W., Deng, X.-W., Valverde, F., and Coupland, G. (2008). Arabidopsis COP1 shapes the temporal pattern of CO accumulation conferring a photoperiodic flowering response. EMBO J. **27**: 1277–1288.

Jarillo, J.A., Gabrys, H., Capel, J., Alonso, J.M., Ecker, J.R., and Cashmore, A.R. (2001). Phototropin-related NPL1 controls chloroplast relocation induced by blue light. Nature **410**: 952–954.

Jeong, R.D., Chandra-Shekara, A.C., Barman, S.R., Navarre, D., Klessig, D.F., Kachroo, A., and Kachroo, P. (2010). Cryptochrome 2 and phototropin 2 regulate resistance protein-mediated viral defense by negatively regulating an E3 ubiquitin ligase. Proc. Natl. Acad. Sci. U. S. A. **107**: 13538–13543.

Jiao, Y., Ma, L., Strickland, E., and Deng, X.W. (2005). Conservation and divergence of light-regulated genome expression patterns during seedling development in rice and Arabidopsis. Plant Cell **17**: 3239–3256.

Job, N., Yadukrishnan, P., Bursch, K., Datta, S., and Johansson, H. (2018). Two B-box proteins regulate photomorphogenesis by oppositely modulating HY5 through their diverse C-terminal domains. Plant Physiol. **176**: 2963–2976.

Jung, J.-H. et al. (2016). Phytochromes function as thermosensors in *Arabidopsis*. Science (80-.). **354**: 886–889.

Kagawa, T., Sakai, T., Suetsugu, N., Oikawa, K., Ishiguro, S., Kato, T., Tabata, S., Okada, K., and Wada, M. (2001). Arabidopsis NPL1: A phototropin homolog controlling the chloroplast high-light avoidance response. Science (80-.). **291**: 2138–2141.

Kaiserli, E. and Jenkins, G.I. (2007). UV-B promotes rapid nuclear translocation of the Arabidopsis UV-B-specific signaling component UVR8 and activates its function in the nucleus. Plant Cell **19**: 2662–2673.

Kang, C.Y., Lian, H.L., Wang, F.F., Huang, J.R., and Yang, H.Q. (2009). Cryptochromes, phytochromes, and COP1 regulate light-controlled stomatal development in arabidopsis. Plant Cell **21**: 2624–2641.

Keller, M.M., Jaillais, Y., Pedmale, U. V., Moreno, J.E., Chory, J., and Ballaré, C.L. (2011). Cryptochrome 1 and phytochrome B control shade-avoidance responses in Arabidopsis via partially independent hormonal cascades. Plant J. **67**: 195–207.

Kim, J., Yi, H., Choi, G., Shin, B., Song, P.S., and Choi, G. (2003). Functional Characterization of Phytochrome Interacting Factor 3 in Phytochrome-Mediated Light Signal Transduction. Plant Cell **15**: 2399–2407.

Kim, L., Kircher, S., Toth, R., Adam, E., Schäfer, E., and Nagy, F. (2000). Light-induced nuclear import of phytochrome-A:GFP fusion proteins is differentially regulated in transgenic tobacco and

Arabidopsis. Plant J. **22**: 125–133.

Kinoshita, T., Doi, M., Suetsugu, N., Kagawa, T., Wada, M., and Shimazaki, K.I. (2001). phot1 and phot2 mediate blue light regulation of stomatal opening. Nature **414**: 656–660.

Kircher, S., Gil, P., Kozma-Bognár, L., Fejes, E., Speth, V., Husselstein-Muller, T., Bauer, D., Ádám, É., Schäfer, E., and Nagy, F. (2002). Nucleocytoplasmic partitioning of the plant photoreceptors phytochrome A, B, C, D, and E is regulated differentially by light and exhibits a diurnal rhythm. Plant Cell **14**: 1541–1555.

Kircher, S., Kozma-Bognar, L., Kim, L., Adam, E., Harter, K., Schäfer, E., and Nagy, F. (1999). Light quality-dependent nuclear import of the plant photoreceptors phytochrome A and B. Plant Cell **11**: 1445–1456.

Kleine, T., Lockhart, P., and Batschauer, A. (2003). An Arabidopsis protein closely related to Synechocystis cryptochrome is targeted to organelles. Plant J. **35**: 93–103.

Kleiner, O., Kircher, S., Harter, K., and Batschauer, A. (1999). Nuclear localization of the Arabidopsis blue light receptor cryptochrome 2. Plant J. **19**: 289–296.

Kliebenstein, D.J., Lim, J.E., Landry, L.G., and Last, R.L. (2002). Arabidopsis UVR8 regulates ultraviolet-B signal transduction and tolerance and contains sequence similarity to human Regulator of Chromatin Condensation 1. Plant Physiol. **130**: 234–243.

Klose, C., Nagy, F., and Schäfer, E. (2020). Thermal Reversion of Plant Phytochromes. Mol. Plant **13**: 386–397.

Klose, C., Viczián, A., Kircher, S., Schäfer, E., and Nagy, F. (2015). Molecular mechanisms for mediating light-dependent nucleo/cytoplasmic partitioning of phytochrome photoreceptors. New Phytol. **206**: 965–971.

Koini, M.A., Alvey, L., Allen, T., Tilley, C.A., Harberd, N.P., Whitelam, G.C., and Franklin, K.A. (2009). High Temperature-Mediated Adaptations in Plant Architecture Require the bHLH Transcription Factor PIF4. Curr. Biol. **19**: 408–413.

Laemmli, U.K. (1970). Cleavage of structural proteins during the assembly of the head of bacteriophage T4. Nature **227**: 680–685.

Lagarias, J.C. and Rapoport, H. (1980). Chromopeptides from Phytochrome. The Structure and Linkage of the PR Form of the Phytochrome Chromophore. J. Am. Chem. Soc. **102**: 4821–4828.

Lau, K., Podolec, R., Chappuis, R., Ulm, R., and Hothorn, M. (2019). Plant photoreceptors and their signaling components compete for COP 1 binding via VP peptide motifs . EMBO J. **38**.

Lau, O.S. and Deng, X.W. (2012). The photomorphogenic repressors COP1 and DET1: 20 years later. Trends Plant Sci. **17**: 584–593.

Laubinger, S., Fittinghoff, K., and Hoecker, U. (2004). The SPA Quartet: A Family of WD-Repeat Proteins with a Central Role in Suppression of Photomorphogenesis in Arabidopsis. Plant Cell **16**: 2293–2306.

Laubinger, S. and Hoecker, U. (2003). The SPA1-like proteins SPA3 and SPA4 repress photomorphogenesis in the light. Plant J. **35**: 373–385.

Laubinger, S., Marchal, V., Le Gourrierec, J., Wenkel, S., Adrian, J., Jang, S., Kulajta, C., Braun, H., Coupland, G., and Hoecker, U. (2006). Arabidopsis SPA proteins regulate photoperiodic flowering and interact with the floral inducer CONSTANS to regulate its stability. Development **133**: 3213–3222.

Lee, J.-H., Terzaghi, W., Gusmaroli, G., Charron, J.-B.F., Yoon, H.-J., Chen, H., He, Y.J., Xiong, Y., and Deng, X.W. (2008). Characterization of Arabidopsis and rice DWD proteins and their roles as substrate receptors for CUL4-RING E3 ubiquitin ligases. Plant Cell **20**: 152–167.

Lee, N. and Choi, G. (2017). Phytochrome-interacting factor from Arabidopsis to liverwort. Curr. Opin. Plant Biol. **35**: 54–60.

Legris, M., Ince, Y.Ç., and Fankhauser, C. (2019). Molecular mechanisms underlying phytochrome-controlled morphogenesis in plants. Nat. Commun. **10**.

Legris, M., Klose, C., Burgie, E.S., Rojas, C.C.R., Neme, M., Hiltbrunner, A., Wigge, P.A., Schäfer, E., Vierstra, R.D., and Casal, J.J. (2016). Phytochrome B integrates light and temperature signals in *Arabidopsis*. Science (80-.). **354**: 897–900.

Leivar, P., Monte, E., Al-Sady, B., Carle, C., Storer, A., Alonso, J.M., Ecker, J.R., and Quaila, P.H. (2008). The Arabidopsis phytochrome-interacting factor PIF7, together with PIF3 and PIF4, regulates responses to prolonged red light by modulating phyB levels. Plant Cell **20**: 337–352.

Leivar, P. and Quail, P.H. (2011). PIFs: Pivotal components in a cellular signaling hub. Trends Plant Sci. **16**: 19–28.

Leivar, P., Tepperman, J.M., Monte, E., Calderon, R.H., Liu, T.L., and Quail, P.H. (2009). Definition of early transcriptional circuitry involved in light-induced reversal of PIF-imposed repression of photomorphogenesis in young Arabidopsis seedlings. Plant Cell **21**: 3535–3553.

Li, F.W., Melkonian, M., Rothfels, C.J., Villarreal, J.C., Stevenson, D.W., Graham, S.W., Wong, G.K.S., Pryer, K.M., and Mathews, S. (2015a). Phytochrome diversity in green plants and the

origin of canonical plant phytochromes. Nat. Commun. **6**.

Li, J., Li, G., Gao, S., Martinez, C., He, G., Zhou, Z., Huang, X., Lee, J.H., Zhang, H., Shen, Y., Wang, H., and Denga, X.W. (2010). Arabidopsis transcription factor ELONGATED HYPOCOTYL5 plays a role in the feedback regulation of Phytochrome a signaling. Plant Cell **22**: 3634–3649.

Li, J., Li, G., Wang, H., and Wang Deng, X. (2011). Phytochrome Signaling Mechanisms. Arab. B. **9**: e0148.

Li, N., Teranishi, M., Yamaguchi, H., Matsushita, T., Watahiki, M.K., Tsuge, T., Li, S.S., and Hidema, J. (2015b). UV-B-induced CPD photolyase gene expression is regulated by UVR8-dependent and-independent pathways in arabidopsis. Plant Cell Physiol. **56**: 2014–2023.

Lian, H.L., He, S.B., Zhang, Y.C., Zhu, D.M., Zhang, J.Y., Jia, K.P., Sun, S.X., Li, L., and Yang, H.Q. (2011). Blue-light-dependent interaction of cryptochrome 1 with SPA1 defines a dynamic signaling mechanism. Genes Dev. **25**: 1023–1028.

Lim, C.W., Baek, W., Han, S.W., and Lee, S.C. (2013). Arabidopsis PYL8 plays an important role for ABA signaling and drought stress responses. Plant Pathol. J. **29**: 471–476.

Lin, C., Robertson, D.E., Ahmad, M., Raibekas, A.A., Jorns, M.S., Dutton, P.L., and Cashmore, A.R. (1995). Association of flavin adenine dinucleotide with the Arabidopsis blue light receptor CRY1. Science (80-.). **269**: 968–970.

Ling, J.J., Li, J., Zhu, D., and Deng, X.W. (2017). Noncanonical role of Arabidopsis COP1/SPA complex in repressing BIN2-mediated PIF3 phosphorylation and degradation in darkness. Proc. Natl. Acad. Sci. U. S. A. **114**: 3539–3544.

Liu, B., Zuo, Z., Liu, H., Liu, X., and Lin, C. (2011). Arabidopsis cryptochrome 1 interacts with SPA1 to suppress COP1 activity in response to blue light. Genes Dev. **25**: 1029–1034.

Liu, H., Yu, X., Li, K., Klejnot, J., Yang, H., Lisiero, D., and Lin, C. (2008a). Photoexcited CRY2 interacts with CIB1 to regulate transcription and floral initiation in Arabidopsis. Science (80-.). **322**: 1535–1539.

Liu, L.J., Zhang, Y.C., Li, Q.H., Sang, Y., Mao, J., Lian, H.L., Wang, L., and Yang, H.Q. (2008b). COP1-mediated ubiquitination of CONSTANS is implicated in cryptochrome regulation of flowering in Arabidopsis. Plant Cell **20**: 292–306.

Liu, Y., Li, X., Li, K., Liu, H., and Lin, C. (2013). Multiple bHLH Proteins form Heterodimers to Mediate CRY2-Dependent Regulation of Flowering-Time in Arabidopsis. PLoS Genet. **9**.

Liu, Z., Li, X., Zhong, F.W., Li, J., Wang, L., Shi, Y., and Zhong, D. (2014). Quenching dynamics of

ultraviolet-light perception by UVR8 photoreceptor. J. Phys. Chem. Lett. **5**: 69–72.

Livak, K.J. and Schmittgen, T.D. (2001). Analysis of relative gene expression data using real-time quantitative PCR and the 2-ΔΔCT method. Methods **25**: 402–408.

Lorrain, S., Allen, T., Duek, P.D., Whitelam, G.C., and Fankhauser, C. (2008). Phytochrome-mediated inhibition of shade avoidance involves degradation of growth-promoting bHLH transcription factors. Plant J. **53**: 312–323.

Lorrain, S., Trevisan, M., Pradervand, S., and Fankhauser, C. (2009). Phytochrome interacting factors 4 and 5 redundantly limit seedling de-etiolation in continuous far-red light. Plant J. **60**: 449–461.

Lu, X.D., Zhou, C.M., Xu, P.B., Luo, Q., Lian, H.L., and Yang, H.Q. (2015). Red-light-dependent interaction of phyB with SPA1 promotes COP1-SPA1 dissociation and photomorphogenic development in arabidopsis. Mol. Plant **8**: 467–478.

Luebbe, A. (2016). Molecular characterisation of domain-specific interaction and subcellular localisation of COP1 and SPA1 in Arabidopsis thaliana. *B.Sc. Thesis*, Universität zu Köln.

Lyapina, S., Cope, G., Shevchenko, A., Serino, G., Tsuge, T., Zhou, C., Wolf, D.A., Wei, N., Shevchenko, A., and Deshaies, R.J. (2001). Promotion of NEDD8-CUL1 conjugate cleavage by COP9 signalosome. Science (80-.). **292**: 1382–1385.

Ma, D., Li, X., Guo, Y., Chu, J., Fang, S., Yan, C., Noel, J.P., and Liu, H. (2016). Cryptochrome 1 interacts with PIF4 to regulate high temperature-mediated hypocotyl elongation in response to blue light. Proc. Natl. Acad. Sci. U. S. A. **113**: 224–9.

Ma, L., Gao, Y., Qu, L., Chen, Z., Li, J., Zhao, H., and Deng, X.W. (2002). Genomic evidence for COP1 as a repressor of light-regulated gene expression and development in Arabidopsis. Plant Cell **14**: 2383–2398.

Ma, L., Li, J., Qu, L., Hager, J., Chen, Z., Zhao, H., and Deng, X.W. (2001). Light Control of Arabidopsis Development Entails Coordinated Regulation of Genome Expression and Cellular Pathways. Plant Cell **13**: 2589–2607.

Ma, L., Wang, X., Guan, Z., Wang, L., Wang, Y., Zheng, L., Gong, Z., Shen, C., Wang, J., Zhang, D., Liu, Z., and Yin, P. (2020). Structural insights into BIC-mediated inactivation of Arabidopsis cryptochrome 2. Nat. Struct. Mol. Biol. **27**: 472–479.

Maier, A., Schrader, A., Kokkelink, L., Falke, C., Welter, B., Iniesto, E., Rubio, V., Uhrig, J.F., Hülskamp, M., and Hoecker, U. (2013). Light and the E3 ubiquitin ligase COP1/SPA control the protein stability of the MYB transcription factors PAP1 and PAP2 involved in anthocyanin

accumulation in Arabidopsis. Plant J. **74**: 638–651.

Mao, J., Zhang, Y.C., Sang, Y., Li, Q.H., and Yang, H.Q. (2005). A role for Arabidopsis cryptochromes and COP1 in the regulation of stomatal opening. Proc. Natl. Acad. Sci. U. S. A. **102**: 12270–12275.

Martínez, C., Nieto, C., and Prat, S. (2018). Convergent regulation of PIFs and the E3 ligase COP1/SPA1 mediates thermosensory hypocotyl elongation by plant phytochromes. Curr. Opin. Plant Biol. **45**: 188–203.

Mas, P., Devlin, P.F., Panda, S., and Kay, S.A. (2000). Functional interaction of phytochrome B and cryptochrome 2. Nature **408**: 207–211.

Mathes, T., Heilmann, M., Pandit, A., Zhu, J., Ravensbergen, J., Kloz, M., Fu, Y., Smith, B.O., Christie, J.M., Jenkins, G.I., and Kennis, J.T.M. (2015). Proton-Coupled Electron Transfer Constitutes the Photoactivation Mechanism of the Plant Photoreceptor UVR8. J. Am. Chem. Soc. **137**: 8113–8120.

Matsushita, T., Mochizuki, N., and Nagatani, A. (2003). Dimers of the N-terminal domain of phytochrome B are functional in the nucleus. Nature **424**: 571–574.

McNellis, T.W., von Arnim, A.G., Araki, T., Komeda, Y., Misera, S., and Deng Xing Wang (1994a). Genetic and molecular analysis of an allelic series of cop1 mutants suggests functional roles for the multiple protein domains. Plant Cell **6**: 487–500.

McNellis, T.W., von Arnim, A.G., and Deng Xing Wang (1994b). Overexpression of Arabidopsis COP1 results in partial suppression of light-mediated development: Evidence for a light-inactivable repressor of photomorphogenesis. Plant Cell **6**: 1391–1400.

Menon, C., Sheerin, D.J., and Hiltbrunner, A. (2016). SPA proteins: SPAnning the gap between visible light and gene expression. Planta **244**: 297–312.

Migliori, V., Mapelli, M., and Guccione, E. (2012). On WD40 proteins propelling our knowledge of transcriptional control? Epigenetics **7**: 815–822.

Morales, L.O., Brosché, M., Vainonen, J., Jenkins, G.I., Wargent, J.J., Sipari, N., Strid, Å., Lindfors, A. V., Tegelberg, R., and Aphalo, P.J. (2013). Multiple roles for UV RESISTANCE LOCUS8 in regulating gene expression and metabolite accumulation in arabidopsis under solar ultraviolet radiation. Plant Physiol. **161**: 744–759.

Moriconi, V., Binkert, M., Costigliolo, C., Sellaro, R., Ulm, R., and Casal, J.J. (2018). Perception of Sunflecks by the UV-B Photoreceptor UV RESISTANCE LOCUS8. Plant Physiol. **177**: 75–81.

Müller, P. and Bouly, J.P. (2015). Searching for the mechanism of signalling by plant photoreceptor cryptochrome. FEBS Lett. **589**: 189–192.

Nagatani, A. (2004). Light-regulated nuclear localization of phytochromes. Curr. Opin. Plant Biol. **7**: 708–711.

Nagatani, A., Chory, J., and Furuya, M. (1991). Phytochrome B Is Not Detectable in the hy3 Mutant of Arabidopsis, Which Is Deficient in Responding to End-of-Day Far-Red Light Treatments. Plant Cell Physiol. **32**: 1119–1122.

Nagatani, A., Reed, J.W., and Chory, J. (1993). Isolation and initial characterization of Arabidopsis mutants that are deficient in phytochrome A. Plant Physiol. **102**: 269–277.

Neff, M.M., Fankhauser, C., and Chory, J. (2000). Light: An indicator of time and place. Genes Dev. **14**: 257–271.

Ni, W., Xu, S.L., Chalkley, R.J., Pham, T.N.D., Guan, S., Maltby, D.A., Burlingame, A.L., Wang, Z.Y., and Quail, P.H. (2013). Multisite light-induced phosphorylation of the transcription factor PIF3 Is necessary for both its rapid degradation and concomitant negative feedback modulation of photoreceptor phyB levels in Arabidopsis. Plant Cell **25**: 2679–2698.

Ni, W., Xu, S.L., Tepperman, J.M., Stanley, D.J., Maltby, D.A., Gross, J.D., Burlingame, A.L., Wang, Z.Y., and Quail, P.H. (2014). A mutually assured destruction mechanism attenuates light signaling in Arabidopsis. Science (80-.). **344**: 1160–1164.

Nixdorf, M. and Hoecker, U. (2010). SPA1 and DET1 act together to control photomorphogenesis throughout plant development. Planta **231**: 825–833.

van Nocker, S. and Ludwig, P. (2003). The WD-repeat protein superfamily in Arabidopsis: Conservation and divergence in structure and function. BMC Genomics **4**.

Oh, E., Kim, J., Park, E., Kim, J. Il, Kang, C., and Choi, G. (2004). PIL5, a phytochrome-interacting basic helix-loop-helix protein, is a key negative regulator of seed germination in Arabidopsis thaliana. Plant Cell **16**: 3045–3058.

Okajima, K. (2016). Molecular mechanism of phototropin light signaling. J. Plant Res. **129**: 149–157.

Ollion, J., Cochennec, J., Loll, F., Escudé, C., and Boudier, T. (2013). TANGO: A generic tool for high-throughput 3D image analysis for studying nuclear organization. Bioinformatics **29**: 1840–1841.

Oravecz, A., Baumann, A., Máté, Z., Brzezinska, A., Molinier, J., Oakeley, E.J., Ádám, É., Schäfer, E., Nagy, F., and Ulm, R. (2006). CONSTITUTIVELY PHOTOMORPHOGENIC1 is required for the UV-B response in Arabidopsis. Plant Cell **18**: 1975–1990.

Ordoñez-Herrera, N., Fackendahl, P., Yu, X., Schaefer, S., Koncz, C., and Hoecker, U. (2015). A cop1 spa mutant deficient in COP1 and SPA proteins reveals partial Co-action of COP1 and SPA during arabidopsis post-embryonic development and photomorphogenesis. Mol. Plant **8**: 479–481.

Osterlund, M.T. and Deng, X.W. (1998). Multiple photoreceptors mediate the light-induced reduction of GUS-COP1 from Arabidopsis hypocotyl nuclei. Plant J. **16**: 201–208.

Osterlund, M.T., Hardtke, C.S., Wei, N., and Deng, X.W. (2000). Targeted destabilization of HY5 during light-regulated development of Arabidopsis. Nature **405**: 462–466.

Pacín, M., Legris, M., and Casal, J.J. (2013). COP1 re-accumulates in the nucleus under shade. Plant J. **75**: 631–641.

Pacín, M., Legris, M., and Casal, J.J. (2014). Rapid decline in nuclear COSTITUTIVE PHOTOMORPHOGENESIS1 abundance anticipates the stabilization of its target ELONGATED HYPOCOTYL5 in the light. Plant Physiol. **164**: 1134–1138.

Pacín, M., Semmoloni, M., Legris, M., Finlayson, S.A., and Casal, J.J. (2016). Convergence of CONSTITUTIVE PHOTOMORPHOGENESIS 1 and PHYTOCHROME INTERACTING FACTOR signalling during shade avoidance. New Phytol. **211**: 967–979.

Paik, I., Chen, F., Ngoc Pham, V., Zhu, L., Kim, J. Il, and Huq, E. (2019). A phyB-PIF1-SPA1 kinase regulatory complex promotes photomorphogenesis in Arabidopsis. Nat. Commun. **10**.

Paik, I. and Huq, E. (2019). Plant photoreceptors: Multi-functional sensory proteins and their signaling networks. Semin. Cell Dev. Biol. **92**: 114–121.

Palágyi, A., Terecskei, K., Ádám, É., Kevei, É., Kircher, S., Mérai, Z., Schäfer, E., Nagy, F., and Kozma-Bognár, L. (2010). Functional analysis of amino-terminal domains of the photoreceptor phytochrome B. Plant Physiol. **153**: 1834–1845.

Park, Y.J., Lee, H.J., Ha, J.H., Kim, J.Y., and Park, C.M. (2017). COP1 conveys warm temperature information to hypocotyl thermomorphogenesis. New Phytol. **3**.

Parks, B.M. and Quail, P.H. (1993). hy8, a new class of arabidopsis long hypocotyl mutants deficient in functional phytochrome A. Plant Cell **5**: 39–48.

Pawley, J.B. (2006). HANDBOOK OF BIOLOGICAL CONFOCAL MICROSCOPY THIRD EDITION.

Pedmale, U. V., Huang, S.S.C., Zander, M., Cole, B.J., Hetzel, J., Ljung, K., Reis, P.A.B., Sridevi, P., Nito, K., Nery, J.R., Ecker, J.R., and Chory, J. (2016). Cryptochromes Interact Directly with PIFs to Control Plant Growth in Limiting Blue Light. Cell **164**: 233–245.

Pepper, A., Delaney, T., Washburnt, T., Poole, D., and Chory, J. (1994). DET1, a negative regulator of light-mediated development and gene expression in arabidopsis, encodes a novel nuclear-localized protein. Cell **78**: 109–116.

Pfeiffer, A., Nagel, M.K., Popp, C., Wüst, F., Bindics, J., Viczián, A., Hiltbrunner, A., Nagy, F., Kunkel, T., and Schäfer, E. (2012). Interaction with plant transcription factors can mediate nuclear import of phytochrome B. Proc. Natl. Acad. Sci. U. S. A. **109**: 5892–5897.

Pham, V.N., Paik, I., Hoecker, U., and Huq, E. (2020). Genomic evidence reveals <scp>SPA</scp> -regulated developmental and metabolic pathways in dark-grown <scp> *Arabidopsis* </scp> seedlings. Physiol. Plant. **169**: 380–396.

Pick, E., Lau, O.-S., Tsuge, T., Menon, S., Tong, Y., Dohmae, N., Plafker, S.M., Deng, X.W., and Wei, N. (2007). Mammalian DET1 Regulates Cul4A Activity and Forms Stable Complexes with E2 Ubiquitin-Conjugating Enzymes. Mol. Cell. Biol. **27**: 4708–4719.

Pokorny, R., Klar, T., Hennecke, U., Carell, T., Batschauer, A., and Essen, L.O. (2008). Recognition and repair of UV lesions in loop structures of duplex DNA by DASH-type cryptochrome. Proc. Natl. Acad. Sci. U. S. A. **105**: 21023–21027.

Ponnu, J. (2020). Molecular mechanisms suppressing <scp>COP1</scp> / <scp>SPA E3</scp> ubiquitin ligase activity in blue light. Physiol. Plant. **169**: 418–429.

Ponnu, J., Riedel, T., Penner, E., Schrader, A., and Hoecker, U. (2019). Cryptochrome 2 competes with COP1 substrates to repress COP1 ubiquitin ligase activity during Arabidopsis photomorphogenesis. Proc. Natl. Acad. Sci. U. S. A. **116**: 27133–27141.

Qian, C., Mao, W., Liu, Y., Ren, H., Sun Lau, O., Ouyang, X., and Huang, X. (2016). Dual-Source Nuclear Monomers of UV-B Light Receptor Direct Photomorphogenesis in Arabidopsis Molecular Plant Letter to the Editor.

Ranjan, A., Dickopf, S., Ullrich, K.K., Rensing, S.A., and Hoecker, U. (2014). Functional analysis of COP1 and SPA orthologs from Physcomitrella and rice during photomorphogenesis of transgenic Arabidopsis reveals distinct evolutionary conservation. BMC Plant Biol. **14**.

Reed, J.W., Nagatani, A., Elich, T.D., Fagan, M., and Chory, J. (1994). Phytochrome A and phytochrome B have overlapping but distinct functions in Arabidopsis development. Plant Physiol. **104**: 1139–1149.

Rizzini, L., Favory, J.J., Cloix, C., Faggionato, D., O'Hara, A., Kaiserli, E., Baumeister, R., Schäfer, E., Nagy, F., Jenkins, G.I., and Ulm, R. (2011). Perception of UV-B by the arabidopsis UVR8 protein.

Science (80-.). **332**: 103–106.

Rockwell, N.C. and Lagarias, J.C. (2006). The structure of phytochrome: A picture is worth a thousand spectra. Plant Cell **18**: 4–14.

Rolauffs, S., Fackendahl, P., Sahm, J., Fiene, G., and Hoecker, U. (2012). Arabidopsis COP1 and SPA genes are essential for plant elongation but not for acceleration of flowering time in response to a low red light to far-red light ratio. Plant Physiol. **160**: 2015–2027.

Saijo, Y., Sullivan, J.A., Wang, H., Yang, J., Shen, Y., Rubio, V., Ma, L., Hoecker, U., and Deng, X.W. (2003). The COP1-SPA1 interaction defines a critical step in phytochrome A-mediated regulation of HY5 activity. Genes Dev. **17**: 2642–2647.

Sakamoto, K. and Nagatani, A. (1996). Nuclear localization activity of phytochrome B. Plant J. **10**: 859–868.

Sambrook, J. and Russell, D.W. (2001). Molecular cloning: a laboratory manual. (Cold Spring Harbor Laboratory Press).

Sang, Y., Li, Q.H., Rubio, V., Zhang, Y.C., Mao, J., Deng, X.W., and Yang, H.Q. (2005). N-terminal domain-mediated homodimerization is required for photoreceptor activity of Arabidopsis Cryptochrome 1. Plant Cell **17**: 1569–1584.

Sarikas, A., Hartmann, T., and Pan, Z.Q. (2011). The cullin protein family. Genome Biol. **12**.

Schindelin, J. et al. (2012). Fiji: An open-source platform for biological-image analysis. Nat. Methods **9**: 676–682.

Schindelin, J., Rueden, C.T., Hiner, M.C., and Eliceiri, K.W. (2015). The ImageJ ecosystem: An open platform for biomedical image analysis. Mol. Reprod. Dev. **82**: 518–529.

Schroeder, D.F., Gahrtz, M., Maxwell, B.B., Cook, R.K., Kan, J.M., Alonso, J.M., Ecker, J.R., and Chory, J. (2002). De-etiolated 1 and damaged DNA binding protein 1 interact to regulate Arabidopsis photomorphogenesis. Curr. Biol. **12**: 1462–1472.

Schwechheimer, C. and Deng, X.W. (2000). The COP/DET/FUS proteins - Regulators of eukaryotic growth and development. Semin. Cell Dev. Biol. **11**: 495–503.

Schwechheimer, C., Serino, G., Callis, J., Crosby, W.L., Lyapina, S., Deshaies, R.J., Gray, W.M., Estelle, M., and Deng, X.W. (2001). Interactions of the COP9 signalosome with the E3 ubiquitin ligase SCFTIR1 in mediating auxin response. Science (80-.). **292**: 1379–1382.

Sellaro, R., Hoecker, U., Yanovsky, M., Chory, J., and Casal, J.J. (2009). Synergism of Red and Blue

Light in the Control of Arabidopsis Gene Expression and Development. Curr. Biol. **19**: 1216–1220.

Seo, H.S. et al. (2003a). LAF1 ubiquitination by COP1 controls photomorphogenesis and is stimulated by SPA1. Nature **423**: 995–999.

Seo, H.S., Watanabe, E., Tokutomi, S., Nagatani, A., and Chua, N.H. (2004). Photoreceptor ubiquitination by COP1 E3 ligase desensitizes phytochrome A signaling. Genes Dev. **18**: 617–622.

Seo, H.S., Yang, J.-Y., Ishikawa, M., Bolle, C., Ballesteros, M.L., and Chua, N.-H. (2003b). LAF1 ubiquitination by COP1 controls photomorphogenesis and is stimulated by SPA1. Nature **423**: 995–999.

Serino, G. and Deng, X.-W. (2003). THE COP9 SIGNALOSOME: Regulating Plant Development Through the Control of Proteolysis. Annu. Rev. Plant Biol. **54**: 165–182.

Sharma, A., Sharma, B., Hayes, S., Kerner, K., Hoecker, U., Jenkins, G.I., and Franklin, K.A. (2019). UVR8 disrupts stabilisation of PIF5 by COP1 to inhibit plant stem elongation in sunlight. Nat. Commun. **10**.

Sharrock, R.A. and Clack, T. (2002). Patterns of expression and normalized levels of the five Arabidopsis phytochromes. Plant Physiol. **130**: 442–456.

Sharrock, R.A. and Quail, P.H. (1989). Novel phytochrome sequences in Arabidopsis thaliana: structure, evolution, and differential expression of a plant regulatory photoreceptor family. Genes Dev. **3**: 1745–1757.

Shaw, P.J. and Brown, J.W. (2004). Plant nuclear bodies. Curr. Opin. Plant Biol. **7**: 614–620.

Sheerin, D.J., Menon, C., zur Oven-Krockhaus, S., Enderle, B., Zhu, L., Johnen, P., Schleifenbaum, F., Stierhof, Y.-D., Huq, E., and Hiltbrunner, A. (2015). Light-Activated Phytochrome A and B Interact with Members of the SPA Family to Promote Photomorphogenesis in Arabidopsis by Reorganizing the COP1/SPA Complex. Plant Cell Online **27**: 189–201.

Shin, A.Y., Han, Y.J., Baek, A., Ahn, T., Kim, S.Y., Nguyen, T.S., Son, M., Lee, K.W., Shen, Y., Song, P.S., and Kim, J. Il (2016). Evidence that phytochrome functions as a protein kinase in plant light signalling. Nat. Commun. **7**: 1–13.

Shin, J., Kim, K., Kang, H., Zulfugarov, I.S., Bae, G., Lee, C.H., Lee, D., and Choi, G. (2009). Phytochromes promote seedling light responses by inhibiting four negatively-acting phytochrome-interacting factors. Proc. Natl. Acad. Sci. U. S. A. **106**: 7660–7665.

Shin, J., Park, E., and Choi, G. (2007). PIF3 regulates anthocyanin biosynthesis in an HY5-dependent manner with both factors directly binding anthocyanin biosynthetic gene promoters in Arabidopsis. Plant J. **49**: 981–994.

Smalle, J. and Vierstra, R.D. (2004). The ubiquitin 26S proteasome proteolytic pathway. Annu. Rev. Plant Biol. **55**: 555–590.

Somers, D.E., Schultz, T.F., Milnamow, M., and Kay, S.A. (2000). ZEITLUPE encodes a novel clock-associated PAS protein from Arabidopsis. Cell **101**: 319–329.

Spector, D.L. (2006). SnapShot: Cellular Bodies. Cell **127**: 1071.e1-1071.e2.

Stacey, M.G. and Von Arnim, A.G. (1999). A novel motif mediates the targeting of the Arabidopsis COP1 protein to subnuclear foci. J. Biol. Chem. **274**: 27231–27236.

Stacey, M.G., Hicks, S.N., and Von Arnim, A.G. (1999). Discrete domains mediate the light-responsive nuclear and cytoplasmic localization of Arabidopsis COP1. Plant Cell **11**: 349–363.

Stacey, M.G., Kopp, O.R., Kim, T.H., and Von Arnim, A.G. (2000). Modular domain structure of Arabidopsis COP1. Reconstitution of activity by fragment complementation and mutational analysis of a nuclear localization signal in planta. Plant Physiol. **124**: 979–989.

Stephenson, P.G., Fankhauser, C., and Terry, M.J. (2009). PIF3 is a repressor of chloroplast development. Proc. Natl. Acad. Sci. U. S. A. **106**: 7654–7659.

Stracke, R., Favory, J.-J., Gruber, H., Bartelniewoehner, L., Bartels, S., Binkert, M., Funk, M., Weisshaar, B., and Ulm, R. (2010). The Arabidopsis bZIP transcription factor HY5 regulates expression of the PFG1 / MYB12 gene in response to light and ultraviolet-B radiation. Plant. Cell Environ. **33**: 88–103.

Su, J., Liu, B., Liao, J., Yang, Z., Lin, C., and Oka, Y. (2017). Coordination of Cryptochrome and Phytochrome Signals in the Regulation of Plant Light Responses. Agronomy **7**: 25.

Subramanian, C., Kim, B.H., Lyssenko, N.N., Xu, X., Johnson, C.H., and Von Arnim, A.G. (2004). The Arabidopsis repressor of light signaling, COP1, is regulated by nuclear exclusion: Mutational analysis by bioluminescence resonance energy transfer. Proc. Natl. Acad. Sci. U. S. A. **101**: 6798–6802.

Tepperman, J.M., Zhu, T., Chang, H.-S.S., Wang, X., and Quail, P.H. (2001). Multiple transcription-factor genes are early targets of phytochrome A signaling. Proc. Natl. Acad. Sci. U. S. A. **98**: 9437–9442.

Tevatia, R. and Oyler, G.A. (2018). Evolution of DDB1-binding WD40 (DWD) in the viridiplantae. PLoS

One **13**.

Torii, K.U., McNellis, T.W., and Deng, X.W. (1998). Functional dissection of Arabidopsis COP1 reveals specific roles of its three structural modules in light control of seedling development. EMBO J. **17**: 5577–5587.

Tuller, T., Diament, A., Yahalom, A., Zemach, A., Atar, S., Chamovitz, D.A., and Birol, I. (2019). The COP9 signalosome influences the epigenetic landscape of Arabidopsis thaliana. Bioinformatics **35**: 2718–2723.

Uljon, S., Xu, X., Durzynska, I., Stein, S., Adelmant, G., Marto, J.A., Pear, W.S., and Blacklow, S.C. (2016). Structural Basis for Substrate Selectivity of the E3 Ligase COP1. Structure **24**: 687–696.

Vaishak, K.P., Yadukrishnan, P., Bakshi, S., Kushwaha, A.K., Ramachandran, H., Job, N., Babu, D., and Datta, S. (2019). The B-box bridge between light and hormones in plants. J. Photochem. Photobiol. B Biol. **191**: 164–174.

Viczián, A., Ádám, É., Wolf, I., Bindics, J., Kircher, S., Heijde, M., Ulm, R., Schäfer, E., and Nagy, F. (2012). A short amino-terminal part of Arabidopsis phytochrome a induces constitutive photomorphogenic response. Mol. Plant **5**: 629–641.

Voityuk, A.A., Marcus, R.A., and Michel-Beyerle, M.E. (2014). On the mechanism of photoinduced dimer dissociation in the plant UVR8 photoreceptor. Proc. Natl. Acad. Sci. U. S. A. **111**: 5219–5224.

Wang, H., Ma, L.G., Li, J.M., Zhao, H.Y., and Xing Wang Deng (2001). Direct interaction of Arabidopsis cryptochromes with COP1 in light control development. Science (80-.). **294**: 154–158.

Wang, Q. et al. (2016). Photoactivation and inactivation of Arabidopsis cryptochrome 2. Science (80-.). **354**: 343–347.

Wang, Q., Liu, Q., Wang, X., Zuo, Z., Oka, Y., and Lin, C. (2018a). New insights into the mechanisms of phytochrome–cryptochrome coaction. New Phytol. **217**: 547–551.

Wang, W., Qu, M., Wang, J., Zhang, X., Zhang, H., Wu, J., Yu, B., Wu, H., Kong, W., and Yu, X. (2018b). Autoubiquitination of feline E3 ubiquitin ligase BCA2. Gene **638**: 1–6.

Wang, X. et al. (2017). A CRY-BIC negative-feedback circuitry regulating blue light sensitivity of Arabidopsis. Plant J. **92**: 426–436.

Wang, X., Li, W., Piqueras, R., Cao, K., Deng, X.W., and Wei, N. (2009). Regulation of COP1 nuclear localization by the COP9 signalosome via direct interaction with CSN1. Plant J. **58**: 655–667.

Wang, X., Wang, Q., Nguyen, P., and Lin, C. (2014). Cryptochrome-mediated light responses in plants. In Enzymes (Academic Press), pp. 167–189.

Wei, N., Serino, G., and Deng, X.W. (2008). The COP9 signalosome: more than a protease. Trends Biochem. Sci. **33**: 592–600.

Wei Ning, Kwok Shing, F., von Arnim, A.G., Lee, A., McNellis, T.W., Piekos, B., and Deng Xing Wang (1994). Arabidopsis COP8, COP10 and COP11 genes are involved in repression of photomorphogenic development in darkness. Plant Cell **6**: 629–643.

Wertz, I.E., O'Rourke, K.M., Zhang, Z., Dornan, D., Arnott, D., Deshaies, R.J., and Dixit, V.M. (2004). Human De-Etiolated-1 Regulates c-Jun by Assembling a CUL4AUbiquitin Ligase. Science **303**: 1371–1374.

Di Wu, Hu, Q., Yan, Z., Chen, W., Yan, C., Huang, X., Zhang, J., Yang, P., Deng, H., Wang, J., Deng, X., and Shi, Y. (2012). Structural basis of ultraviolet-B perception by UVR8. Nature **484**: 214–219.

Wu, G. and Spalding, E.P. (2007). Separate functions for nuclear and cytoplasmic cryptochrome 1 during photomorphogenesis of Arabidopsis seedlings. Proc. Natl. Acad. Sci. U. S. A. **104**: 18813–18818.

Wu, M., Strid, Å., and Eriksson, L.A. (2014). Photochemical reaction mechanism of UV-B-induced monomerization of UVR8 dimers as the first signaling event in UV-B-regulated gene expression in plants. J. Phys. Chem. B **118**: 951–965.

Xu, X., Paik, I., Zhu, L., Bu, Q., Huang, X., Deng, X.W., and Huq, E. (2014). PHYTOCHROME INTERACTING FACTOR1 enhances the E3 ligase activity of CONSTITUTIVE PHOTOMORPHOGENIC1 to synergistically repress photomorphogenesis in Arabidopsis. Plant Cell **26**: 1992–2006.

Xu, X., Paik, I., Zhu, L., and Huq, E. (2015). Illuminating Progress in Phytochrome-Mediated Light Signaling Pathways. Trends Plant Sci. **20**: 641–650.

Yamaguchi, R., Nakamura, M., Mochizuki, N., Kay, S.A., and Nagatani, A. (1999). Light-dependent translocation of a phytochrome B-GFP fusion protein to the nucleus in transgenic Arabidopsis. J. Cell Biol. **145**: 437–445.

Yanagawa, Y., Sullivan, J.A., Komatsu, S., Gusmaroli, G., Suzuki, G., Yin, J., Ishibashi, T., Saijo, Y., Rubio, V., Kimura, S., Wang, J., and Deng, X.W. (2004). Arabidopsis COP10 forms a complex with DDB1 and DET1 in vivo and enhances the activity of ubiquitin conjugating enzymes. Genes Dev. **18**: 2172–2181.

Yang, H.-Q., Tang, R.-H., and Cashmore, A.R. (2001). The Signaling Mechanism of Arabidopsis CRY1 Involves Direct Interaction with COP1. Plant Cell **13**: 2573–2587.

Yang, J., Lin, R., Hoecker, U., Liu, B., Xu, L., and Wang, H. (2005a). Repression of light signaling by Arabidopsis SPA1 involves post-translational regulation of HFR1 protein accumulation. Plant J. **43**: 131–141.

Yang, J., Lin, R., Sullivan, J., Hoecker, U., Liu, B., Xu, L., Xing, W.D., and Wang, H. (2005b). Light regulates COP1-mediated degradation of HFR1, a transcription factor essential for light signaling in Arabidopsis. Plant Cell **17**: 804–821.

Yang, J. and Wang, H. (2006). The central coiled-coil domain and carboxyl-terminal WD-repeat domain of Arabidopsis SPA1 are responsible for mediating repression of light signaling. Plant J. **47**: 564–576.

Yang, Y. and Xiaodan, Y. (2003). Regulation of apoptosis: the ubiquitous way. FASEB J. **17**: 790–799.

Yi, C. and Deng, X.W. (2005). COP1 - From plant photomorphogenesis to mammalian tumorigenesis. Trends Cell Biol. **15**: 618–625.

Yin, R., Skvortsova, M.Y., Loubéry, S., and Ulm, R. (2016). COP1 is required for UV-B-induced nuclear accumulation of the UVR8 photoreceptor. Proc. Natl. Acad. Sci. U. S. A. **113**: E4415–E4422.

Yin, R. and Ulm, R. (2017). How plants cope with UV-B: from perception to response. Curr. Opin. Plant Biol. **37**: 42–48.

Yu, J.W. et al. (2008). COP1 and ELF3 Control Circadian Function and Photoperiodic Flowering by Regulating GI Stability. Mol. Cell **32**: 617–630.

Yu, X., Sayegh, R., Maymon, M., Warpeha, K., Klejnot, J., Yang, H., Huang, J., Lee, J., Kaufman, L., and Lina, C. (2009). Formation of nuclear bodies of Arabidopsis CRY2 in response to blue light is associated with its blue light-dependent degradation. Plant Cell **21**: 118–130.

Yu, X., Shalitin, D., Liu, X., Maymon, M., Klejnot, J., Yang, H., Lopez, J., Zhao, X., Bendehakkalu, K.T., and Lin, C. (2007). Derepression of the NC80 motif is critical for the photoactivation of Arabidopsis CRY2. Proc. Natl. Acad. Sci. U. S. A. **104**: 7289–7294.

Zeng, X., Ren, Z., Wu, Q., Fan, J., Peng, P.P., Tang, K., Zhang, R., Zhao, K.H., and Yang, X. (2015). Dynamic crystallography reveals early signalling events in ultraviolet photoreceptor UVR8. Nat. Plants **1**: 1–6.

Zhang, Y., Feng, S., Chen, F., Chen, H., Wang, J., McCall, C., Xiong, Y., and Xing, W.D. (2008). Arabidopsis DDB1-CUL4 associated factor1 forms a nuclear E3 ubiquitin ligase with DDB1 and

CUL4 that is involved in multiple plant developmental processes. Plant Cell **20**: 1437–1455.

Zhang, Y., Mayba, O., Pfeiffer, A., Shi, H., Tepperman, J.M., Speed, T.P., and Quail, P.H. (2013). A Quartet of PIF bHLH Factors Provides a Transcriptionally Centered Signaling Hub That Regulates Seedling Morphogenesis through Differential Expression-Patterning of Shared Target Genes in Arabidopsis. PLoS Genet. **9**: e1003244.

Zheng, X. et al. (2013). Arabidopsis phytochrome B promotes SPA1 nuclear accumulation to repress photomorphogenesis under far-red light. Plant Cell **25**: 115–133.

Zhu, D., Maier, A., Lee, J.H., Laubinger, S., Saijo, Y., Wang, H., Qu, L.J., Hoecker, U., and Deng, X.W. (2008). Biochemical characterization of Arabidopsis complexes containing constitutively photomorphogenic1 and suppressor of PHYA proteins in light control of plant development. Plant Cell **20**: 2307–2323.

Zimmerman, E.S., Schulman, B.A., and Zheng, N. (2010). Structural assembly of cullin-RING ubiquitin ligase complexes. Curr. Opin. Struct. Biol. **20**: 714–721.

Zuo, Z., Liu, H., Liu, B., Liu, X., and Lin, C. (2011). Blue light-dependent interaction of CRY2 with SPA1 regulates COP1 activity and floral initiation in arabidopsis. Curr. Biol. **21**: 841–847.

Zuo, Z.C., Meng, Y.Y., Yu, X.H., Zhang, Z.L., Feng, D.S., Sun, S.F., Liu, B., and Lin, C.T. (2012). A study of the blue-light-dependent phosphorylation, degradation, and photobody formation of Arabidopsis CRY2. Mol. Plant **5**: 726–733.

7 SUPPLEMENTS

Supplemental Figure S 1: Multiple sequence alignment of Arabidopsis COP1 and SPA1-4 peptide sequences.

Amino acid sequences of Arabidopsis COP1, SPA1, SPA2, SPA3 and SPA4 were aligned with the ClustalW algorithm using standard parameters. Consensus identity depicts degree of sequence identity and consensus sequence. Predicted protein domains were annotated with the program Geneious. NLS and CLS were manually annotated as described by previous studies (Deng et al., 1991; Hoecker et al., 1998)
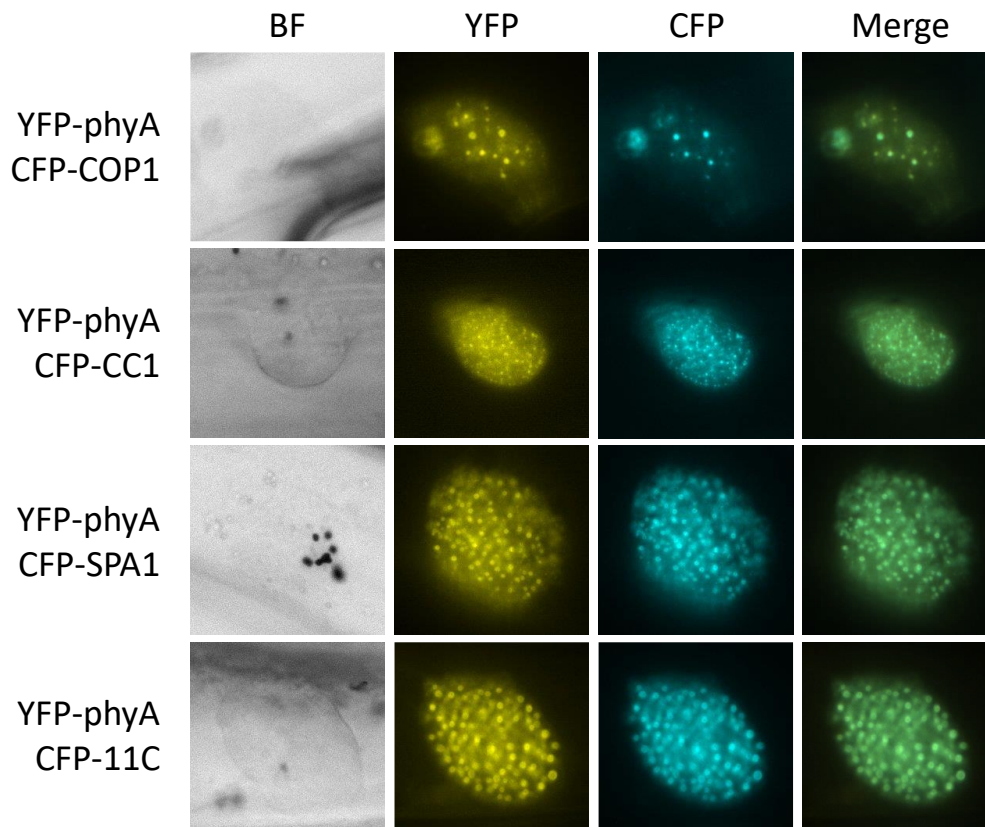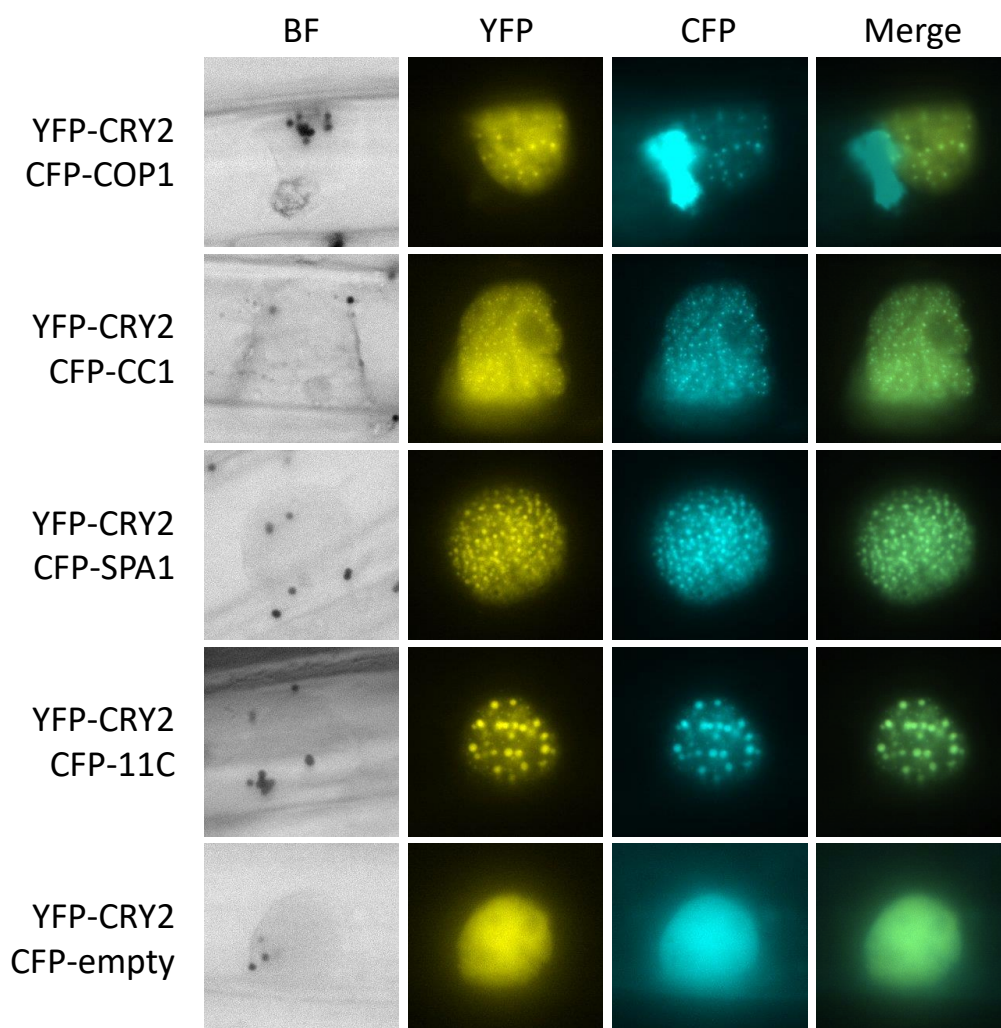
Supplemental Figure S 2: Chimeric COP1/SPA1 domain-swap proteins co-localize with phyA.

Fluorescence microscopy images visualizing co-localization of fluorescence-tagged COP1, SPA1 and domain-swap proteins with phyA. Proteins fused to either YFP or CFP were co-expressed in leek epidermal cells and analyzed using confocal laser scanning microscopy. Columns (left to right): Bright field (BF), image captured in the YFP channel (YFP); image captured in the CFP channel (CFP); YFP and CFP images layers on top of each other (merge).
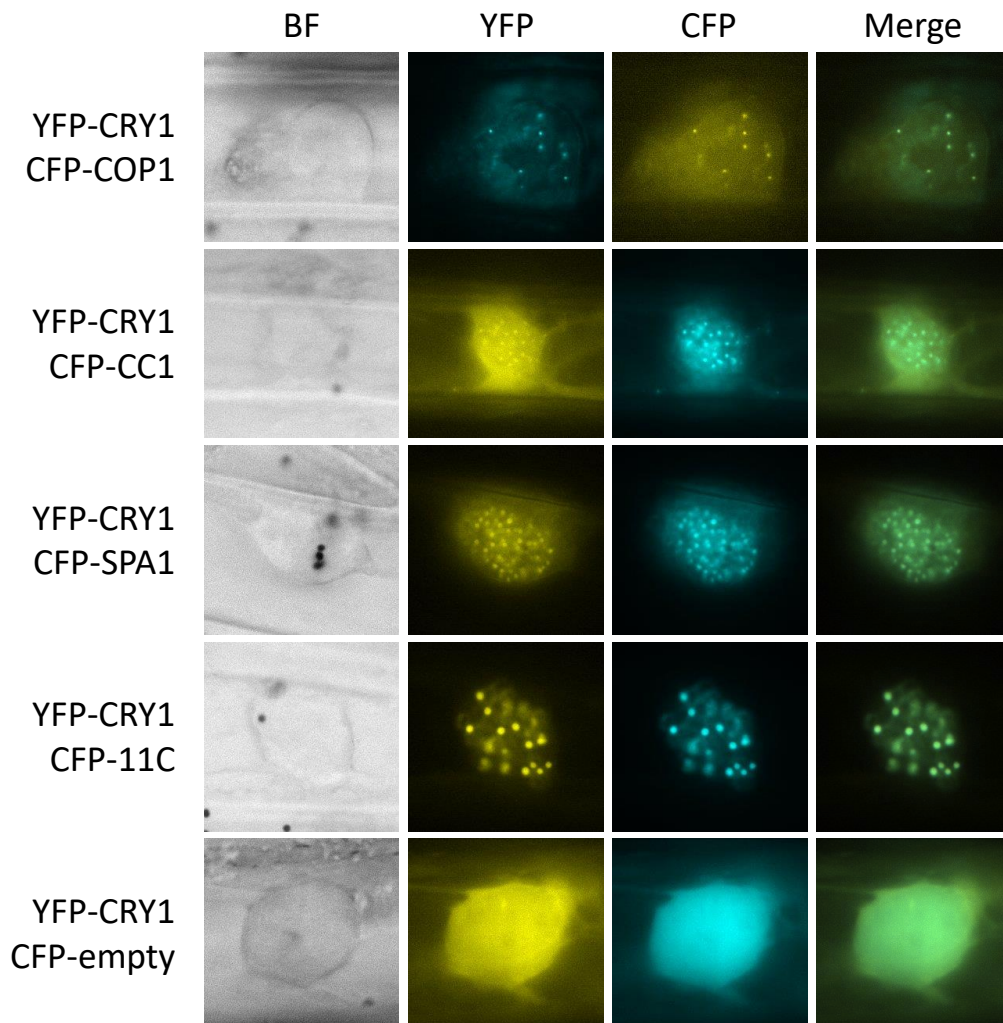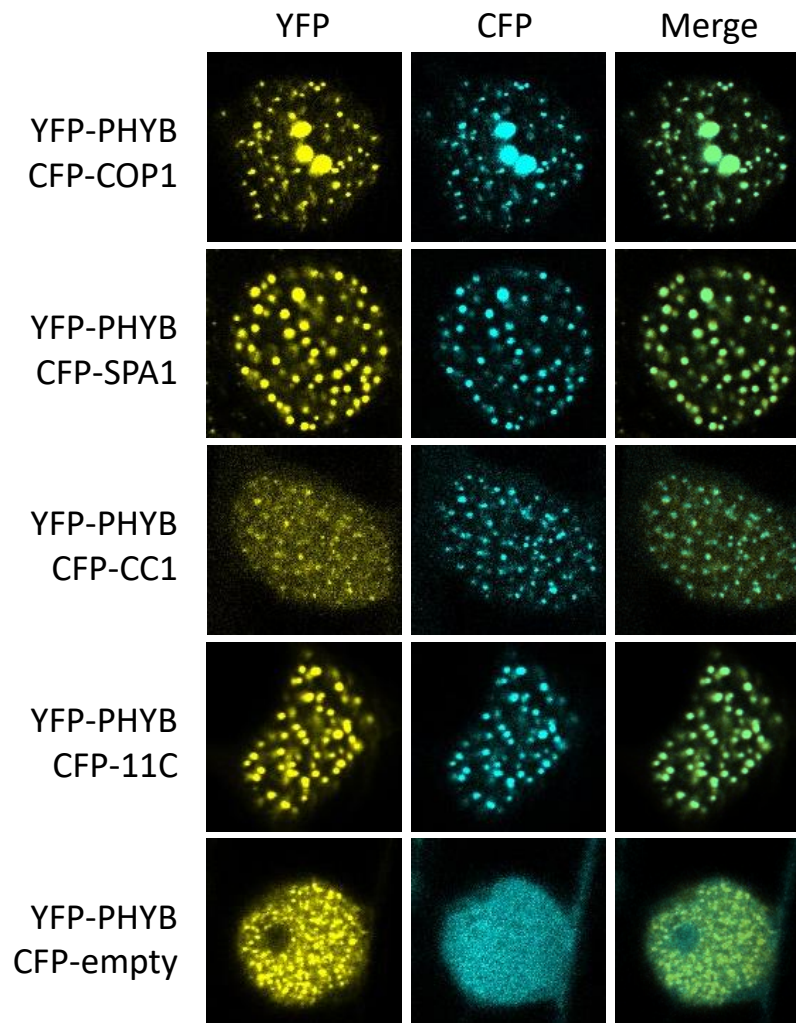
Supplemental Figure S 3: Chimeric COP1/SPA1 domain-swap proteins co-localize with cry1.

Confocal laser scanning microscopy images visualizing co-localization of fluorescence-tagged COP1, SPA1 and domain-swap proteins with cry1. Proteins fused to either YFP or CFP were co-expressed in leek epidermal cells and analyzed using confocal laser scanning microscopy. Columns (left to right): Bright field (BF), image captured in the YFP channel (YFP); image captured in the CFP channel (CFP); YFP and CFP images layers on top of each other (merge).

Supplemental Figure S 4 : Chimeric COP1/SPA1 domain-swap proteins co-localize with cry2.

Fluorescence microscopy images visualizing co-localization of fluorescence-tagged COP1, SPA1 and domain-swap proteins with cry2. Proteins fused to either YFP or CFP were co-expressed in leek epidermal cells and analyzed using confocal laser scanning microscopy. Columns (left to right): Bright field (BF), image captured in the YFP channel (YFP); image captured in the CFP channel (CFP); YFP and CFP images layers on top of each other (merge).

Supplemental Figure S 5: Chimeric COP1/SPA1 domain-swap proteins co-localize with phyB.

Fluorescence microscopy images visualizing co-localization of fluorescence-tagged COP1, SPA1 and domain-swap proteins with phyB. Proteins fused to either YFP or CFP were co-expressed in leek epidermal cells and analyzed using confocal laser scanning microscopy. Columns (left to right): Bright field (BF), image captured in the YFP channel (YFP); image captured in the CFP channel (CFP); YFP and CFP images layers on top of each other (merge).
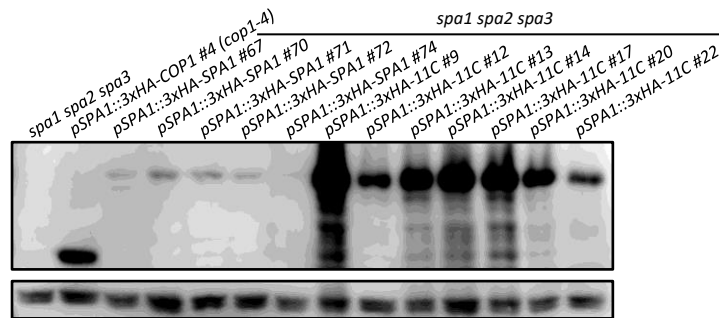
Supplemental Figure S 6: 11C protein accumulates to a much higher degree than SPA1 in most transgenic lines.

Immunodetection of either 3xHA-SPA1 or 3xHA-11C protein dark grown transgenic T2 seedlings. Multiple genetically independent transgenic lines in the T2 generation were germinated in darkness and total protein was extracted from dark-grown seedlings after four days. Total protein extracts were separated using SDS-PAGE and fixated onto PVDF membranes. Protein extracted from *spa1 spa2 spa3* triple mutants was used as a negative control, and protein extracts from the *pSPA1::3xHA-COP1 #4 (cop1-4)* line was used as a reference. HSC70 was used as a loading control. Proteins were detected using HRP-coupled anti-HA antibody or anti-HSC70 primary antibody.
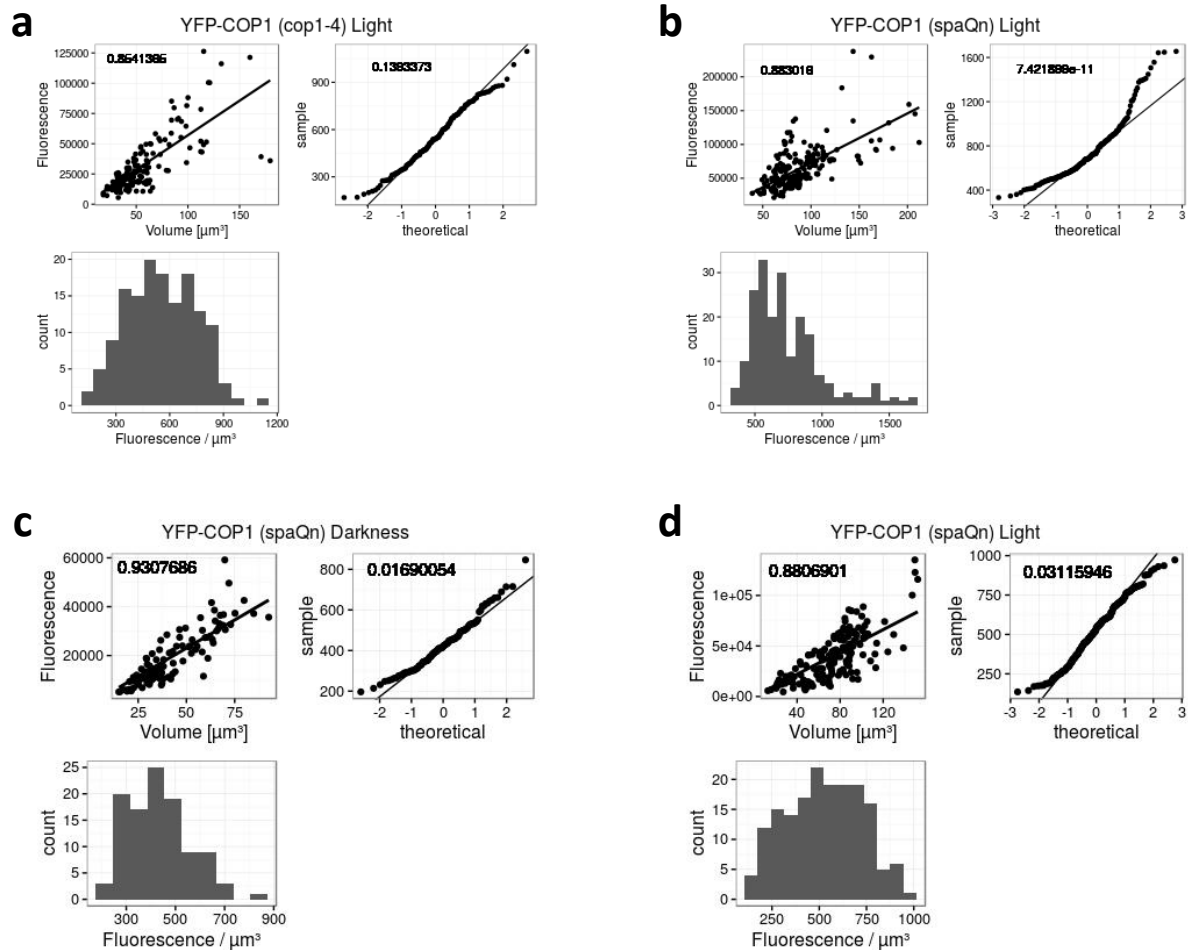
a

b
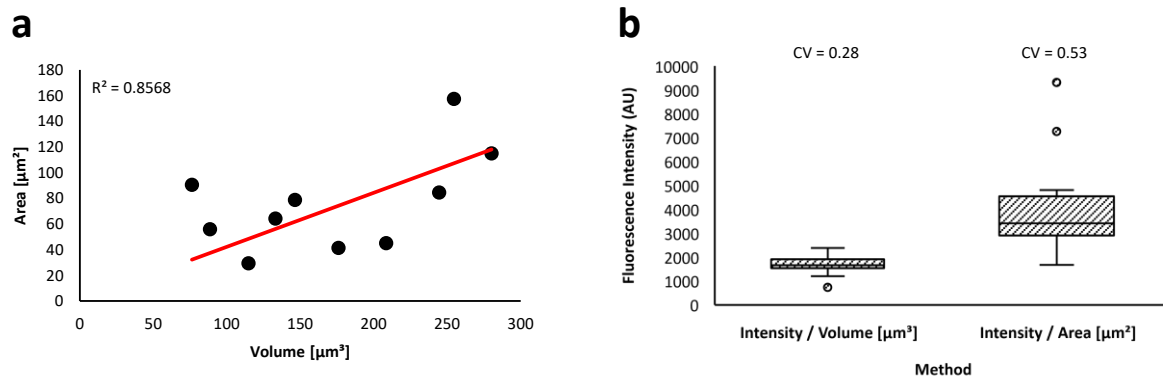
Supplemental Figure S 7: Nuclear fluorescence intensity can be measured more precisely in 3-dimensional images.

(a) Z-stacks obtained from confocal laser scanning microscopy visualizing 3-dimensional models of DAPI-stained nuclei were analyzed for nuclear volume. To calculate nuclear volume, ROIs were defined in slices of z-stacks which showed DAPI-stained nuclei. For each nucleus individually, the area of a ROI was measured, and each ROI are was multiplied by the distance between each slice and summed up. For area, area measurements from each slice of a ROI were compared, and the slice with the biggest area was used. For ten randomly picked nuclei, its area was subsequently plotted against its volume measurement. Red line indicates linear regression model with $R^2 = 0.2306$. **(b)** For the same nuclei that were randomly picked in (a), total fluorescence intensity was measured in 3-dimensional z-stacks. Fluorescence intensity per μm^3 (previously obtained volume measurements) showed a significantly lower variance with a coefficient of variation (CV) = 27.9% than fluorescence intensity per μm^2 (previously obtained area measurements) with a CV = 53.3%. Coefficient of variation is calculated as the standard deviation of a set of datapoints divided by its mean.
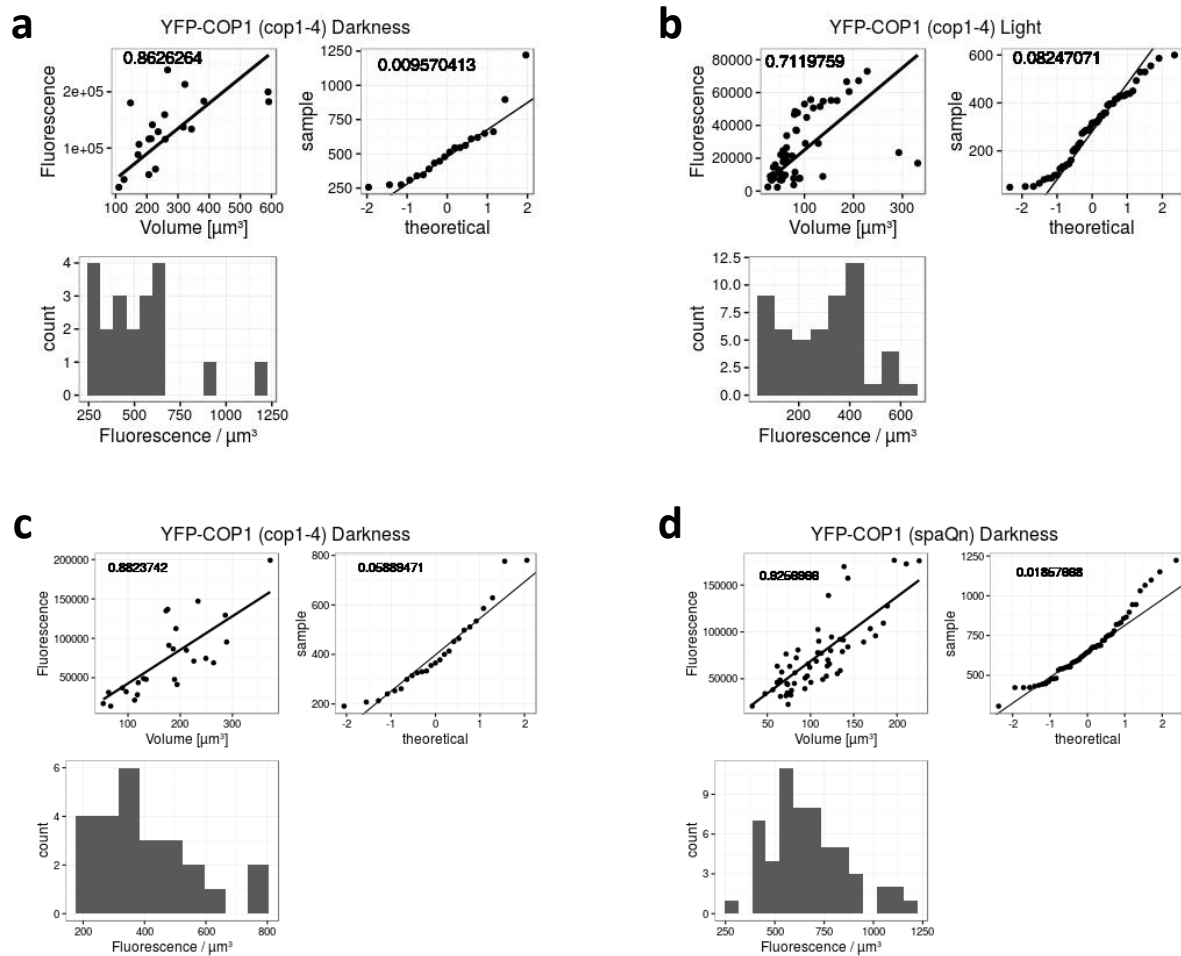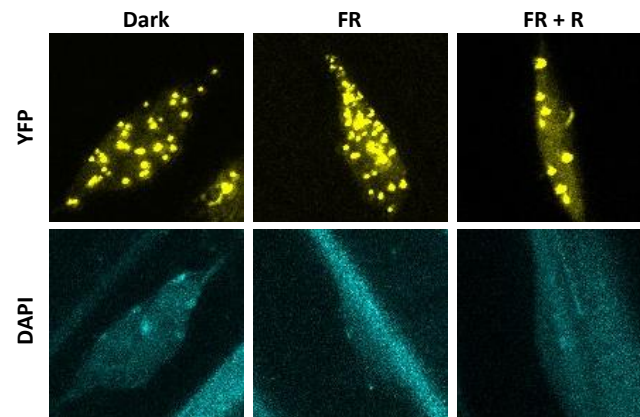
Supplemental Figure S 8: Quality assessment of datasets used for quantitative analysis in Fig.2.10.

Datasets generated and used for quantitative analysis of nuclear fluorescence intensity as depicted in Figure 3.10 were investigated for data quality. In total, four distinct datasets were generated for the quantification of nuclear fluorescence intensity described in Figure 3.10. Plots in **(a+b)** correspond to datasets used in Figure 3.10b; plots in **(c+d)** correspond to datasets used in Figure 3.10d. (a-d) top-left: Analysis of the correlation between fluorescence intensity (y-axis) and volume measurements (x-axis) for each individual nucleus measured. Black line symbolizes linear regression model of datasets. Number represents R^2 value for the regression model. Top-right: Normal quantile-quantile plot assessing the distribution pattern of datasets. Quantiles of sample points (y-axis) are plotted against hypothetical quantiles of a normal distribution (x-axis). If the dataset has a normal distribution, data points will follow the plotted line. Number represents *p*-value obtained from Shapiro-Wilk test. If $p <$ 0.05, then the null hypothesis that the respective dataset is normally distributed can be rejected to a confidence of 95%. Bottom left: histogram of the distribution of data points expressed in terms of fluorescence intensity per μm^3.

Supplemental Figure S 9: Quality assessment of datasets used for quantitative analysis in Fig.2.11.

Datasets generated and used for quantitative analysis of nuclear fluorescence intensity as depicted in Figure 3.11 were investigated for data quality. In total, four distinct datasets were generated for the quantification of nuclear fluorescence intensity described in Figure 3.11. Plots in **(a+b)** correspond to datasets used in Figure 3.11b; plots in **(c+d)** correspond to datasets used in Figure 3.11d. (a-d) top-left: Analysis of the correlation between fluorescence intensity (y-axis) and volume measurements (x-axis) for each individual nucleus measured. Black line symbolizes linear regression model of datasets. Number represents R^2 value for the regression model. Top-right: Normal quantile-quantile plot assessing the distribution pattern of datasets. Quantiles of sample points (y-axis) are plotted against hypothetical quantiles of a normal distribution (x-axis). If the dataset has a normal distribution, data points will follow the plotted line. Number represents *p*-value obtained from Shapiro-Wilk test. If $p < 0.05$, then the null hypothesis that the respective dataset is normally distributed can be rejected to a confidence of 95%. Bottom left: histogram of the distribution of data points expressed in terms of fluorescence intensity per μm^3.

Supplemental Figure S 10: YFP-SPA1 speckle formation is not abolished by FR or R induction.

Confocal laser scanning microscopy visualization of nuclear YFP-SPA1 in hypocotyl cells of dark grown transgenic *35S::HA-YFP-SPA1* Arabidopsis seedlings. Seedlings were grown in darkness for 4 days and then either kept in darkness (Dark), shifted to FR for 6 h (FR) or shifted to FR for 6 h and subsequently shifted to R for an additional 6 h (FR + R). Seedlings were stained with DAPI solution and analyzed for DAPI and YFP fluorescence.

Supplemental Table S 1: Phenotypic data collected from transgenic lines expressing *COP1, SPA1, CC1* or *11C.*

Arabidopsis *cop1-4* or *spa1 spa2 spa3* mutants were transformed with constructs containing either full-length *COP1, SPA1* or chimeric *CC1/11C* and seeds were screened for transformants by Kan[R] selection. Independent transgenic lines were then propagated into the T2 generation, where they were analyzed for segregation of resistant vs non-resistant plants as well seedling phenotypes in 4 days of darkness or 4 days of 60 µmol m^{-2} s^{-1} Rc. Genetically independent transgenic lines that segregated to a ratio of 3 (resistant) to 1 (non-resistant) and showed the majority phenotype of all transgenic lines with the same transgene were propagated to the T3 generation (propagated lines marked in grey).

genotype	line	#resistant	#susceptible	segregation	dark phenotype	Rc phenotype
pSPA1::COP1 (cop1-4)	1	all	0	15:1	much shorter than Col-0	almost cop1-4
pSPA1::COP1 (cop1-4)	2	all	0	15:1	like Col-0	like Col-0
pSPA1::COP1 (cop1-4)	4	50	7	7.142857143	like Col-0	slighty shorter than Col-0
pSPA1::COP1 (cop1-4)	5	31	10	3.1	like Col-0	like Col-0
pSPA1::COP1 (cop1-4)	6	all	0	15:1	like Col-0	like Col-0
pSPA1::COP1 (cop1-4)	11	37	11	3.363636364	like Col-0	slighty shorter than Col-0
pSPA1::COP1 (cop1-4)	12	60	17	3.529411765	like Col-0	almost cop1-4
pSPA1::COP1 (cop1-4)	13	all	0	15:1	like Col-0	like Col-0
pSPA1::COP1 (cop1-4)	14	all	0	15:1	like Col-0	like Col-o
pSPA1::COP1 (cop1-4)	15	42	9	4.666666667	like Col-0	like Col-0
pSPA1::COP1 (cop1-4)	16	all	0	15:1	like Col-0	like Col-0
pSPA1::COP1 (cop1-4)	17	28	10	2.8	low germination	low germination
pSPA1::COP1 (cop1-4)	18	46	15	3.066666667	like Col-0	like Col-0
pSPA1::COP1 (cop1-4)	20	all	0	15:1	like Col-0	like Col-0
pSPA1::CC1 (cop1-4)	1	16	5	3.2	low germination	low germination
pSPA1::CC1 (cop1-4)	2	19	5	3.8	low germination	low germination
pSPA1::CC1 (cop1-4)	3	32	5	6.4	no seeds	no seeds
pSPA1::CC1 (cop1-4)	5	27	4	6.75	low germination	low germination
pSPA1::CC1 (cop1-4)	6	30	7	4.285714286	almost Col-0	almost cop1-4
pSPA1::CC1 (cop1-4)	7	many	2	15:1	almost Col-0	almost cop1-4
pSPA1::CC1 (cop1-4)	8	many	2	15:1	as long as Col-0 open cotyledons	almost cop1-4
pSPA1::CC1 (cop1-4)	9	42	5	8.4	as long as Col-0 open cotyledons	almost cop1-4
pSPA1::CC1 (cop1-4)	10	29	9	3.222222222	as long as Col-0 open cotyledons	almost cop1-4
pSPA1::CC1 (cop1-4)	11	35	13	2.692307692	as long as Col-0 open cotyledons	almost cop1-4
pSPA1::CC1 (cop1-4)	12	35	8	4.375	as long as Col-0 open cotyledons	almost cop1-4
pSPA1::CC1 (cop1-4)	13	61	19	3.210526316	as long as Col-0 open cotyledons	almost cop1-4
pSPA1::CC1 (cop1-4)	14	many	1	15:1	low germination	almost cop1-4
pSPA1::CC1 (cop1-4)	15	44	11	4	low germination, almost Col-0	low germ, almost cop1-4
pSPA1::CC1 (cop1-4)	16	35	9	3.888888889	shorter than Col-0	almost cop1-4
pSPA1::CC1 (cop1-4)	17	41	12	3.416666667	as long as Col-0 open cotyledons	almost cop1-4
pSPA1::CC1 (cop1-4)	18	27	15	1.8	as long as Col-0 open cotyledons	almost cop1-4
pSPA1::CC1 (cop1-4)	20	31	9	3.444444444	low germ, almost Col-0	low germination, almost cop1-4
pSPA1::SPA1 (spa123)	11	all	0	15:1	like spa234	longer than spa234
pSPA1::SPA1 (spa123)	13	all	0	15:1	like spa234	longer than spa234
pSPA1::SPA1 (spa123)	42	35	11	3.181818182	like spa234	longer than spa234
pSPA1::SPA1 (spa123)	46	37	5	7.4	like spa234	longer than spa234
pSPA1::SPA1 (spa123)	54	all	0	15:1	like spa234	like spa234
pSPA1::SPA1 (spa123)	55	all	0	15:1	like spa234	like spa234
pSPA1::SPA1 (spa123)	56	all	0	15:1	like spa234	like spa234
pSPA1::SPA1 (spa123)	57	all	0	15:1	like spa234	like spa234
pSPA1::SPA1 (spa123)	58	48	13	3.692307692	like spa234	like spa234
pSPA1::SPA1 (spa123)	59	34	10	3.4	like spa234	like spa234
pSPA1::SPA1 (spa123)	60	15	1	15	like spa234	like spa234
pSPA1::SPA1 (spa123)	61	30	2	15	like spa234	like spa234
pSPA1::SPA1 (spa123)	62	42	3	14	like spa234	like spa234
pSPA1::SPA1 (spa123)	63	40	12	3.333333333	like spa234	like spa234
pSPA1::SPA1 (spa123)	64	15	1	15	like spa234	like spa234
pSPA1::SPA1 (spa123)	65	59	19	3.105263158	like spa234	like spa234
pSPA1::SPA1 (spa123)	67	35	12	2.916666667	like spa234	like spa234
pSPA1::SPA1 (spa123)	70	15	1	15	like spa234	like spa234
pSPA1::SPA1 (spa123)	71	15	1	15	like spa234	like spa234
pSPA1::SPA1 (spa123)	72	35	13	2.692307692	like spa234	like spa234
pSPA1::SPA1 (spa123)	74	all	0	15:1	like spa234	like spa234
pSPA1::11C (spa123)	4	16	5	3.2	slightly longer than spa123	like spa234
pSPA1::11C (spa123)	9	17	7	2.428571429	like spa123	like spa234
pSPA1::11C (spa123)	13	15	6	2.5	like spa123	like spa234
pSPA1::11C (spa123)	14	all	0		like spa123	like spa234
pSPA1::11C (spa123)	18	21	7	3	like spa123	like spa234
pSPA1::11C (spa123)	12	17	10	1.7	like spa123	like spa234
pSPA1::11C (spa123)	17	all	0		like spa123	like spa234
pSPA1::11C (spa123)	20	27	7	3.857142857	like spa123	like spa234
pSPA1::11C (spa123)	23	all	0		like spa123	like spa234
pSPA1::11C (spa123)	38	30	8	3.75	like spa123	like spa234
pSPA1::11C (spa123)	43	18	5	3.6	like spa123	like spa234
pSPA1::11C (spa123)	48	32	12	2.666666667	like spa123	like spa234
pSPA1::11C (spa123)	49	17	5	3.4	like spa123	like spa234
pSPA1::11C (spa123)	50	31	3	10.33333333	like spa123	like spa234
pSPA1::11C (spa123)	24	all	0		like spa123	like spa234
pSPA1::11C (spa123)	22	37	2	18.5	like spa123	like spa234
pSPA1::11C (spa123)	44	50	12	4.166666667	like spa123	like spa234

8 ACKNOWLEDGEMENTS

Although I am the author of this work, there are many people who supported me both personally and professionally and I would have never been able to finish this work without them. Four and a half years of my work life have been poured into this work, and some stretches of the journey have been far from easy. In this regard, I am first and foremost eternally thankful to Ute Höcker for her unmatched guidance, and her unique ability to provide exactly the right amount of support in every situation. Her investment in both my professional and personal development since my Bachelor studies more than seven years ago and her encouragement to always find new challenges has made this work, and so much more, possible to begin with.

I would like to thank Martin Hülskamp and Thomas Wiehe for being part of the examination committee. I am also grateful to Philipp Schiffer and Kay Hofmann for their guidance in my Thesis Advisory Committee and Isabell Witt for her excellent organization of all things around the GSfBS.

In times when the lab was my second home, my lab buddies where like roommates to me. I would like to thank every single lab member of the Höcker group for being such excellent people and scientists. I am especially grateful to Martin and Xu, who welcomed me into the lab so kindly and helped me on my first steps as a PhD student. Thank you to Christian, Eva, Jathish, Krzysztof, Laura, Martina, Melanie, Natalia, Pan Pan and Tobi, as well as all bachelor/master students and student helpers (both past and present), for countless hours of fun in the lab, great scientific discussions, apple breaks™ and overall great memories. You all made my time in this group unforgettable.

As a lab member, but more importantly as a friend, I owe so much to Oliver for his eternal patience and kindness. Thank you to Beatrix, Nikolai and Philipp for sharing the insane experience that was the organization of the YRSPP 2018, and to Karin Körner for helping me find peace of mind during rough times.

For the last ten years, Sophie has been by my side through some of the best, and some of the toughest, parts of my life. I could not imagine where I would be today without her unconditional support and kindness. We have fought our demons, and enjoyed the spoils, together. I will always be thankful for everything she has given me.

Finally, I would not be here without the support of all my family members, especially my sister and mother, Katharina and Barbara. Although he is no longer here to witness all of this, I know that my dad would be immeasurably proud, and I am eternally thankful to him for setting me on the path to everything I have managed to accomplish.
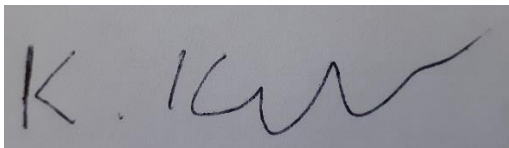
9 ERKLÄRUNG

Gemäß der Promotionsordnung vom 12. März 2020

„Hiermit versichere ich an Eides statt, dass ich die vorliegende Dissertation selbstständig und ohne die Benutzung anderer als der angegebenen Hilfsmittel und Literatur angefertigt habe. Alle Stellen, die wörtlich oder sinngemäß aus veröffentlichten und nicht veröffentlichten Werken dem Wortlaut oder dem Sinn nach entnommen wurden, sind als solche kenntlich gemacht. Ich versichere an Eides statt, dass diese Dissertation noch keiner anderen Fakultät oder Universität zur Prüfung vorgelegen hat; dass sie - abgesehen von unten angegebenen Teilpublikationen und eingebundenen Artikeln und Manuskripten - noch nicht veröffentlicht worden ist sowie, dass ich eine Veröffentlichung der Dissertation vor Abschluss der Promotion nicht ohne Genehmigung des Promotionsausschusses vornehmen werde. Die Bestimmungen dieser Ordnung sind mir bekannt. Darüber hinaus erkläre ich hiermit, dass ich die Ordnung zur Sicherung guter wissenschaftlicher Praxis und zum Umgang mit wissenschaftlichem Fehlverhalten der Universität zu Köln gelesen und sie bei der Durchführung der Dissertation zugrundeliegenden Arbeiten und der schriftlich verfassten Dissertation beachtet habe und verpflichte mich hiermit, die dort genannten Vorgaben bei allen wissenschaftlichen Tätigkeiten zu beachten und umzusetzen. Ich versichere, dass die eingereichte elektronische Fassung der eingereichten Druckfassung vollständig entspricht."

Teilpublikationen:

Balcerowicz, M., Kerner, K., Schenkel, C., and Hoecker, U. (2017). SPA proteins affect the subcellular localization of COP1 in the COP1/SPA ubiquitin ligase complex during photomorphogenesis. Plant Physiol. **174**: 1314–1321.

_____

21. September 2020, Konstatin Kerner